Quantifying Seasonal, Hemispheric, and Interannual Variations in Cyclone Impacts on Sea Ice

By

Claire Mundi

A dissertation submitted in partial fulfillment of
the requirements for the degree of

Doctor of Philosophy
(Atmospheric and Oceanic Sciences)

at the
UNIVERSITY OF WISCONSIN-MADISON
2026

Date of final oral examination: 3/26/2026

The dissertation is approved by the following members of the Final Oral Committee:
Tristan L'Ecuyer, Professor, Atmospheric and Oceanic Sciences
Jonathan Martin, Professor, Atmospheric and Oceanic Sciences
Steve Vavrus, Scientist, Center for Climatic Research
Till Wagner, Associate Professor, Atmospheric and Oceanic Sciences
Hannah Zanowski, Assistant Professor, Atmospheric and Oceanic Sciences

Abstract

Quantifying Seasonal, Hemispheric, and Interannual Variations in Cyclone Impacts on Sea Ice

by Claire Mundi

Earth's energy balance is strongly modulated by sea ice cover. Cyclones can impact sea ice extent by amplifying wave activity, promoting ice breakup, advecting heat and moisture, and enhancing sea ice drift. Due to the range of atmospheric and oceanic processes involved, the net effect of intense cyclones on sea ice within the marginal ice zone (MIZ) has yet to be quantified. Here we first assess the impact of Arctic summer storms from an observational perspective, which is when the sea ice is likely at its most vulnerable to further decreases in ice area. Guided by the opposing ice tendencies of two case studies, 264 strong (minimum surface pressure below 984 hPa) summer cyclones were analyzed to quantify the net ice impacts in the present-day Arctic (2010–19) and early satellite era (1982–91). We find that early summer storms tend to decrease the MIZ ice area more than late summer storms and that wind direction and SST trends partially reconcile the wide range of MIZ ice area changes due to cyclone passage. Additionally, recent summer cyclones had more negative impacts on the ice than storms in the 1980s. Based on these results, understanding how these effects may evolve in the future is critical for accurately predicting future ice loss. We use output from the Community Earth System Model version 2 Large Ensemble (CESM2-LE) to compare intense summer cyclone impacts on the MIZ with observed responses. We find that CESM2-LE reproduces observed net

impacts but exhibits compensating biases, where fewer intense cyclones reach the MIZ but decrease ice area more than observed. In a future emission scenario, CESM2-LE predicts more frequent intense cyclones, but as the Arctic warms and late summer ice cover lessens, fewer storms will interact with the retreating ice edge. Subsequently, the largest effects shift earlier in the year, and ice loss from these storms declines after present day, suggesting intense summer cyclone impacts have reached a maximum. Finally, the effects of intense cyclones are assessed in all seasons and in both hemispheres using observations, finding that storms enhance the seasonal ice growth and decay cycle in both hemispheres. Cyclones intensify equatorward winds and ice advection within a cooling ocean during the cold season and enhance poleward motion within a warming ocean during the warm season, collectively increasing global annual mean ice area. Southern hemisphere cyclones have the strongest influence on global ice area, with autumn and early winter cyclones strongly expanding ice area. While these increases are partially offset by ice losses in early austral summer, the low overall Antarctic sea ice extent in late summer limits further losses, leading to an asymmetric annual cycle where intense cyclones enhance global ice area from April through October but only destroy it in November and December.

Acknowledgements

I am so incredibly grateful to every single person who has offered support throughout this journey. I would first like to acknowledge my advisor Tristan L'Ecuyer, who has provided unending encouragement over the years. I appreciate his guidance and mentorship, which have helped me become the scientist I am today. My gratitude also extends to my PhD committee members: Jon Martin, Till Wagner, Steve Vavrus, and Hannah Zanowski for their helpful suggestions and advice throughout the research progress. Their support of this work has been invaluable. I would also like to extend my sincere thanks to Alice DuVivier for her assistance, not only with the ins and outs of CESM but also with putting together applications for my visit to NCAR and for being such an amazing host. Her feedback greatly improved my second paper, which is reproduced here as Chapter 4. And thank you to the greater AOS community for creating such a supportive environment. To any curious STEM pen pals or high school science class adopters who have happened upon this work, thank you for your curiosity-driven questions and important reminders about why this field is so interesting and why I started down this path. Finally, I would not have made it this far without the support of my family. I very much appreciate all their encouragement and unwavering belief in my abilities. Special thanks to my parents for nurturing my curiosity and love of learning, and for always printing out my papers even if they remain unread. Thanks also to Poppi for being a source of unending happiness.

Contents

Abstract **i**

Acknowledgements **iii**

Contents **iv**

List of Figures **vi**

List of Tables **xiii**

1 Introduction **1**

2 Data and Methods **8**
2.1 Data 8
2.1.1 Observational Datasets 8
2.1.2 Atmospheric reanalysis 11
2.1.3 Large Ensemble 13
2.2 Methods 15
2.2.1 Arctic cyclone identification 15
2.2.2 Sea ice area trend metrics 18

3 Is the Modern Arctic Marginal Ice Zone More Susceptible to Summer Cyclones? **20**
3.1 Preface 20
3.2 Census of Summer Arctic Cyclones 22
3.3 Results 25
3.3.1 Decreasing MIZ Area: August 5, 2017 26
3.3.2 Increasing MIZ Area: September 9, 2011 29
3.3.3 Composite Analysis 33
3.3.4 Comparison with earlier Arctic epoch (1982–1991) 37
3.4 Discussion 41
3.5 Conclusions 43

4 Have Impacts of Intense Arctic Cyclones on Summer Sea Ice Reached a Maximum? 56
4.1 Introduction . . . 56
4.2 Adapting Cyclone Detection Methods to CESM2-LE . . . 58
4.3 Results . . . 59
4.3.1 Differences in Cyclone Detection . . . 59
4.3.2 Impacts of Intense Cyclones on MIZ Ice Area . . . 61
4.3.3 Net Impact . . . 64
4.4 Evolution of Intense Cyclone Impacts in Future Decades . . . 64
4.5 Conclusions . . . 68

5 Intense Storms Increase Global Ice Area 70
5.1 Preface . . . 70
5.2 Adapting Methods to the Southern Hemisphere . . . 71
5.2.1 Sensitivity to Chosen Thresholds . . . 72
5.3 Storms Can Expand or Reduce Ice Area . . . 72
5.4 Storm-Induced Changes in the MIZ Environment . . . 76
5.5 The Net Cyclone Impact on Global Sea Ice . . . 79
5.6 Discussion . . . 80

6 Conclusions 83
6.1 Synthesis . . . 83
6.2 Future Work . . . 86

A Supplementary Information for Chapter 3 87

B Supplementary Information for Chapter 4 94

C Supplementary Information for Chapter 5 99

Bibliography 109

List of Figures

2.1 Study area (red dashed) of two cyclone events based on the 1000 hPa pressure contours over the three days of each storm. The 990 hPa contour is also shown for each day. The accumulated MIZ area within this study area is outlined in black and shaded in blue. Note in (b) that a second storm was identified just south of the main storm. Since the detection algorithm groups cyclones by spatial proximity, these two systems are classified as the same storm event and their impact on the MIZ will be considered jointly. 17

3.1 Distributions of minimum sea level pressure for (a) June and July and (b) August and September cyclones. Confidence levels at which the distributions of the two decades differ for Student's t-test (t), non-parametric Mann-Whitney U test (MW), and Kolmogorov-Smirnov test (KS) are listed (as in Finocchio et al. (2022)). Minimum pressures of the two case studies are also shown. Spatial distribution of storms for (c) early summer 2010–2019, (d) early summer 1982–1991, (e) late summer 2010–2019, and (f) late summer 1982–1991. Shading represents the minimum pressure reached by the cyclone throughout its development. The mean 15% (solid) and 80% (dotted) sea ice concentration contours are also shown. 23

3.2 Normalized changes in MIZ ice area relative to the start of the analysis time window for early- and late-summer months in (a) and (c) 2010–2019 and (b) and (d) 1982–1991. Line coloring indicates the percentage of ice that is present within the storm area on the first day of the cyclone. The mean and standard deviation of all curves are plotted in red. The mean trend in (a), (b), and (d) are significantly different from zero based on a Student's t-test at the 95% level. Panel (c) also shows the time series for the ice-increasing and ice-decreasing cyclones selected as case studies in the thick blue and black lines, respectively. 25

3.3 (a-c) Change in sea ice concentration over the three days of a storm that reduces ice area within the MIZ region. The accumulated MIZ area is outlined in black. The location of the storm's minimum pressure from each earlier day is identified by a yellow star. (d-f) Change in sea surface temperature over the three days of the storm. The 15% and 80% contours of the earlier day (outlined in gray) and daily averaged 10-meter wind vectors from the earlier day are displayed in all plots. 26

3.4 Time series of (a) sea ice area, (b) wind values, and (c) SST (black) and air temperature (green dashed) values within the MIZ from one week before the start of the storm to two weeks after. Note in (a) that the area time series is not detrended as in Figure 3.2. Dashed lines indicate climatological averages from 2010–2019, with one standard deviation shown in gray shading. Mean upper-ocean temperature profiles averaged over the MIZ area for key dates surrounding the cyclone's development are shown in (d). 27

3.5 (a-c) Change in sea ice concentration over the three days of a storm that increases ice area within the MIZ region. The accumulated MIZ area is outlined in black. The location of the storm's minimum pressure from each earlier day is identified by a yellow star. (d-f) Change in sea surface temperature over the three days of the storm. The 15% and 80% contours of the earlier day (outlined in gray) and daily averaged 10-meter wind vectors from the earlier day are displayed in all plots. 30

3.6 Time series of (a) sea ice area, (b) wind values, and (c) SST (black) and air temperature (green dashed) values within the MIZ from one week before the start of the storm to two weeks after. Note in (a) that the area time series is not detrended as in Figure 3.2. Dashed lines indicate climatological averages from 2010–2019, with one standard deviation shown in gray shading. Mean upper-ocean temperature profiles averaged over the MIZ area for key dates surrounding the cyclone's development are shown in (d). 31

3.7 Composite plots showing the normalized change in MIZ ice area for the three weeks around cyclones occurring in late summer 2010–2019, separated into categories based on the primary wind direction within the storm area. The mean values and the 5th, 25th, 75th, and 95th percentiles are plotted. The arrows represent the portion of the plot where the distribution of slopes of the mean normalized area time series has a statistically significant ($p < 0.05$) difference from zero. The slopes are computed over different sections of the time series: the week leading up to the storm (days -7 to 0; top of plots), after the storm (days 0 to 3, 0 to 7, 0 to 14; top of plots), or over the full three-week time series (days -7 to 14; bottom of plots). A version of this plot without normalization is available in Figure A.1. 34

3.8 As in Figure 3.7, but separated into categories based on the primary wind direction and SST trend during the time of the cyclone. A version of this plot without normalization is available in Figure A.1. 35

3.9 As in Figures 3.7 and 3.8, but for early-summer months in 2010–2019. A version of this plot without normalization is available in Figure A.2. 49

3.10 (a) Comparison of monthly mean sea ice extent for both decades. Gray dotted line shows the mean ice extent for July 2010-2019 to highlight its similarity to the 1982-1991 August and September extents. (b) Comparison of monthly mean sea surface temperatures in open water north of 67°N for both decades. 50

3.11 As in Figures 3.7 and 3.8, but for late-summer months in 1982–1991. A version of this plot without normalization is available in Figure A.3. 51
3.12 As in Figures 3.7 and 3.8, but for early-summer months in 1982–1991. A version of this plot without normalization is available in Figure A.4. 52
3.13 (a) Normalized changes in MIZ ice area relative to the start of the analysis time window for four decades of cyclone events. The legend includes the percentage of early-summer storms and the number of total storms for that decade in parentheses. A version of this plot without normalization is available in Figure A.5. (b) Monthly counts of both early- and late-summer storms in each decade. (c) Normalized changes in MIZ ice area relative to the start of the analysis time window for each month in 2010–2019 (top) and 1982–1991 (bottom). 53
3.14 As in Figure 3.7, but for early-summer months (a,b) and late-summer months (c,d) in 1990–1999. A version of this plot without normalization is available in Figure A.6. 54
3.15 Net change in MIZ ice area for cyclones in the present-day Arctic (2010–2019, left column) and early in the satellite era (1982–1991, right column), for each decade (a,b), for early-summer months (c,d), and for late-summer months (e,f), relative to the climatological mean for each storm and the initial ice area one week before the start of the storm. Line coloring indicates the percentage of ice that is present within the storm area on the first day of the cyclone. The mean and standard deviation of all curves are plotted in red. The mean trends in (a), (c), and (f) are significantly different from zero based on a Student's t-test at the 95% level. Values in red (upper left) denote the mean net change in area after two weeks. . . . 55

4.1 June through September storm counts for 2010-2019 (a) and 1982-1991 (b) in CESM (left) and ERA5 (right). The mean total annual count per ensemble member (n) is indicated at the top of each bar. Colors describe the filters applied to the census of cyclones and are discussed in text. “Remaining Cyclones" (red) are storms considered in this study, with the mean annual count shown in parentheses. (c-f) Distribution of ensemble annual-mean storm counts (dots and boxplot) compared with ERA5 (cross) for total storm counts (blue) and remaining cyclones (red). (g-j) Frequency of June-September mean sea level pressure values falling below 986 hPa. ERA5 data is scaled to match the resolution of CESM2. 60

4.2 (a-d) Net change in MIZ ice area, relative to one week before the storm. Mean storm impact for each ensemble member is shown in gray, with the mean and standard deviation across members shown in red. The mean observational response is shown in blue. (e) Fraction of cyclones in each ensemble member that causes a net decrease in MIZ ice area two weeks after the storm's passage or (f) have a corresponding increase in SST during the storm lifetime. (g) Total net sea ice change for each month/decade grouping. Red dots and box plots show the distribution of ensemble member values. Blue crosses show the corresponding mean value for cyclones detected in ERA5. Asterisk depicts no statistically significant difference at the 99.9% level (e-f all show significant differences). 62

4.3 Monthly mean (a) MIZ ice area, (b) storm count, (c) number of storms that interact with the MIZ, per latitude band. (d) Annual storm counts (green) and MIZ area (brown crosses) for both CESM2-LE (no marker) and observed storms (circles). Dashed lines indicate storms that interact with the MIZ and solid lines show total storm count. (e) Observed annual mean MIZ latitude (green) and MIZ area (brown) over the satellite record. 65

4.4 Changes in MIZ ice area due to cyclones for May, June, July, August, September, and total change for all five months (columns) and four selected decades (rows). Thick black lines depict the ensemble and decadal mean sea ice extent on the first day of the month. Thin contours indicate the mean number of days of each decade with storms occurring in that location. Monthly and total time series on the right show the change in MIZ area for all decades from the early satellite era through 2100. Markers correspond to the four selected decades shown in the maps. 67

5.1 **Example Case Study: April 15, 2011. a**, Storm area (navy) defined by daily mean 980 hPa contours (pink). Shaded area indicates the MIZ. Light blue and black contours indicate the sea ice extent on the the first day (April 15) and the last day (April 18) of the storm. **b**, Change in sea ice concentration over the duration of the storm. Daily mean wind vectors are shown for the second day of the storm. The location of the storm's minimum pressure is noted with a yellow star. **c-d**, Daily time series from one week before the storm to two weeks after for (**c**) sea ice area (solid; dashed line depicts the climatological mean ice change for this storm area), (**d**) meridional winds, computed within the MIZ and storm area for this case. **e**, Normalized mean change in MIZ ice area for all southern hemisphere April and May storms in 2010-2019 (gray). The red line depicts the mean MIZ ice area evolution for these storms, and the blue line is the normalized time series for this case study. 73

5.2 **Monthly Mean Change in MIZ Ice Area. a-d**, Normalized mean change in MIZ ice area for the northern (**a,b**) and southern (**c,d**) hemispheres across two decades (**a,c**) 1982-1991 and (**b,d**) 2010-2019. January-March months in the southern hemisphere are excluded due to small sample size. 75

5.3 **Modified Taylor Diagram Showing Main Environmental Conditions. a-d**, Monthly mean meridional wind (X), ice motion (diamond), and change in SST (circle) for (**a**,**b**) ice-increasing months and (**c**,**d**) ice-decreasing months in the Arctic and Antarctic, with outlined markers indicating the more recent decade. **e**, Range of values for each environmental variable. 77

5.4 **Monthly Mean 3-, 7-, and 14-day Changes in MIZ Ice Area. a**, Monthly changes in MIZ ice area due to cyclone influence across three timescales (light = 3 days, medium = 7 days, and dark = 14 days) in the Arctic (blue) and Antarctic (brown) for 2010-2019 (solid) and the two-week change for 1982-1991 (dashed). Net annual changes are shown for each hemisphere (Total). The MIZ-area-weighted monthly mean insolation is shown for the northern (blue solid line) and southern (brown dashed line) hemispheres for reference. **b**, Summed changes for each month. Colors indicate which hemisphere has the larger impact in each month. The total global change across all months is shown in grayscale. 82

A.1 Composite plots showing the change in MIZ ice area for the three weeks around cyclones occurring in late-summer 2010–2019 (as in Section 3c of the main text, but without the normalization procedure applied). (a-b) Categories based on the primary wind direction and within the storm area. (c-f) Categories are based on the primary wind direction and SST trend during the time of the cyclone. The mean values and the 5th, 25th, 75th, and 95th percentiles are plotted. The arrows represent the portion of the plot where the distribution of slopes of the mean normalized area time series has a statistically significant ($p < 0.05$) difference from zero. The slopes are computed over different sections of the time series: the week leading up to the storm (days -7 to 0; top of plots), after the storm (days 0 to 3, 0 to 7, 0 to 14; top of plots), or over the full three-week time series (days -7 to 14; bottom of plots). 88

A.2 As in Figure A.1, but for early-summer months in 2010–2019. 89

A.3 As in Figure A.1, but for late-summer months in 1982–1991. 90

A.4 As in Figure A.1, but for early-summer months in 1982–1991. 91

A.5 Change in MIZ ice area relative to the start of the analysis time window for four decades of cyclone events (as in Figure 14a of Chapter 3, but without the normalization procedure applied). 92

A.6 As in Figure 15 of Chapter 3, but without the normalization procedure applied. Categories are based on the primary wind direction for early-summer months (a,b) and late-summer months (c,d) in 1990–1999. 93

B.1 ERA5 mean sea level pressure at the original resolution (a-c) and scaled to match the resolution of CESM2 (d-f). Magenta and red contours indicate the 984 and 1000 hPa isobars in (a-c) and the 986 and 1002 hPa isobars in (d-f). Yellow stars mark the location of the minimum pressure. The horizontal and temporal resolutions of the datasets are listed alongside the minimum pressure (p_{min}) used for cyclone detection. Sea ice concentration for August 1, 2017, from (g) satellite observations and (h) one ensemble member of the CESM2-LE. Sea ice concentration contours for 15% (solid) and 80% (dashed) are shown in red. The root mean square (RMS) equivalent contours are shown in yellow, indicating the same fractional area as the 15% and 80% contours in satellite observations. (i) Example cyclone event. Black dashed line indicates the storm area based on the daily 1002 mb contours (grayscale). Yellow shaded area is the equivalent MIZ area used to determine the cyclone's interaction with the MIZ. Red shaded area is region MIZ ice area is tracked, defined as all 15%-80% sea ice concentration points from one day before to one day after the storm. 96

B.2 Normalized changes in the MIZ ice area relative to the start of the analysis time window for each month in (top) 2010–19 and (bottom) 1982–91 for modeled (solid) and observed (dashed) storms. Storm time series were normalized by the range (minimum value subtracted from the maximum value) of the series to composite cyclone effects without preferentially weighting spatially larger storms, as in Mundi and L'Ecuyer (2025). 97

B.3 Number of July storms across the 40 ensemble members considered for the six decades from the 1980s to the 2030s. Value and dashed line indicate the average storm count across the ensemble members for each decade. Asterisk depicts a statistically significant difference in count distributions at the 95% level. The 2010s has the fewest number of cyclones, contributing to the minimum in total cyclone impacts in Figure 4.4. 98

C.1 **Monthly Minimum Storm Pressures. a-b**, Mean and standard deviation minimum storm pressures for each month for (**a**) Arctic and (**b**) Antarctic storms, with the 1980s shown in blue and 2010s in red. Shaded regions indicate statistically significant distributions in central pressures between the two decades. 100

C.2 **Correlation Matrix of Environmental Characteristics. a-d**, Correlation values for mean changes in each variables over two weeks following storm starts from both decades for (**a**,**c**) ice-increasing months and (**b**,**d**) ice-decreasing months in the Arctic and Antarctic. 101

C.3 **Modified Taylor Diagram Showing Main Environmental Conditions One Week After Storm. a-d**, Monthly mean meridional wind (X), ice motion (diamond), and change in SST (circle) for (**a**,**b**) ice-increasing months and (**c**,**d**) ice-decreasing months in the Arctic (**a**,**c**) and Antarctic (**b**,**d**), with outlined markers indicating the more recent decade. The range of values for each environmental variable is shown in the table. 102

C.4 **Modified Taylor Diagram Showing Atmosphere Conditions. a-d**, Monthly mean atmosphere conditions during intense cyclone events. Mean meridional wind (X) and 2 m air temperature (triangle) for (**a**,**b**) ice-increasing months and (**c**,**d**) ice-decreasing months in the Arctic and Antarctic, are shown with outlined markers indicating the more recent decade. The range of values for each environmental variable is shown in the table. 103

C.5 **Modified Taylor Diagram Showing Ocean Conditions. a-d**, Monthly mean ocean conditions during intense cyclone events. Mean significant wave height (triangle), change in SST (circle), and change in upper ocean temperature (star) for (**a**,**b**) ice-increasing months and (**c**,**d**) ice-decreasing months in the Arctic and Antarctic, are shown, with outlined markers indicating the more recent decade. The range of values for each environmental variable is shown in the table. 104

C.6 **Modified Taylor Diagram Showing Sea Ice Conditions. a-d**, Monthly mean ocean conditions during intense cyclone events. Mean sea ice concentration (SIC) gradient (square), mean SIC at the start of each storm (star), and mean meridional ice motion (diamond) for (**a**,**b**) ice-increasing months and (**c**,**d**) ice-decreasing months in the Arctic and Antarctic, are shown, with outlined markers indicating the more recent decade. The range of values for each environmental variable is shown in the table. 105

C.7 **Modified Taylor Diagram Showing Main Environmental Conditions during Ice Maximum Months. a-d**, Monthly mean meridional wind (X), ice motion (diamond), and change in SST (circle) for (**a**,**b**) one-week timescales and (**c**,**d**) two-week timescales in the Arctic (**a**,**c**) and Antarctic (**b**,**d**), with outlined markers indicating the more recent decade. The range of values for each environmental variable is shown in the table. 106

C.8 **Monthly Storm Counts.** Monthly intense cyclone counts for Northern Hemisphere (blue) and Southern Hemisphere (brown) for each decade. . . 107

C.9 **Monthly Mean 3-, 7-, and 14-day Changes in MIZ Ice Area. a-b**, Monthly changes in MIZ ice area due to cyclone influence across three timescales (light = 3 days, medium = 7 days, and dark = 14 days) in the Arctic (blue) and Antarctic (brown) for (**a**) 1982-1991 and (**b**) 2010-2019 Net annual changes are shown for each hemisphere (Total). **c-d** Summed changes for each month for (**c**) 1982-1991 and (**d**) 2010-2019. Colors indicate which hemisphere has the larger impact in each month. The total global change across all months is shown in grayscale. 108

List of Tables

3.1 Average net change and standard deviation in normalized area. 39

Chapter 1

Introduction

Global sea ice cover is a key component in determining the amount of sunlight absorbed to heat the surface and, in turn, Earth's energy balance (Trenberth et al., 2014, von Schuckmann et al., 2016, Zhou et al., 2025). The Arctic, in particular, has been experiencing a rapid decline in sea ice cover due to significant warming over the last few decades (Box et al., 2019, Carmack et al., 2015, Stroeve and Notz, 2018). During the summer months, in particular, the average sea ice extent has declined by over 40% since 1979 (Koyama et al., 2017, Stroeve et al., 2012). Additionally, sea ice has become thinner and younger in more recent years, making it more susceptible to further seasonal melting (Comiso, 2012, Lindsay and Schweiger, 2015). More specifically, the marginal ice zone (MIZ) has

This chapter is comprised of modified portions of the peer-reviewed publications:
Mundi, C., & L'Ecuyer, T. (2025). Is the modern Arctic marginal ice zone more susceptible to summer cyclones?. *Journal of Climate*, 38(1), 403-422.
Mundi, C. L., L'Ecuyer, T. S., & DuVivier, A. K. (2025). Have Impacts of Intense Arctic Cyclones on Summer Sea Ice Reached a Maximum?. *Geophysical Research Letters*, 52(19), e2025GL117848.

widened in recent years due to the decline of thick, multiyear ice (Strong and Rigor, 2013). However, the MIZ has also been retreating poleward, causing the total extent of the MIZ to remain unchanged (Rolph et al., 2020).

Antarctic sea ice, on the other hand, steadily increased between 2000 and 2014, followed by a rapid decrease in recent years (Eayrs et al., 2021). The resulting decrease in global ice cover has lead to greater areas of open ocean in the polar regions and subsequently greater heat uptake. This is especially important in the Arctic where heat is readily absorbed in the shallow mixed layer, and heat uptake provides extra energy to melt sea ice, creating a feedback that accelerates Arctic warming (Hansen et al., 2011, Prince and L'Ecuyer, 2024).

With the total global sea ice extent decreasing over the recent decades, understanding the mechanisms that influence sea ice cover, specifically around the ice edge, has become increasingly important. Sea ice can be altered through changes in the surface energy budget, including anomalous cloud cover or changes in precipitation (Kapsch et al., 2016, Screen and Simmonds, 2012). Ice is also subject to dynamic influences where strong winds contribute to a decrease in ice extent through poleward advection and ice convergence (Ogi et al., 2008). Additionally, changes in ice cover itself can perpetuate additional loss through the ice-albedo feedback (Perovich et al., 2008, Serreze and Barry, 2011). As the surface albedo decreases due to greater areas of open water, nearby SSTs increase due to enhanced solar absorption and subsequently cause more ice melt. The capacity for these

changes all together is likely at its largest during the summer, when the ice extent is at its smallest and the ice is most vulnerable to environmental forcings.

One prominent aspect of the climate system that can exert a rapid influence on sea ice by simultaneously altering surface fluxes, cloud cover, precipitation, and wind patterns is the passage of Arctic cyclones. The dominant mechanism governing these sea ice changes appears to be the strong winds associated with cyclones, that are, on average, about 1 m s^{-1} greater than climatological winds without a cyclone present, and more intense storms can have even greater deviations (Schreiber and Serreze, 2020). These strong winds can cause divergent or convergent advection and can ultimately lead to ice breakup or ridging (Brümmer et al., 2008, Itkin et al., 2017). The divergence of ice forms leads that create regions of low-albedo open water, furthering the absorption of solar radiation. These leads also generate avenues for future ice growth, given sufficiently cool conditions. Convergence, on the other hand, causes ice to ridge, forming regions of thicker ice. This simultaneously leads to more open water at the ice edge, but the thicker ice is potentially more resilient to future cyclone-induced changes (Brümmer et al., 2008, Itkin et al., 2017).

In addition to changing the characteristics of the ice itself, the resultant ice motion can also change the environment in which the ice resides by advecting ice floes into regions of warmer or cooler ocean and increasing upper-ocean mixing. For example, in a numerical modeling study of the intense August 2012 storm, Zhang et al. (2013) attributed the observed decline in sea ice to the resulting upward transport of heat from

the enhanced upper-ocean mixing. These two factors, along with other contributions such as the radiative effects of variations in cloud and precipitation properties (Kapsch et al., 2016, Screen and Simmonds, 2012), help define the wide range of sea ice outcomes from cyclones.

This range of atmospheric and oceanic processes involved has prompted considerable research to quantify the effects of cyclones on sea ice, especially during the summer melt period in the Arctic. Current literature appears divided on the net impact of these events, with some studies claiming cyclones work against the climatological decline of sea ice (Schreiber and Serreze, 2020), while others cite increased sea ice loss following a storm (Kriegsmann and Brümmer, 2014). Schreiber and Serreze (2020) found that, overall, summer storms tend to limit the seasonal decline of ice primarily through increased cloud cover. This result was supported for storms that occur earlier in the summer season, during May and June (Finocchio et al., 2020). In contrast, late-summer storms in July and August have been shown to cause slightly more sea ice loss (Finocchio and Doyle, 2021, Finocchio et al., 2022). Additionally, in July and August, storms with stronger winds are associated with greater changes in ice area than storms with weaker winds (Finocchio et al., 2020). This result is explained, in part, by the presence of thinner ice (which becomes more prominent later in the summer season) that is more responsive to wind forcing (Kwok et al., 2013, Spreen et al., 2011).

However, only a few of these previous studies focused specifically on the sea ice within the MIZ. In doing so, these studies take a statistical approach of analyzing many cyclones

over large regions. As suggested by Clancy et al. (2022), this spatial averaging does not consider variations within a single cyclone or differences between individual storm events leading to generalized impacts that can vary depending on the methodology applied. The MIZ is critical for defining the total ice extent and is likely more vulnerable to storm forcings, providing a more targeted perspective than considering the entire ice area Finocchio et al. (2022), Schreiber and Serreze (2020). Since the solid ice pack is more rigid and less susceptible to winds, the net effect of cyclones on the MIZ provides a good proxy for their effect on global sea ice cover.

Given this focus in the literature on Arctic summer storms, the effects of southern hemisphere storms and the annual cycle of cyclone impacts are also still uncertain. Ice cover changes have been shown to be both accelerated and slowed by cyclones throughout the year, particularly in the Arctic. Different processes tend to dominate at different times of year, with refreezing after cyclone passage leading to increases in ice mass in the winter whereas warmer ocean conditions lead to increased melt after cyclone passage (Kriegsmann and Brümmer, 2014). Differences in cyclone intensity broadly causes larger impacts in the cold season (Aue and Rinke, 2023). Alternatively, Schreiber and Serreze (2020) suggest cyclones generally increase sea ice concentration across all months, or other studies suggest that there is little net impact across all months as positive and negative impacts tend to cancel out (Clancy et al., 2022, Spensberger et al., 2026).

Much less attention has been paid to the role of Antarctic cyclones throughout the year, with emphasis generally placed on autumn and winter storm impacts (Ward et al., 2023).

For example, several consecutive intense cyclones led to the record low ice cover in the Weddell Sea in April and May 2019, due to a combination of poleward winds and waves and upward mixing of ocean heat (Jena et al., 2022). An explosive cyclone occurring in July 2017 was found to redistribute ice within the Antarctic MIZ (Vichi et al., 2019). Yet, a systematic understanding of how southern hemisphere cyclones impact the ice edge is still lacking.

Ultimately, due to the complex nature of storm-sea ice interactions, the net effect of cyclones on the global MIZ is still uncertain, and, given the large changes occurring in the polar regions, particularly the Arctic, understanding how these impacts might evolve in the future under changing ice conditions have yet to be addressed. This dissertation aims to answer the following research questions:

1. Is the modern Arctic MIZ more susceptible to summer cyclones?
2. Have impacts of intense Arctic cyclones on summer sea ice reached a maximum?
3. How do storm impacts vary seasonally and in the southern hemisphere?

In answering these questions, Chapter 3 analyzes summer storm impacts in the Arctic over two decades using the observational record. Next, we use the Community Earth System Model Version 2 to explore future Arctic summer cyclone impacts in Chapter 4. Finally, Chapter 5 expands upon the results of Chapter 3 by including the full seasonal cycle and global impacts of cyclones on the MIZ. By addressing these research questions,

we aim to provide comprehensive insights into the impacts intense weather events have on the underlying sea ice within the MIZ

Chapter 2

Data and Methods

2.1 Data

2.1.1 Observational Datasets

The National Snow and Ice Data Center (NSIDC) reports daily average sea ice concentrations across the Arctic on a polar stereographic grid at 25 km resolution by combining passive microwave data from three different sensors (Scanning Multichannel Microwave Radiometer, Special Sensor Microwave Imager, Special Sensor Microwave Imager/Sounder) utilizing the NASA Bootstrap algorithm as part of their Climate Data Record product (Meier et al., 2017, Peng et al., 2013). Sea ice concentration data from 1982–1991 and

This chapter is adapted from the peer-reviewed publications:
Mundi, C., & L'Ecuyer, T. (2025). Is the modern Arctic marginal ice zone more susceptible to summer cyclones?. *Journal of Climate*, 38(1), 403-422.
Mundi, C. L., L'Ecuyer, T. S., & DuVivier, A. K. (2025). Have Impacts of Intense Arctic Cyclones on Summer Sea Ice Reached a Maximum?. *Geophysical Research Letters*, 52(19), e2025GL117848.

2010–2019 is used to establish pre-storm ice cover and track changes in ice area within the MIZ. This product does have missing data during July and August 1984, however, this affects a very small subset of cyclones that are considered in this analysis. We also relied on the Polar Pathfinder Daily 25 km EASE-Grid Sea Ice Motion Vectors (Tschudi et al., 2019) to quantify ice advection during the storms

We define the MIZ area for each cyclone event as the accumulated area of all locations with sea ice concentration between 15 and 80 percent (Strong and Rigor, 2013) from one day before the start of the storm to one day after the end of the storm. Having a constant area allows for all changes within the domain to be accounted for, whereas looking at the changes in 15-80% ice concentration cover from day-to-day causes the analysis area to vary and may mask important signals caused by cyclone interactions. With this definition, variations arise solely from changes in sea ice concentration and not from an expansion or reduction in analysis area. While this definition does include changes in the adjacent pack ice, these additional changes are important for describing the overall evolution of the MIZ and ice edge as a whole. We then track how the total sea ice area within this region evolves from one week before through two weeks after cyclone passage. We also calculate the total ice area within the region of storm influence to ensure the storm significantly interacts with the ice edge by only selecting storms with a pack ice area (concentrations greater than 80%) of at least 20% and no more than 80% of the domain on the first day of the cyclone.

This focus on changes in the MIZ is motivated by the fact that this region is likely

most sensitive to storm influences. Strong winds over largely open ocean regions can generate large shear fields leading to the breakdown of larger ice floes into smaller floes that are easier to advect via the same winds (Holt and Martin, 2001). Additionally, lower concentration ice experiences not only surface and basal melt but also lateral ice melt from the surrounding open ocean (Tsamados et al., 2015).

To characterize changes in the ocean environment where the ice resides, estimates of daily mean Arctic Ocean sea surface temperature (SST) from the NOAA Optimum Interpolation (OI) High Resolution Dataset are utilized (Huang et al., 2021). This product incorporates both in situ data (from ships, buoys, and Argo floats) and satellite (Advanced Very High Resolution Radiometer and Visible Infrared Imaging Radiometer Suite) observations and is provided on a 0.25-degree resolution global grid. Data from this product is available from September 1981 through present. To compute time series of SST over the analysis period, we use daily regions of ice between 15 and 80 percent concentration (Strong and Rigor, 2013). Therefore, most of the variation in SST comes from the day-to-day variations in the location of low-concentration sea ice. By doing so, we emphasize the role of SST within the regions where marginal ice is present.

In addition to trends in surface temperature, we also computed mean volume temperatures within the MIZ down to 35 m depth using the Global Ocean Reanalysis Product (GLORYS; Lellouche et al., 2021). GLORYS data has an eddy-resolving horizontal resolution of $1/12^{\circ}$ and 50 vertical levels within the ocean model NEMO (Nucleus for European Modeling of the Ocean; Madec et al., 2017). The model is driven by European Centre for

Medium-Range Weather Forecasts ERA-Interim data at the surface. We find that SST trends during the time of the cyclone are similar to trends of mean upper-ocean temperature. Additionally, since GLORYS is only available starting in 1993, observations of upper ocean characteristics are not readily available for the earlier decade analyzed. We therefore use SST observations to represent the upper ocean characteristics.

Regardless of whether the observed changes in SST are seen as driving changes in sea ice concentration or as a result of the melt and growth of nearby ice, the ocean environment is still a key factor in the evolution of sea ice within the MIZ. SST can be influenced by a number of factors such as mixing, heat transport, or ice cover prior to the cyclone (Wang et al., 2019) and is an important factor for the lateral and basal melt of ice (Stroeve et al., 2014). These melting processes especially have the greatest influence within the MIZ and during late-summer months as the lesser ice cover enhances solar absorption and warming of the upper ocean (Steele et al., 2010).

2.1.2 Atmospheric reanalysis

To identify and establish characteristics of the cyclones analyzed, European Centre for Medium-Range Weather Forecasts ERA5 reanalysis was used (C3S, 2023, Hersbach et al., 2020). ERA5 improves upon the ERA-Interim reanalysis, with enhancements in horizontal and temporal resolutions, as well as in the 4-D variable data assimilation process used. ERA5 data is available from 1940 to present day on a $0.25° \times 0.25°$ grid. In this study, we use hourly mean sea level pressure, as well as 10-meter wind and 2-m air temperature products. Overall, compared with independent observations over the eastern Fram Strait,

ERA5 was found to provide the most accurate wind and atmospheric profiles compared to other reanalyses (Graham et al., 2019a).

Hourly mean sea level pressure (SLP) is used to identify the location and duration of Arctic cyclones across two decades. The SLP field is then tracked over the lifetime of the storms to determine the total impact area of the cyclones. We also incorporate 2-meter air temperature trends over the lifetime of each cyclone case to begin to understand some of the atmospheric effects of a passing storm on the sea ice. To investigate the effects of storm-enhanced winds on the underlying ice, hourly 10-meter winds were utilized to calculate wind speeds associated with the cyclone as well as investigate the impacts of meridional and zonal winds. The mean values and mean direction (when considering directional signs) within the MIZ in the storm region for each day are considered. The dominant winds within the storm regions are based on the sign of the mean winds.

In incorporating an analysis of the near-surface winds, we link prevailing wind directions to local changes in sea ice concentration. It should be noted that Ekman motion theory states surface ocean currents move at an angle to the right of prevailing near-surface winds. When considering sea ice advection, however, a wide range of factors affect the precise direction of the ice. It has been shown that ice generally moves in line with the geostrophic winds (Kwok et al., 2013, Tschudi et al., 2020), where the geostrophic winds explain more than 70% of the variance in daily ice velocities (Thorndike and Colony, 1982). Overall, the exact conditions for strengthened Ekman veering depend on the properties of the ice and are difficult to ascertain throughout the entire Arctic. In this study, we focus mainly

on the meridional component of the winds to describe possible ice motion from higher to lower latitudes (or vice versa). By considering one direction of motion alone, the effect of Ekman drift (and the resulting angle of ice motion) on the results is minimized since the same meridional direction is generally maintained. Discussion of ERA5 10 m winds, 2 m air temperature, and significant wave height products within the cyclone environment are also included.

2.1.3 Large Ensemble

To assess future cyclone impacts in the Arctic, we use output from the Community Earth System Model Version 2 (CESM2), which is a free running, fully coupled climate model with approximately 1° horizontal resolution (Danabasoglu et al., 2020). CESM2 utilizes the Los Alamos Sea Ice Model version 5.1.2 (CICE5; Hunke et al., 2017) to represent sea ice, the Parallel Ocean Program version 2 (POP2) for the ocean component of the model, and the Community Atmosphere Model version 6 (CAM6) to represent the atmosphere. Sea ice concentration and sea surface temperature (SST) values are output daily, and mean sea level pressure values are available 6-hourly. From 1850 to 2014, CESM2 is forced by CMIP6 historical forcing and, from 2015 onward, by the Shared Socioeconomic Pathways (SSP) forcing scenario SSP3-7.0 (Rodgers et al., 2021). The large ensemble consists of 100 members, where 50 members use standard CMIP6 historical forcing and 50 use smoothed biomass burning emissions in the historical period, which are known to impact Arctic sea ice trends (DeRepentigny et al., 2022). For this study, we used 40 of the 50 members with consistent smoothed forcing. We present results from the early satellite

era, 1982 through 1991, and the modern-day Arctic, 2010 through 2019, to establish model performance relative to observations and then extend the analysis through 2100 to understand predicted future sea ice changes.

The CESM2 was selected for use in this study based on its wide usage for studying the Arctic. Given its relatively high spatial resolution, we find that intense low pressure systems were able to be represented within CESM2, especially at lower latitudes. An analysis of 14 CMIP6 climate models found similar biases in summer storm tracks, with too few storms occurring over the Arctic Ocean (Song et al., 2021). Generally, both high- and low- resolution models simulated fewer cyclones within the Arctic, with higher-resolution models tending to reproduce the storm tracks from reanalysis better than a lower resolution model (Song et al., 2021). Additionally, Simpson et al. (2020) described notable improvements in the representation of NH summer storm tracks in CESM2 compared to CESM1, ranking within the top 10% of CMIP models. Improvements have also been made in the representation of Arctic sea ice in CESM2, compared with the previous version. CICE model version 5.1.2 (Hunke et al., 2017) uses the new mushy-layer thermodynamics compared with the earlier version producing thicker and more extensive sea ice (which is particularly important within the marginal ice zone; Bailey et al., 2020). Even with this improvement, the CESM2 September sea ice extent is consistently smaller in area compared with the CESM1 Large Ensemble and most CMIP6 models leading to a faster decline in summer ice area in future decades (DeRepentigny et al., 2020). These caveats are important to keep in mind when assessing the results of this study.

2.2 Methods

2.2.1 Arctic cyclone identification

To gain insight into the sea ice response to a variety of different events, a census of cyclone cases was identified for the months of June through August for both a recent decade (2010–2019) and an earlier decade (1982–1991). Like many previous studies, minimum SLP was selected as the primary variable for cyclone detection (Neu et al., 2013). To restrict the focus to stronger storms, we first identified low-pressure systems by determining local minima in sea level pressure, where the minimum value reaches below 984 hPa (similar to the 985 hPa threshold used by Rinke et al. (2017) and Lukovich et al. (2021) to define “extreme" Arctic cyclones). While this threshold is an arbitrary choice, the addition of higher-pressure storms into the analysis did not widely change the main results of this work, with the exception of making mean trends slightly less well-defined. We also find that background mean sea level pressures across the summer months do not widely vary in the Arctic, so using the same minimum pressure cutoff for each month demonstrates the same deviation from mean conditions.

To account for the development of the cyclone, low-pressure grid boxes with SLP less than 990 hPa in each hourly SLP map were clustered into a single event. Grid cells located more than 15 degrees east or west of the next closest SLP minimum cell were considered separate storm systems. This approach aligns with previous studies (Serreze et al., 1997, Zhang et al., 2004) that require separation of 1200 km (lowered from the original choice

of 1400 km, based on Serreze (1995)) to identify individual cyclones. The value used here is slightly more strict since the pressure centers do not represent the full radius of the cyclone, only the width of the low-pressure center (i.e., the 990 hPa contour). A 50-degree longitude threshold was also applied to the locations of absolute minimum pressure of the identified clusters to further separate storms developing in different regions. This choice also groups low-pressure events that occur in series, affecting the same region of ice. Additionally, low-pressure locations that occur in the same location but are more than 6 hours apart are regarded as different cyclone events.

To remove any short-lived cyclone events, each storm was required to last a minimum of 2 days. As discussed in Wernli and Schwierz (2006), many of these selected parameters are somewhat arbitrary, especially when considering the selected minimum storm duration. The choice of 2 days represents a compromise between other studies that adopted thresholds of 12 hours, 1 day, or 3 days (e.g., Crawford and Serreze, 2016, Hoskins and Hodges, 2002, Sickmöller et al., 2000, Zhang et al., 2004). Additionally, this choice focuses on storms that develop over the ice edge and have a more prolonged interaction with the ice edge, without largely minimizing the sample of cyclones analyzed.

Unlike other algorithms (Neu et al., 2013), we did not mask for high elevation or account for the bias imposed by non-equal area grids. Since only storms that interact with the ice edge—thus occurring within a small latitude band—are considered in this census, variations in horizontal spatial resolution due to using a longitude-based grid (not equal area) do not largely bias the cyclones identified. Additionally, since most of the cyclones

that interact with the ice edge develop over the ocean, these storms only partially interact with the coastline, again minimizing any impact from higher-elevation regions. Lastly, storms that only partially interact with the ice edge or that pass over mostly high-concentration ice were removed to ensure that changes in the marginal ice zone are well-represented. Thus, only cyclones with a defined storm area (see Figure 2.1) that contains 20–80% of non-MIZ ice are considered.

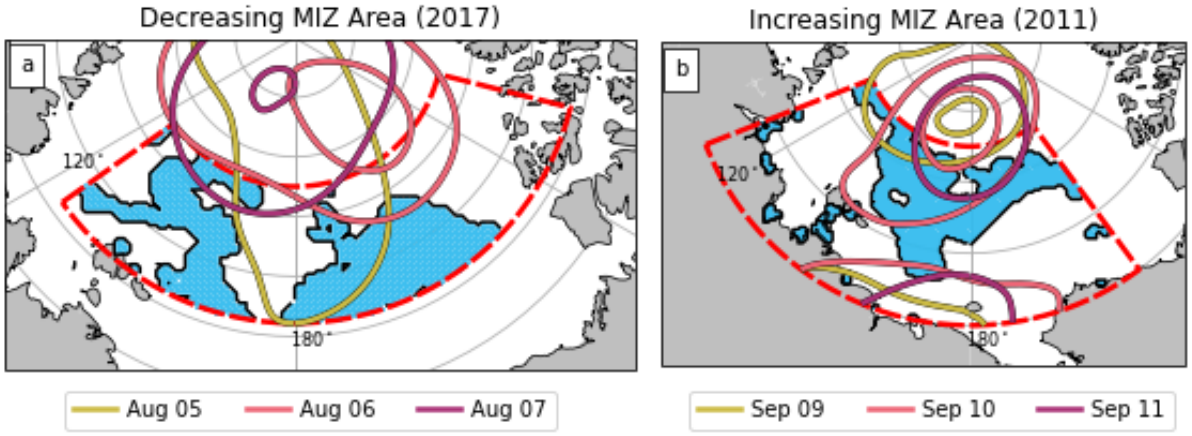

Figure 2.1: Study area (red dashed) of two cyclone events based on the 1000 hPa pressure contours over the three days of each storm. The 990 hPa contour is also shown for each day. The accumulated MIZ area within this study area is outlined in black and shaded in blue. Note in (b) that a second storm was identified just south of the main storm. Since the detection algorithm groups cyclones by spatial proximity, these two systems are classified as the same storm event and their impact on the MIZ will be considered jointly.

To describe the region of impact of the storm, the daily-averaged 1000 hPa contours of the event were mapped out over the storm duration (defined as the days the storm's minimum pressure was below 990 hPa to account for the development of the storm around its minimum pressure). A bounding box was then created based on the minimum and maximum latitudes and longitudes of these contours (Fig. 2.1). To avoid this box becoming increasingly wide as the storm approaches the north pole, a maximum northern latitude

was defined as 85°N. While this cutoff was applied for both decades of the analysis, the poleward retreat of the MIZ may cause the area within the storm domain to be slightly limited during the more recent decade. However, for consistency, the same limits were applied. Within this box, the area of ice within the MIZ was calculated, and wind and SST values within the MIZ area were isolated for analysis. Other storm areas such as using the daily 990 hPa contours to define the edges of the bounding box, analyzing the variables in the area within the 1000 hPa contours themselves (without forming a bounding box), and using a 500-km radius from the center of the storm were also considered. The net impact of the cyclone on the underlying sea ice is not largely influenced by the selection of how the impact area of the storm is defined. This result is also mathematically supported by the fact that the decadal mean trend is removed from the MIZ area time series, so the areal changes present within the storm boundary are due to the current dynamics plus small deviations from the mean.

2.2.2 Sea ice area trend metrics

To quantify the impact of each cyclone on the MIZ within the storm area, the evolution of ice area within the MIZ from a week prior to the storm through two weeks after was examined. Since the cyclones occur during the period when sea ice is naturally declining, climatological trends due to the seasonal ice melt within the storm area must be removed to isolate the influence of storms. A background climatology of sea ice change is defined as the trend of sea ice area within the MIZ within any analyzed storm region averaged over 2010–2019 for the more recent decade and averaged over 1982–1991 for the earlier

storms. The total ice area within the accumulated MIZ was computed for each year of the climatology and averaged for each day of the three-week time series. Then to remove this mean seasonal decline of the ice area, the climatology was subtracted from the time series of MIZ ice area during the storm.

To account for differences in storm area, the sea ice area time series were normalized before compositing. First, the change in detrended ice area was made relative to one week before the storm by subtracting the initial value of the time series, and then the three-week time series was normalized by the range (minimum value subtracted from the maximum value) of the series. By rescaling the data, composite cyclone influences can be assessed without preferentially weighting spatially larger storms. In doing so, we examine the ice response (increasing or decreasing) to any given cyclone rather than quantifying the net effects dominated by a few large cyclones. This methodology is useful for understanding the processes behind cyclone-ice interactions, as opposed to emphasizing total changes happening to the sea ice, which are controlled by the scale of the storms.

Chapter 3

Is the Modern Arctic Marginal Ice Zone More Susceptible to Summer Cyclones?

3.1 Preface

While it is possible to demonstrate many of the atmospheric and oceanic processes by which Arctic cyclones interact with sea ice using models of varying scales and complexity, establishing the net effect of storms on the ice edge requires a comprehensive analysis of available satellite observations and reanalyses that capture the ensemble of the multiple effects Arctic cyclones exert on sea ice within the MIZ. As a step toward a more complete understanding of the role Arctic cyclones play in shaping the early-summer (June and

This chapter is adapted from the peer-reviewed publication:
Mundi, C., & L'Ecuyer, T. (2025). Is the modern Arctic marginal ice zone more susceptible to summer cyclones?. *Journal of Climate*, 38(1), 403-422.

July) and late-summer (August and September) ice edge, this study examines the impacts of cyclone-induced near-surface winds and the local sea surface temperature field within the MIZ. At these times of the year, Arctic sea ice is melting, approaching its minimum extent, and likely increasingly susceptible to passing storms. September storms are included in this analysis for their importance in influencing not only in the seasonal melting of Arctic sea ice, but also the regrowth of ice occurring near the end of the month.

To account for the longer-term effects of changes in the ocean environment after cyclone passage, we track ice area within the MIZ from one week before each storm to two weeks after its passage, extending the analysis period further than previous studies (e.g., Aue et al., 2022, Finocchio and Doyle, 2021), to allow for multiple time scales to be investigated (as suggested by Schreiber and Serreze, 2020). The effects of clouds in modulating surface radiative fluxes implicitly factor into the analysis but are not explicitly investigated since storm-to-storm changes in cloud cover are more difficult to capture in reanalyses than storm location, intensity, and winds. Surface characteristics (i.e., ice concentration and ocean temperatures) are established using satellite observations.

Two individual case studies are first examined in detail revealing two distinct mechanisms by which cyclones impact observed sea ice concentrations within the local marginal ice zone. Characteristics of these events are used to establish a framework for analyzing a full census of 264 intense storms to quantify the net effect of Arctic cyclones on the MIZ and attempt to distinguish between storms that enhance and impede sea ice loss. A recent decade (2010–2019) is contrasted with an earlier one (1982–1991) to investigate

how cyclone impacts may have evolved with the increase in seasonal ice cover (Haine and Martin, 2017, Landrum and Holland, 2020).

3.2 Census of Summer Arctic Cyclones

A total of 133 ice-influencing strong storms were identified between 1982 and 1991 and 131 storms were identified in the more recent decade, from 2010 to 2019. Figure 3.1 shows the distributions of each cyclone's central minimum pressure for each decade separated by month of the year. There are generally more storms in late-summer months than in early summer, and late-summer storms are slightly more intense (consistent with Zhang et al., 2004). Mean central pressures are around 980 hPa in June and July and around 977 hPa in August and September. For storms occurring in June and July, the frequency of intense cyclones may have also slightly increased in the more recent decade, with statistically significant differences observed in the two distributions. There is no statistically significant difference in intensity between late-summer storms between the two decades. Figure 3.1 also shows the locations of each storm, with a slight poleward shift of storms during the more recent decade. While this result is consistent with recent findings from Zhang et al. (2023), it should also be noted that the storms shown in Figure 3.1 only consider cyclones impacting the ice edge. Since the ice edge is retreating poleward, an associated shift in cyclone locations is expected in this study.

This cyclone identification algorithm identifies a wide range of intense storm events over the entire Arctic. Figure 3.2 shows the fractional impact on MIZ ice area of all storms

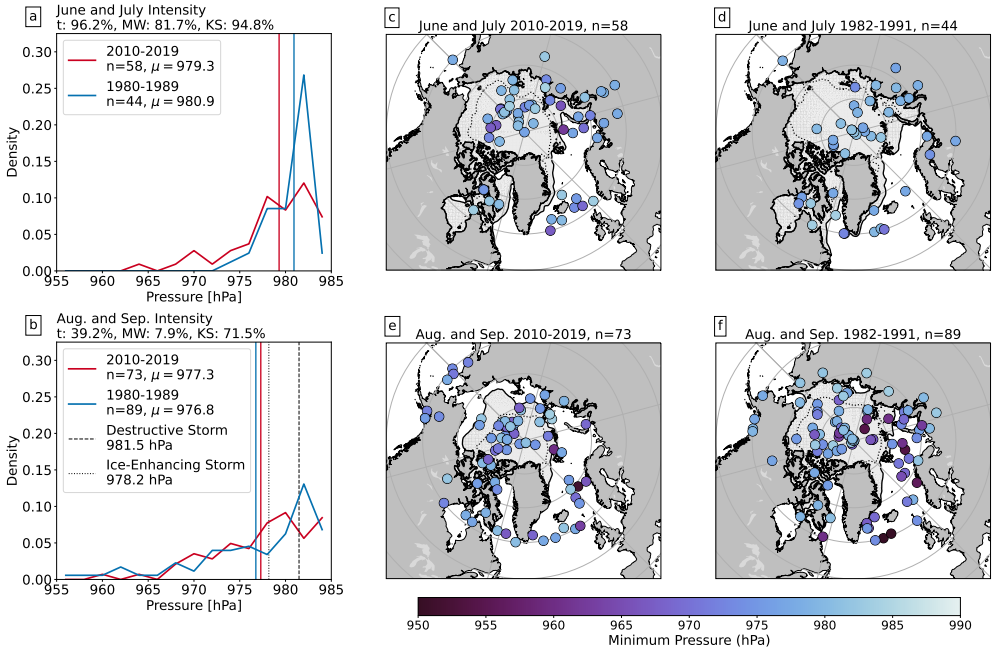

Figure 3.1: Distributions of minimum sea level pressure for (a) June and July and (b) August and September cyclones. Confidence levels at which the distributions of the two decades differ for Student's t-test (t), non-parametric Mann-Whitney U test (MW), and Kolmogorov-Smirnov test (KS) are listed (as in Finocchio et al. (2022)). Minimum pressures of the two case studies are also shown. Spatial distribution of storms for (c) early summer 2010–2019, (d) early summer 1982–1991, (e) late summer 2010–2019, and (f) late summer 1982–1991. Shading represents the minimum pressure reached by the cyclone throughout its development. The mean 15% (solid) and 80% (dotted) sea ice concentration contours are also shown.

identified in this study sorted by season and decade. Storms have widely varying impacts on the sea ice. Early-summer storms tend to reduce the area of ice present within the MIZ more than late-summer storms across both decades. Nearly 80% of June and July storms decrease sea ice area relative to climatology in the current period while only 68% reduce ice area in the earlier decade. Additionally, the net changes in area are greater for early-summer storms in the 2010s that decrease ice area, with those storms reducing area by about 16% more than storms in the earlier period that also decrease ice. Perhaps

surprisingly, on average, late-summer cyclones tend to have no net effect in the later decade, with about half (48%) of the storms resulting in an increase in ice and about half (52%) decreasing the MIZ ice area (Fig. 3.2c). In the earlier decade, storms cause a statistically significant increase in MIZ ice area, with over 57% of storms resulting in an increased area. However, this effect is much smaller than the large spread in effects that individual cyclones impart.

Overall, nearly two-thirds of storms in the more recent decade result in less sea ice within the MIZ two weeks after a cyclone, whereas in the earlier decade, only about half of all storms have this effect. This result is due in part to the notable shift in the distribution of when storms occur. While about 130 storms were identified in each decade, the seasonality of the storms is quite different between the two periods. In the earlier decade, only a third of storms occurred in early-summer months when storms tend to decrease the ice area within the MIZ. Nearly half of the storms in the more recent decade occurred in June or July. As ice retreats earlier in recent years (Sledd et al., 2023), there is more open water in June and July, generating greater moisture fluxes and a less rough surface for storm development, allowing stronger storms to develop (Valkonen et al., 2021). This result then causes a greater number of June and July storms to meet our criteria of an intense storm and leads to a larger fraction of storms that reduce ice area overall.

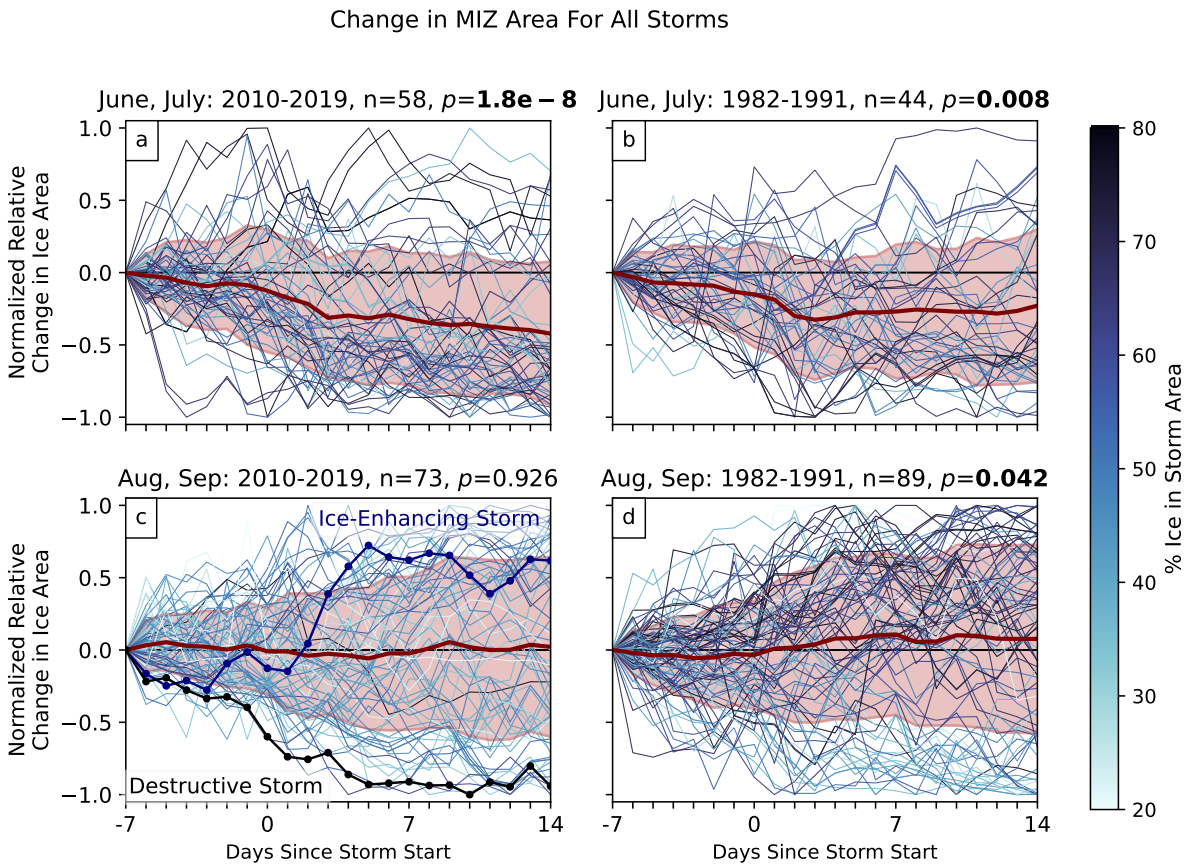

Figure 3.2: Normalized changes in MIZ ice area relative to the start of the analysis time window for early- and late-summer months in (a) and (c) 2010–2019 and (b) and (d) 1982–1991. Line coloring indicates the percentage of ice that is present within the storm area on the first day of the cyclone. The mean and standard deviation of all curves are plotted in red. The mean trend in (a), (b), and (d) are significantly different from zero based on a Student's t-test at the 95% level. Panel (c) also shows the time series for the ice-increasing and ice-decreasing cyclones selected as case studies in the thick blue and black lines, respectively.

3.3 Results

To better understand the wide range of sea ice responses shown in Figure 3.2, we analyze two storms with opposing effects on sea ice. The first case shows an instance where the cyclone increases ice area within the MIZ and the second case decreases ice area. Examining the conditions that led to these two opposite sea ice outcomes reveals two

mechanisms by which cyclones can modulate sea ice cover in the MIZ. Following these results, we determine the extent to which MIZ responses to all cyclones can be explained by similar basic mechanisms.

3.3.1 Decreasing MIZ Area: August 5, 2017

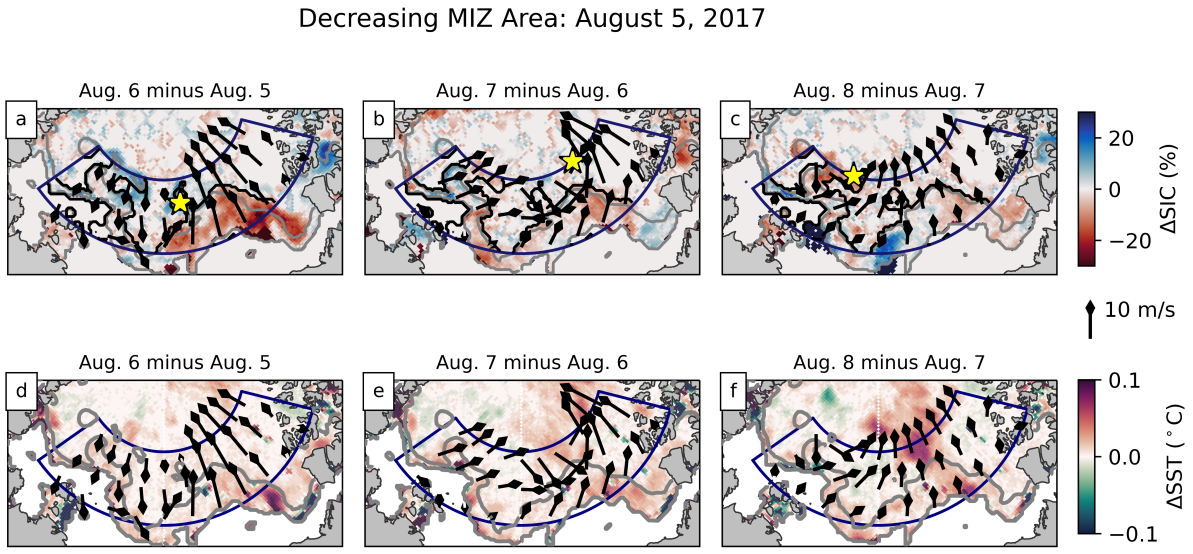

Figure 3.3: (a-c) Change in sea ice concentration over the three days of a storm that reduces ice area within the MIZ region. The accumulated MIZ area is outlined in black. The location of the storm's minimum pressure from each earlier day is identified by a yellow star. (d-f) Change in sea surface temperature over the three days of the storm. The 15% and 80% contours of the earlier day (outlined in gray) and daily averaged 10-meter wind vectors from the earlier day are displayed in all plots.

Beginning August 5, 2017, a low-pressure minimum was identified over the ice pack spanning across the East Siberian and Chukchi seas. At its greatest strength, the cyclone's minimum pressure was 981.5 hPa, and maximum near-surface winds were over 19 m s^{-1}, based on ERA5. The cyclone began to dissipate after a lifetime of three days. In total, within the storm area defined by the bounding box, there was 1,477,900 km^2 of ice on the first day of the storm (August 5), with 434,194 km^2 (about 29%) within the MIZ.

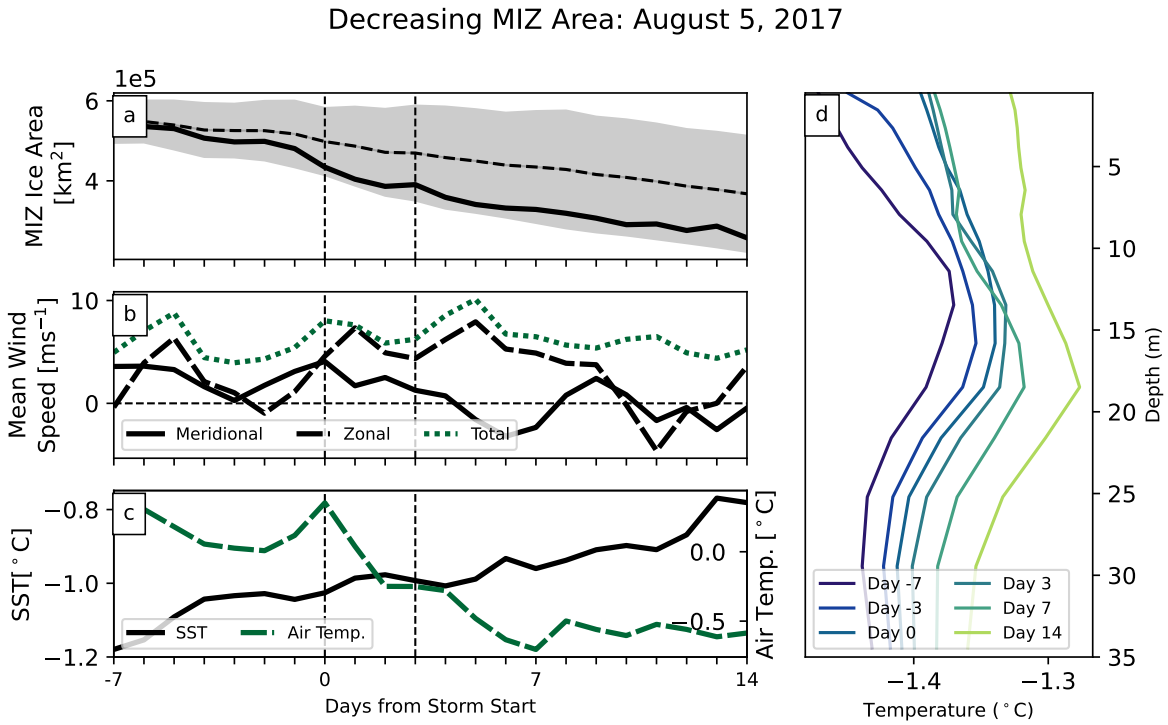

Figure 3.4: Time series of (a) sea ice area, (b) wind values, and (c) SST (black) and air temperature (green dashed) values within the MIZ from one week before the start of the storm to two weeks after. Note in (a) that the area time series is not detrended as in Figure 3.2. Dashed lines indicate climatological averages from 2010–2019, with one standard deviation shown in gray shading. Mean upper-ocean temperature profiles averaged over the MIZ area for key dates surrounding the cyclone's development are shown in (d).

Figure 3.3 highlights two potential avenues for enhanced ice loss due to this event. During the storm, enhanced winds on the eastern flank of the storm may move ice northward or compress the ice pack (Clancy et al., 2022). This corresponds to the large decreases in sea ice concentration shown on the first two days of the cyclone. On the western side of the storm, winds also advect sea ice into warmer waters (Fig 3.3d-f). On the first day of the cyclone northerly winds are present above regions of ice concentration gain. During the last two days, those regions exhibit mostly ice loss. This suggests warmer water may enhance ice loss through accelerated melting long after the storm passes.

The time series of ice area within this region from a week before the storm start to two weeks afterward is presented in Fig. 3.4a, confirming the accelerated decline in area observed. During the storm, there is a net decrease in ice within the MIZ of 43,706 km^2. This loss of ice is 14,951 km^2 more than the climatological average 28,755 km^2 loss expected during this time of year, based on the observed average decrease in ice area within this region from 2010–2019. We also see the time series depart from the climatological mean near the start date of the cyclone. Furthermore, there are net mean decreases in the areas with southerly winds over the course of the cyclone and net increases in regions with northerly winds.

Leading up to the storm and throughout its lifetime, there were mostly southerly winds associated with the northward advection of ice and the decrease in ice area. In an effort to quantify the role of winds and SST in the observed change in ice area, the wind and SST values within the MIZ were averaged for each day (Fig. 3.4b,c). Winds are strongest earlier in the storm's life cycle. In the days after storm passage, the mean wind direction in this area transitions to northerly. Then, later in the analysis period, the mean meridional wind speed weakens and oscillates between primarily northerly and southerly. Throughout the duration of the storm, winds are persistently westerly.

During the days following the start of the storm, the overall sea surface temperature in the MIZ increases and continues to increase for the two weeks after the storm. The temperature profile of this storm (Fig. 3.4d) demonstrates that this warming is consistent throughout the upper layer of the ocean, with temperatures near the surface warming

faster than those at depth. Temperatures near the surface during the storm become similar to temperatures at about 10-15 m depth, suggesting that the change in SST around the cyclone may partly be due to upwelling and vertical mixing of the water column. In contrast to the warming of ocean temperatures within the MIZ, the mean air temperature in the area is steadily decreasing over the lifetime of the storm.

Summing these effects, there is an overall large decline in the MIZ ice area during this storm. This net result is due to a variety of factors, including the advection of ice into regions of higher SST on the western side of the storm area (that may be a result of localized upwelling of warmer water near the surface) and compression of ice from southerly winds on the eastern side of the cyclone, as well as a retreat of sea ice out of the analysis region. This single cyclone illustrates two pathways by which other cyclones with similar wind patterns may reduce ice cover, either through compression or through a change in the ocean environment surrounding the ice within the MIZ. However, Figure 3.2 shows that many storms have the opposite effect, causing ice areas within the MIZ to increase, potentially due to differing wind or ocean conditions.

3.3.2 Increasing MIZ Area: September 9, 2011

To provide an example of a cyclone that induces the opposite ice response within the MIZ, a second storm located in a similar region as the first cyclone is analyzed. This storm developed in the center of the Chukchi Sea starting on September 9, 2011, reaching a minimum pressure of 978 hPa, about 3 hPa less than the previous storm. Its maximum winds reached over 18 m s^{-1}, slightly less than the previous case.

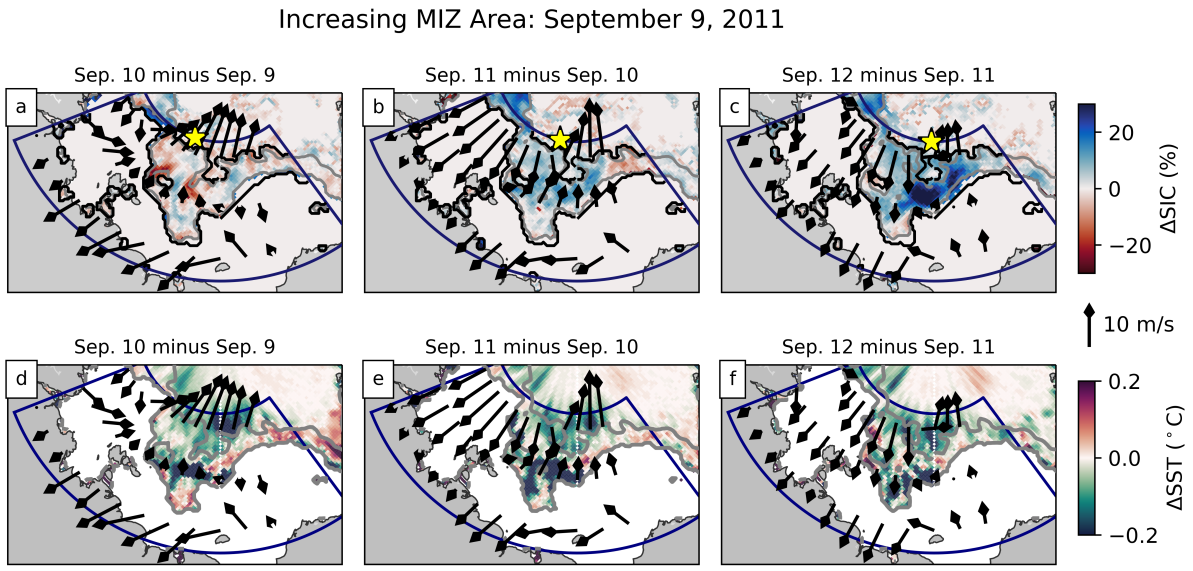

Figure 3.5: (a-c) Change in sea ice concentration over the three days of a storm that increases ice area within the MIZ region. The accumulated MIZ area is outlined in black. The location of the storm's minimum pressure from each earlier day is identified by a yellow star. (d-f) Change in sea surface temperature over the three days of the storm. The 15% and 80% contours of the earlier day (outlined in gray) and daily averaged 10-meter wind vectors from the earlier day are displayed in all plots.

The impact area of this storm is shown in Figure 3.5. This storm interacted with about a third of the area of ice as the previous event (498,744 km^2 on the first day of the cyclone) but, 351,962 km^2 of ice (or about 70.6% of the total ice area) lies within the MIZ, a much greater fraction than the previous case. Figure 3.5a-c shows the evolution of the winds from September 9 to September 11 overlaid on changes in sea ice concentration. Like the first case, the western side of the storm experiences strong northerly winds and the eastern side has enhanced southerlies. However, on the first day of the storm, the wind structure is less cyclonic in nature as the storm begins to develop, with small regions of increases and decreases in sea ice concentration throughout the MIZ area. As the storm continues to develop, we see that the northerly winds dominate most of the storm area and much of

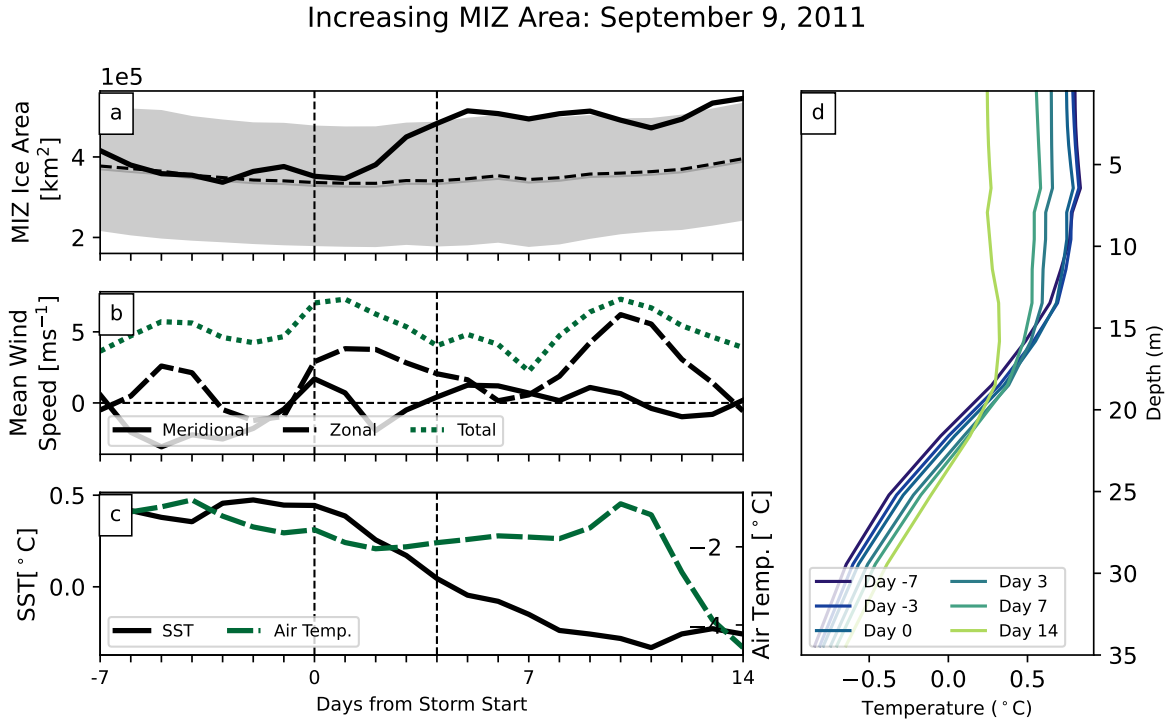

Figure 3.6: Time series of (a) sea ice area, (b) wind values, and (c) SST (black) and air temperature (green dashed) values within the MIZ from one week before the start of the storm to two weeks after. Note in (a) that the area time series is not detrended as in Figure 3.2. Dashed lines indicate climatological averages from 2010–2019, with one standard deviation shown in gray shading. Mean upper-ocean temperature profiles averaged over the MIZ area for key dates surrounding the cyclone's development are shown in (d).

the MIZ experiences an increase in ice concentration. In particular, the largest increases in concentration appear to be in regions where the southerly flow converges with the northerly winds, compressing ice into regions of lower SST. This convergence of winds suggests a surface cold front that aligns over the MIZ, a characteristic of this storm that is not present in the previous case.

The time series of ice area within this region from a week prior to the storm start to two weeks afterward is presented in Figure 3.6a. There is not an obvious decline in ice, as

there was in the first case. In fact, during the 3-day storm period, there was a net gain of 131,200 km^2 of ice within the MIZ, while based on the mean climatology, a much smaller ice gain was expected (about 3,958 km^2). Like the previous event, this deviation in ice area from the climatological mean coincides well with the start of the storm. Though, through both the time series and Figure 3.5a-c, the largest gains in area occur in the later days of the storm, with much of the MIZ experiencing an increase in sea ice concentration between the 11th and 12th. MIZ ice area the day following the end of the storm already exceeds one standard deviation away from the mean climatology, and remains around this value for the following two weeks. This result differs from the previous storm, where the ice area continued to decline in the weeks after the storm. Initially, southerly winds corresponded to a decrease in MIZ ice area, followed by an increase in area during the second half of the storm. Northerly winds corresponded to a net increase in ice.

Similar to the previous case, the zonal winds are persistently westerly throughout the storm and the total wind speed is larger at the start of the storm and weakens throughout the cyclone's lifetime. However, in this case, the mean meridional wind direction is northerly over the lifetime of the storm (Fig. 3.6b). In contrast to the decrease in upper-ocean temperature, the mean air temperature within the MIZ remained fairly constant around 2°C (Fig. 3.6c).

SST values within the region of the storm are shown in Figure 3.5d-f, along with the MIZ area for each day. SSTs steadily decrease over the 3-day period of the storm, as confirmed by both Figure 3.6c, showing the time series of daily SST values within the MIZ,

and Figure 3.6d, the evolution of the upper-ocean temperature profile within the MIZ. Interestingly, while the upper 20 m of the ocean profile shows decreasing temperatures, the layer beneath that is warming over the duration of the storm, suggesting that the cyclone-induced changes to the surface characteristics largely influence the ocean environment of the sea ice within the MIZ for this event. Additionally, like the previous case, surface temperatures during the storm match those at about 15 m depth in the week before the storm, again suggesting that there may be some vertical mixing occurring due to oceanic upwelling. However, unlike the first case, there is no near-surface ocean temperature maximum just below the surface that could promote enhanced ice melt.

Whereas winds in the first case resulted in a decrease in area, likely due to a combination of ice compression from southerly winds on the east, retreat out of the analysis region, and advection of ice on the west into regions of higher SSTs (possibly as a result of mixing near the surface), an increase in ice area is evident in this case which is associated with a decrease in SST. The dominant southerly winds in this case cause the MIZ to widen into the region of cooler SSTs and lead to an increase in area. While far from exhaustive, these two very different responses illustrate the distinct ice behaviors in the MIZ possible due to intense summer cyclones, offering some insight into the origins of the range of results present in current literature.

3.3.3 Composite Analysis

Motivated by these examples, we attempt to introduce some structure to the results shown in Figure 3.2 and better understand the dominant impacts that storm-induced

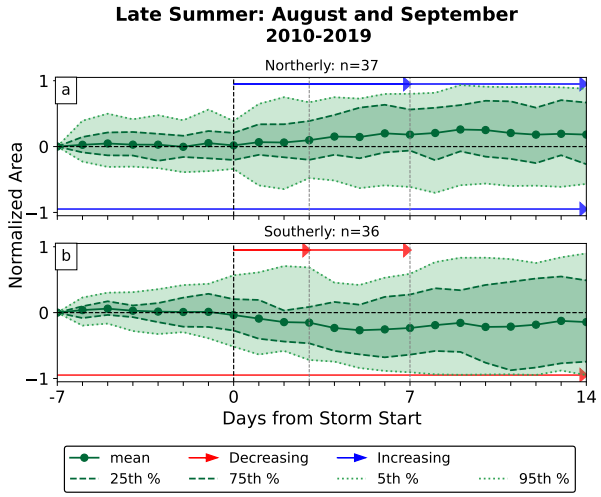

Figure 3.7: Composite plots showing the normalized change in MIZ ice area for the three weeks around cyclones occurring in late summer 2010–2019, separated into categories based on the primary wind direction within the storm area. The mean values and the 5th, 25th, 75th, and 95th percentiles are plotted. The arrows represent the portion of the plot where the distribution of slopes of the mean normalized area time series has a statistically significant ($p < 0.05$) difference from zero. The slopes are computed over different sections of the time series: the week leading up to the storm (days -7 to 0; top of plots), after the storm (days 0 to 3, 0 to 7, 0 to 14; top of plots), or over the full three-week time series (days -7 to 14; bottom of plots). A version of this plot without normalization is available in Figure A.1.

near-surface winds and nearby SSTs have on sea ice within the MIZ by sorting the 131 cases from the recent decade and the 133 cases from the earlier decade based on dominant wind direction and SST trends in the MIZ. First, cyclone events were separated into two categories based on the cyclone's mean wind direction over the duration of the cyclone (northerly or southerly). Then, based on the post-storm ice behavior in the two case studies, SST trends (warming or cooling) were incorporated to represent possible influences on melt following storm passage. Daily SST changes within the MIZ were calculated over the storm duration and were sorted based on the mean change in SST over that period. To avoid obscuring the main effects of these two factors by incorporating series with small

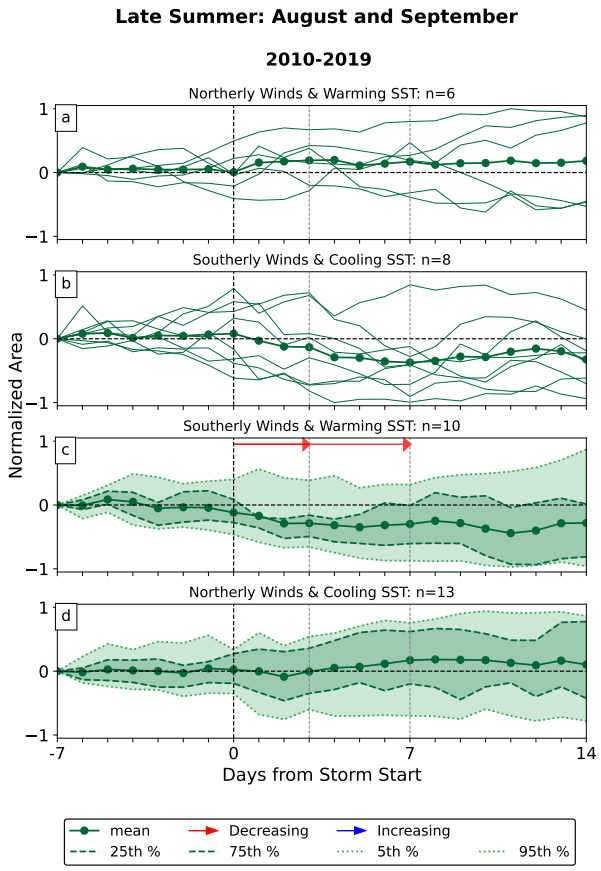

Figure 3.8: As in Figure 3.7, but separated into categories based on the primary wind direction and SST trend during the time of the cyclone. A version of this plot without normalization is available in Figure A.1.

signals during the cyclone event, SST changes were required to exceed a magnitude of 0.01 °C per day and mean meridional winds (including directional signs) had to exceed a magnitude of 0.1 m s^{-1} for a cyclone to be categorized. The main conclusions drawn from this composite analysis are not sensitive to these choices, which simply represent small deviations from zero. Applying these thresholds results in fewer storms being categorized when considering both wind values and SST trends than when considering the effect of winds alone, so sample sizes are reported in the titles of all figures for reference.

All storms identified during the late summer months of the most recent decade are shown in Figure 3.7, separated based on dominant wind direction. As in Figure 3.2, different cyclone events during this period have a wide range of impacts on MIZ sea ice, even when sorted by wind direction. However, the ensemble of storms with mostly northerly winds results in statistically significant increases in normalized MIZ ice area over the three-week period while the ensemble with predominantly southerly winds results in statistically significant decreases in area in the weeks following the storm.

Further sorting storms by SST trends in addition to dominant wind direction does not substantially alter this finding (Fig. 3.8). The two categories with dominant northerlies still show small increases in MIZ ice area in the two weeks following the storm (although now without statistical significance) and the two categories with dominant southerly winds still show short-term decreases in MIZ ice area in the days following the cyclone. The spread in sea ice responses appears to be slightly reduced when SST trends are also accounted for.

A similar decomposition method is applied to storms observed in June and July, and the results are presented in Figure 3.9. In recent years, mean sea ice changes due to early-summer storms generally show that storms tend to enhance MIZ ice loss as suggested by Figure 3.2, regardless of categorization. While there is still considerable variability when separating by winds alone, storms with dominant southerly winds have a greater capacity for reducing MIZ ice area than those with northerly winds. Generally, regardless of accompanying SST trends, storms with northerly winds tend to have smaller mean

effects on ice areas within the MIZ. On the other hand, while storms with prevailing southerly wind show considerable decreases around the start of the storm, those that also increase SSTs have longer-lasting impacts, with a significant decreasing trend over the entire 3-week period analyzed.

The pre-storm decreases in Figure 3.9c may be due to how these storms approach the ice edge as they develop. This change could also be attributed to the interannual timing of the cyclones. If the storms in a particular category are from years that deviate similarly from the climatological mean decline, a significant mean pre-storm trend may emerge when the expected behavior is subtracted out.

3.3.4 Comparison with earlier Arctic epoch (1982–1991)

Considering the different impacts between early-summer storms and late-summer storms, the amount of sea ice interacting with the storm clearly plays an important role in a cyclone's impact, as suggested by Finocchio and Doyle (2021). In the Arctic, a significant shift in sea ice cover has been observed over the past few decades. The mean state of Arctic sea ice has dramatically shifted toward seasonal ice cover from more persistent inter-annual ice cover in recent years (Haine and Martin, 2017, Landrum and Holland, 2020). Thick, multiyear ice area, for example, has been observed to be declining at a rate of over 17% per decade since 1979 (Comiso, 2012). These changing ice conditions have the potential to impact the net ice response to the passage of a cyclone.

To assess whether cyclone influences on sea ice are changing, a similar analysis was applied

to the earlier decade of storms (1982–1991) shown in Figures 3.1d and 3.1f. For context, Figure 3.10a shows the monthly mean ice extent for each month included in the analysis for both decades. The recent decade shows a considerably smaller ice extent across all months. Notably, the late-summer months in 1982–1991 have a similar ice extent to July in the recent decade. SST values also tend to be lower throughout the summer in the earlier decade than in the present-day Arctic, except for July which has a slightly higher mean SST in the earlier decade (Fig. 3.10b).

Sea ice responses observed during the late summer of 1982–1991 are quite similar to the trends of the same months in the more recent decade (Fig. 3.11). Storms with dominant northerlies over the MIZ tend to result in mean increases in MIZ ice area that last over a week after storm passage and storms with dominant southerlies result in short-term decreases in ice area. Classifying these events by changes in SST enhances these trends. Most of the storms with dominant southerly winds also experience decreases in SSTs and result in significant decreases in MIZ ice area within a few days following the start of the storm. This result is opposite that of the more recent decade, where increases in SST along with southerly winds led to larger decreases in MIZ ice area, suggesting a greater dependence on wind direction than SST in understanding changes occurring within the MIZ. Storms with mostly northerly winds over the MIZ are evenly split based on cooling and warming SST trends. Of these storms, those with increases in SST have much greater variability and shorter-lasting impacts than those with decreases in SST. With cooling trends, however, MIZ ice areas remain high well after the storm, with a majority of cases resulting in positive net change in the two weeks following the storm.

Like the late-summer responses, the impacts of early-summer storms early in the satellite era are fairly similar to the impacts of early-summer storms in the recent decade (Fig. 3.12). Again, as suggested by Figure 3.2, most storms in this time period tend to decrease the MIZ ice area relative to climatology. Unlike the early-summer storms in the recent decade, storms dominated by northerly winds tend to have longer-lasting impacts than storms with mostly southerly winds over the MIZ. Even when further classifying storms by changes in SST within the storm region, mean decreases in ice area within the MIZ last for at least a week after the start of the storm for northerly-dominant cyclones. The mean area changes due to storms with mostly southerly winds over the MIZ are less consistent. Overall, variations in SST during this period are small, resulting in small sample sizes when considering both mean wind direction and trends in SST.

Time	All Cyclones	Northerly Winds	Southerly Winds
1982–1991 JJ	**-0.229 ± 0.53** (44)	**-0.308 ± 0.49 (18)**	-0.174 ± 0.55 (26)
1982–1991 AS	**0.076 ± 0.65 (89)**	**0.184 ± 0.58 (53)**	-0.136 ± 0.7 (34)
2010–2019 JJ	**-0.422 ± 0.5 (58)**	**-0.293 ± 0.51 (31)**	**-0.57 ± 0.45 (27)**
2010–2019 AS	0.022 ± 0.62 (73)	**0.182 ± 0.53 (37)**	**-0.143 ± 0.66 (36)**

Table 3.1: Average net change and standard deviation in normalized area from one week before the start of the cyclone to two weeks after for all storms, those with dominant northerly winds, and those with dominant southerly winds. Total storm counts in each category are shown in parentheses. Values in bold are statistically significant at the 95% confidence level. JJ refers to storms occurring in June and July and AS refers to storms occurring in August and September.

Overall, in all categories and for each decade and month pairing, there is a large amount of variability in the observed sea ice outcomes. Table 3.1 summarizes the net change in normalized ice area within the MIZ from one week before the start of the cyclone to two weeks after. These values, of course, disregard that some cyclone effects could be short-lived and are therefore not fully represented by a single value. However, they

represent the general findings well; cyclones occurring earlier in the season tend to locally enhance the climatological decline of sea ice within the MIZ while, later in the season, cyclones have much more variable impacts (with mean sea ice changes near zero and large standard deviations). The means of the late-summer categories tend to be much smaller in magnitude than the early-summer means across most categories. Cyclones with dominant southerly winds within the MIZ region lead to mean decreases in MIZ ice area. Predominant northerlies lead to mean decreases in MIZ ice area in early-summer months and mean increases in MIZ ice area in late-summer months. Still, the standard deviations of each category are relatively large and indicate that not every storm within each category produces a similar sea ice response.

On average, we find early-summer storms locally decrease ice area more than late-summer storms. This result reflects the results of Kriegsmann and Brümmer (2014), who find that cyclones accelerate summer ice loss due to enhanced ice breakup and the subsequent decrease in surface albedo and increase in ice dispersion. These effects are likely largest at the beginning of the warm season as the ice extent is just beginning to retreat. There are also notable differences between storms with different dominant wind directions, where mostly southerly winds generally lead to decreases in ice area within the MIZ and storms with mostly northerly winds over the ice edge tend to have split results, depending on the seasonality of the cyclone. This result appears to be robust across the seasons and epochs analyzed.

3.4 Discussion

Throughout this chapter, we have established two climate regimes; the first occurring early in the satellite era, when sea ice was relatively thick and covered a large areal extent and the second being the most recent decade, when sea ice extent is more seasonally varying and vulnerable to changes. These two decades, the 1980s and 2010s, respectively, also demonstrate a notable shift in the number of intense cyclone events occurring in the early- and late-summer periods resulting in different mean sea ice changes in response to cyclone activity. In the recent decade, a greater fraction of storms occurred earlier in the summer than in the 1980s causing summertime cyclones in the more recent decade to result in more MIZ ice area loss than the earlier period. This result is summarized in Figure 3.13a. Note that the sharpest changes in normalized MIZ ice area occur just after the start of the cyclone, as indicated by the two case studies. As expected, storms occurring in the 1980s resulted in only a small mean change in area over the three-week period analyzed.

Figure 3.13b shows the number of intense storms occurring in each month of each decade. The 1980s also have the greatest number of September storms. Breaking the storm impacts down by month, Figure 3.13c shows that the September storms, on average, contribute positively in both the recent decade and earlier in the satellite era, suggesting these storms may be a critical factor in this decade's smaller net response.

Additionally, the differences in total mean MIZ ice area changes correspond well to the

differences in wind characteristics of the storms for the two decades. In the more recent decade, the higher frequency of southerly wind cases leads to larger mean decreases in sea ice area. However, in the 1980s, the mean storm impact appears to be driven by the greater number of northerly cases that tend to result in an increase in MIZ ice area.

Figure 3.13a also includes mean trends from 2000–2009 and 1990–1999 as a way to bridge the two extremes. Both the 2000s and 2010s experienced more storms during the earlier months of the summer, and subsequently led to greater mean decreases in MIZ ice area. A notable exception to this trend is the 1990s. As opposed to showing a sequential shift from the 1980s to the 2000s, the 1990s exhibit the largest mean decrease in normalized area out of the four decades. This period also fails to follow the trend of storms occurring earlier in the season and has the lowest percentage of early-summer storms.

Interestingly, the late-summer storms in the 1990s also do not follow the same pattern of wind-induced impacts as the August and September storms in the 2010s and 1980s. While the northerly-dominated late-summer storms in those decades were often associated with slight increases in MIZ ice area, similar cyclones in the 1990s tended to lead to decreases in MIZ ice area (Fig. 3.14). This decade also has the greatest number of August storms and the least number of September storms, which jointly contribute to this large negative effect (Fig. 3.13b). By analyzing the impacts of these four decades of intense summer cyclones on ice within the MIZ, we see evolving impacts based on storm timing and how the cyclonic winds interact with the ice edge.

3.5 Conclusions

NSIDC sea ice observations, NOAA SST observations, and ERA5 reanalyses from two decades were examined to characterize the influence of Arctic cyclones on sea ice cover. When analyzing a large census of cyclone events, we find that storms generally tend to locally decrease ice area rather than increase MIZ ice area, with 42.4% of all storms causing an increase in area and 57.6% of storms causing a decrease in MIZ ice area two weeks after the storm. We find that present-day cyclones are more likely to cause a decrease in ice area within the MIZ relative to climatology (64.1% of all storms in this decade), while cyclones in the 1980s, early in the satellite record, are more evenly split in terms of MIZ ice area impact with 51.1% of storms resulting in a decrease in MIZ ice area at the end of the 3-week study period.

The difference in storm impacts demonstrated in this study is largely explained by a shift toward more storms that interact with the MIZ occurring earlier in the summer in recent years, likely as a result of decadal variability. Early-summer storms tend to reduce MIZ ice area more than late-summer storms, with nearly three-quarters of all early-summer storms across both decades decreasing ice area. Early-summer storms both decrease MIZ ice area more on average and occur more frequently in the recent decade compared to the 1980s. Late-summer storms that dominated the early satellite record tend to slightly enhance the ice area within the MIZ, with 53.1% of storms corresponding with increases in area. This split may be explained by the competing effects of the storm cases surrounding

the Arctic's minimum sea ice extent, as August storms tend to cause a mean enhancement of MIZ area loss and September storms generally lead to increases in MIZ ice area.

In addition to storm timing, the effects of cyclones on sea ice are also found to vary depending on the dominant wind direction and, to a lesser extent, nearby ocean temperatures. Generally, late-summer storms across both decades result in changes that are primarily wind-driven. Cyclones that primarily enhance southerly winds result in decreases in MIZ ice area, and cyclones that enhance northerly winds result in increases in MIZ ice area. Likewise, even though most storms occurring earlier in the season tend to decrease the area of ice within the MIZ, the main meridional wind direction of the cyclone over the ice edge affects how early-summer storms impact the MIZ. Southerly winds tend to have much greater and longer-lasting impacts than northerly winds in the recent decade, while dominant northerly winds correspond to greater changes in the earlier decade.

Overall, cyclones across all months of the summer season tend to locally decrease MIZ ice area more in recent years than earlier in the satellite era. This result highlights a transition in the Arctic from an established state of resilient ice and mostly late-summer storms to a state with more vulnerable marginal ice and a greater frequency of early-summer storm events.

Comparing the effects of storms as a function of wind direction and SST changes necessitated normalization to account for the very different MIZ ice areas impacted by each storm. There is, however, considerable value in quantifying the net impact of Arctic cyclones on MIZ ice area in today's Arctic and how this impact has changed relative to

those early in the satellite record. The net impact of all storms on absolute MIZ ice area, without normalizing by the minimum and maximum values, is shown in Figure 3.15. On average, cyclones in the 1980s had no statistically significant net effect owing to the near cancellation of accelerated ice loss from early-season storms and ice enhancements from late-season storms that resulted in a small net gain of just over 4,000 km^2 of MIZ ice two weeks after storm passage. Recent storms, however, have had a much larger impact on MIZ ice area, decreasing the area of MIZ ice by over ten times as much (40,000 km^2 per storm) on average. This reflects the change in storm seasonality with more storms occurring in June and July in the more recent decade. This effect is compounded by the fact that early-season storms decrease more than three times more ice in the modern era than the early-summer changes observed in the 1980s (over 80,000 km^2 of ice loss compared to over 25,000 km^2). Late-summer storms decrease the ice-covered area of the MIZ much less, with just under 8,000 km^2 of sea ice loss within the MIZ in the recent decade but this contrasts with late-season storms causing a gain of over 18,000 km^2 in the earlier period.

In bridging these two decades at the start and end of the satellite record, we have noted an important exception to these results occurring in the 1990s, where summer cyclones led to an enhanced decline in MIZ ice area due to differences in storm timing and wind-induced impacts. Previous studies suggest this intensified response may also be due to large-scale circulation changes that resulted in a change in the distribution of sea ice (Wei et al., 2019, Zhang et al., 2004). This result may be indicative of the importance of the background state of the ice and the confounding effects of large-scale circulation changes in predicting

the impact cyclones will impart and highlights a potentially important implication of the recent shift toward seasonal ice cover in the Arctic.

While many of the responses documented here are statistically significant, there remains a large amount of variability from case to case across all time periods. While some of this uncertainty may be due to the limited sample size of storms that can be analyzed, this outcome suggests that wind direction and nearby SSTs alone do not fully determine the effects of extreme cyclones on Arctic sea ice. The varied responses of sea ice can also be attributed to other variable causes. For example, regions of ridge ice may be more resilient to cyclone-induced changes, whereas the associated increase in open water could either further melt through increased solar absorption or motivate additional ice growth under cool enough conditions. So, while the effects of cyclonic winds and associated SST changes capture some of the underlying physics, these mechanisms alone cannot fully predict sea ice outcomes.

The results presented here diverge from previous studies, such as Schreiber and Serreze (2020) and Finocchio et al. (2020), in that we find that a majority of storms tend to decrease MIZ ice area. While these two studies similarly focus on sea ice within the MIZ, the unique methods presented here highlight important considerations not addressed in previous work. Firstly, a different subset of cyclone events is used in this analysis, where we emphasize the role of the most intense cyclones. The signals presented in previous works may be dominated by the impacts of many less intense storms. Secondly, we isolated the impacts only within a predefined area outlining the MIZ. Previous studies that

considered cyclone impacts on the MIZ include all sea ice points along the ice periphery regardless of concentration. By focusing on only a subset of these points, we prioritize the changes occurring to the most vulnerable ice, which may have a different net response than all points along the ice edge.

Other factors not addressed here, such as storm location and differences in storm structure, also complicate the influence of each cyclone event. The location where the storm develops can have different effects on not only the strength of the storm but also how the sea ice responds (e.g., Aue et al., 2022, Finocchio et al., 2022, Schreiber and Serreze, 2020). Yet another complicating factor is the orientation of the ice edge relative to the storm winds. The first case study had meridional winds that were near-perpendicular to the ice edge. This is not necessarily true of the entire extent of the second case. Additionally, the second case had a cold front that aligned well with the MIZ, which further promoted an increase in MIZ ice area, whereas the first case did not. Methods could be developed for incorporating aspects of these factors into observation-based analyses. For example, further investigation of how storms approach the ice edge and subsequently impact the ice is recommended. Future analysis could also consider the effects of ocean upwelling in more detail by expanding the analysis of vertical temperature profiles or making use of models that better capture vertical ocean processes. The effect of cyclone-induced upwelling and upward heat transport has been shown to largely influence sea ice changes (Peng et al., 2021, Zhang et al., 2013). Incorporating this extended analysis may help clarify some of the questions raised here, but may suffer from the limited availability of profile measurements in the Arctic.

The impacts of cyclones clearly depend on a large number of different factors and as a result, are widely varied. Nevertheless, the proposed mechanisms described here appear to provide robust insights into how the cyclonic winds and associated SST changes of intense summertime storms can impact the underlying marginal ice zone. We have also demonstrated the importance of the background state of the ice, which will continue to evolve in a warming climate.

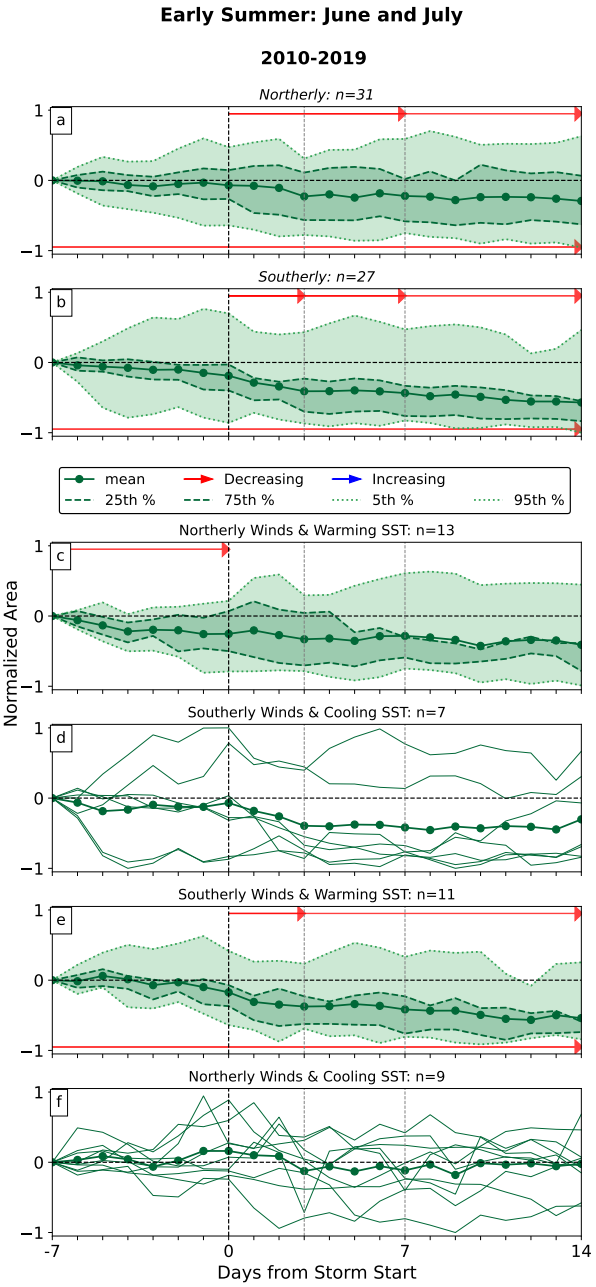

Figure 3.9: As in Figures 3.7 and 3.8, but for early-summer months in 2010–2019. A version of this plot without normalization is available in Figure A.2.

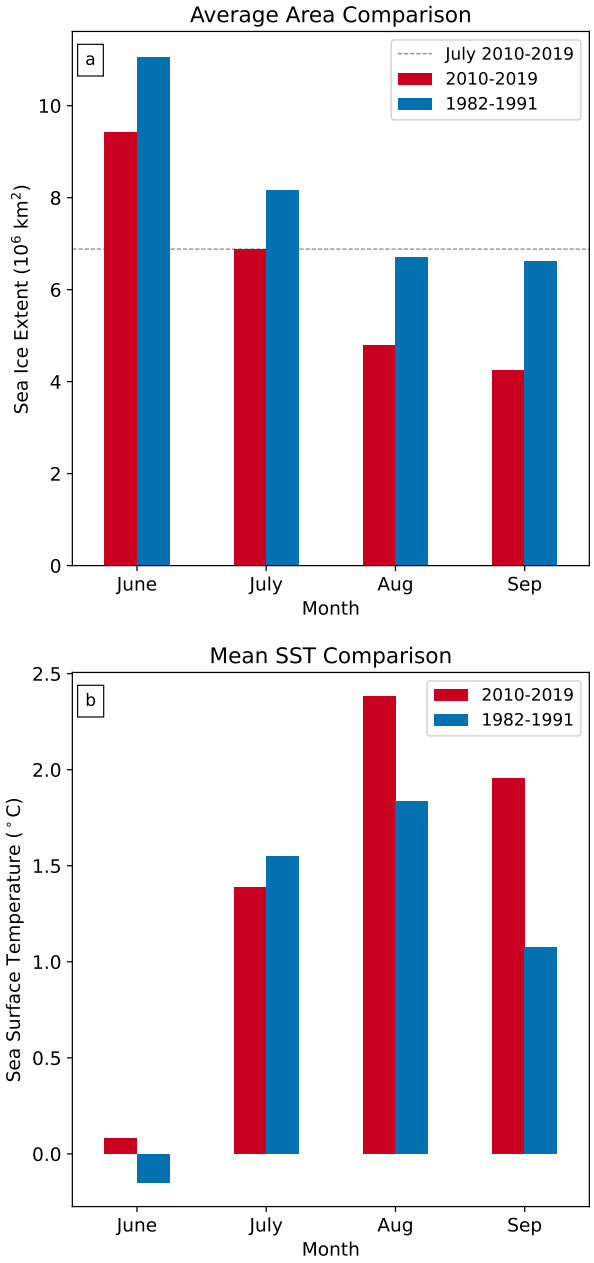

Figure 3.10: (a) Comparison of monthly mean sea ice extent for both decades. Gray dotted line shows the mean ice extent for July 2010-2019 to highlight its similarity to the 1982-1991 August and September extents. (b) Comparison of monthly mean sea surface temperatures in open water north of 67°N for both decades.

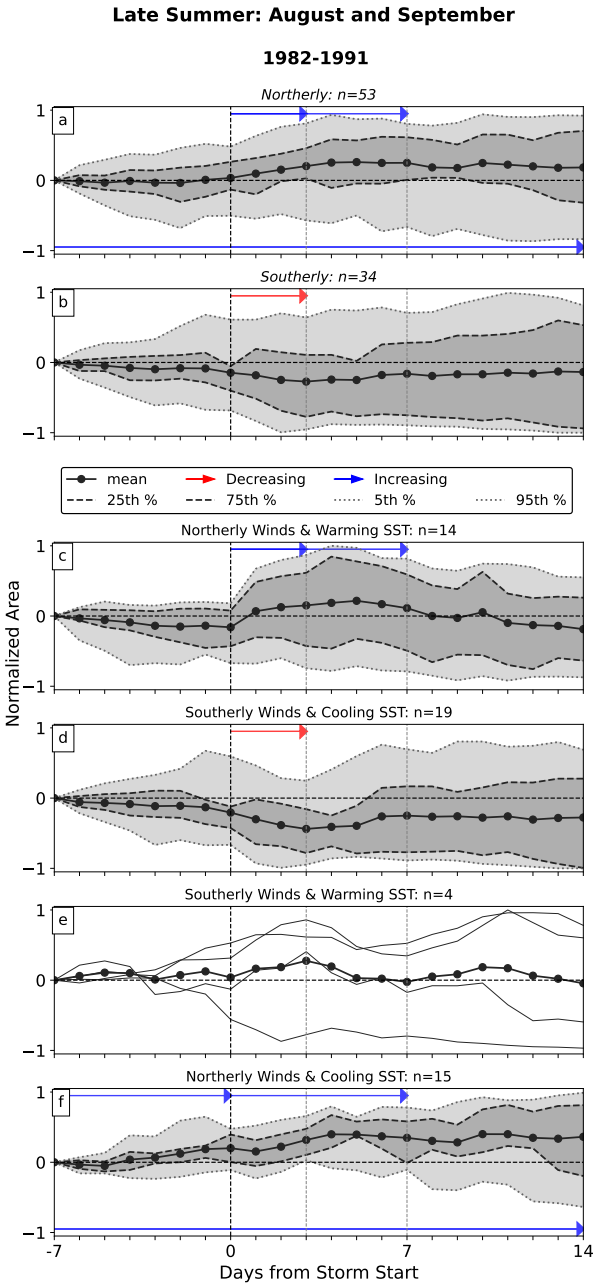

Figure 3.11: As in Figures 3.7 and 3.8, but for late-summer months in 1982–1991. A version of this plot without normalization is available in Figure A.3.

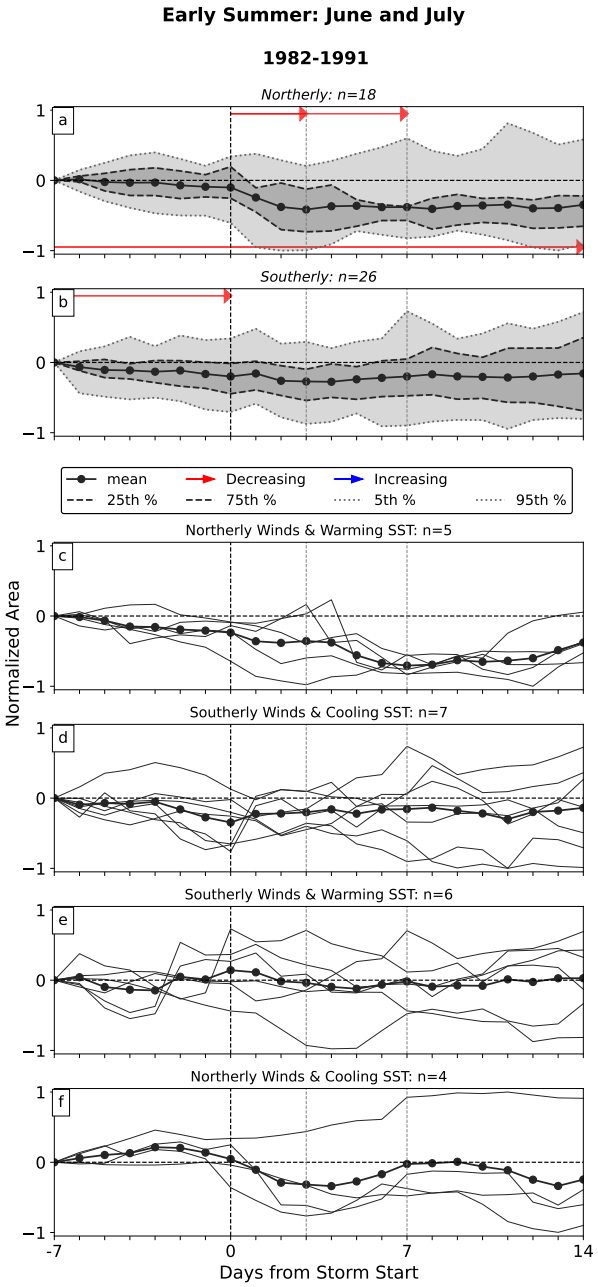

Figure 3.12: As in Figures 3.7 and 3.8, but for early-summer months in 1982–1991. A version of this plot without normalization is available in Figure A.4.

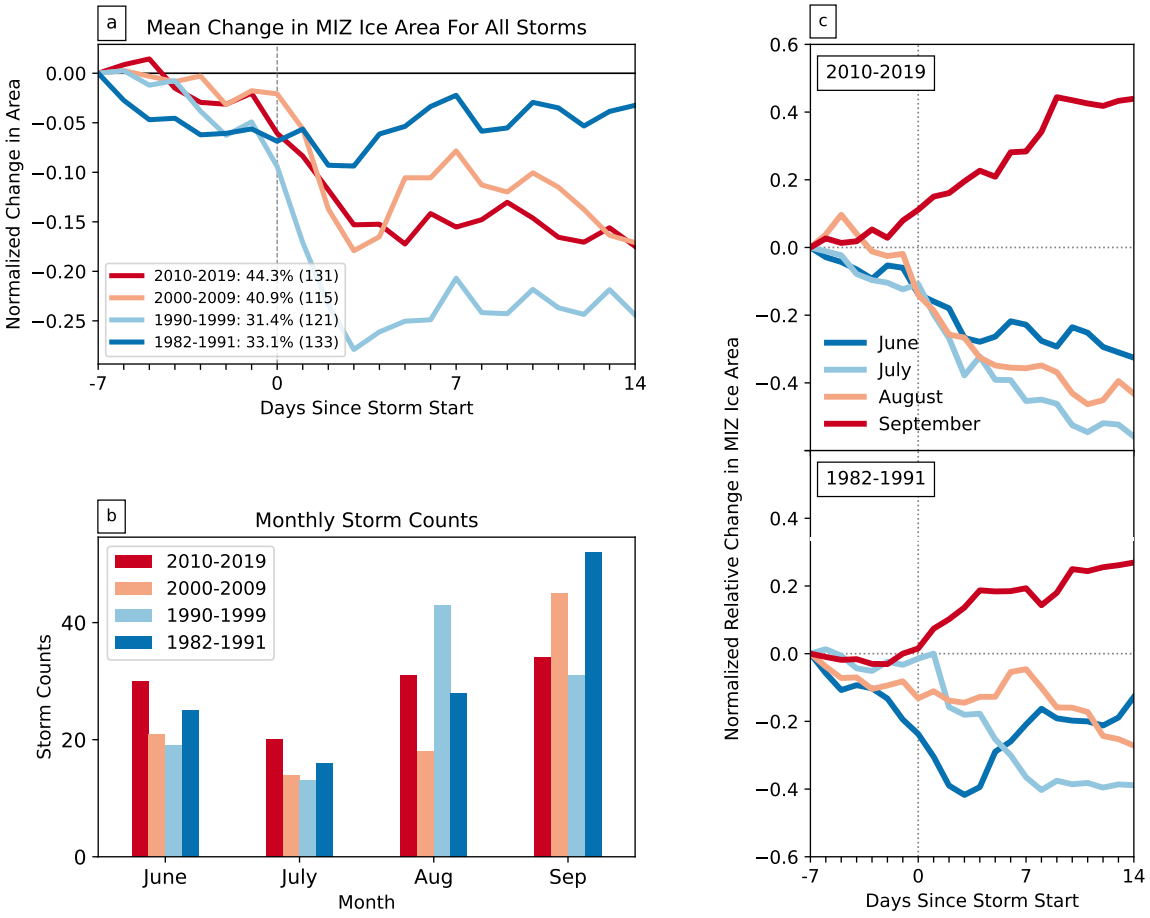

Figure 3.13: (a) Normalized changes in MIZ ice area relative to the start of the analysis time window for four decades of cyclone events. The legend includes the percentage of early-summer storms and the number of total storms for that decade in parentheses. A version of this plot without normalization is available in Figure A.5. (b) Monthly counts of both early- and late-summer storms in each decade. (c) Normalized changes in MIZ ice area relative to the start of the analysis time window for each month in 2010–2019 (top) and 1982–1991 (bottom).

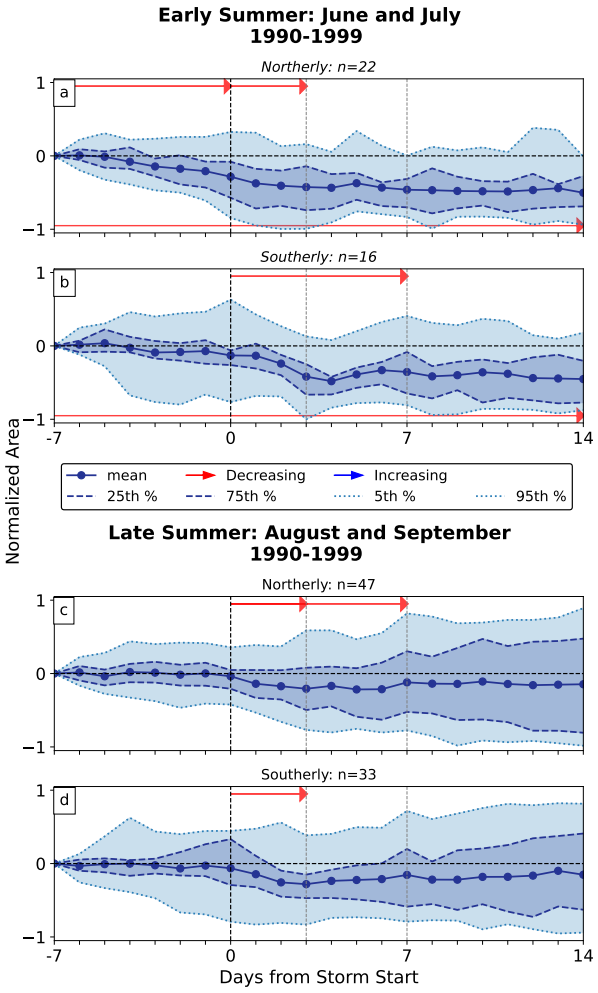

Figure 3.14: As in Figure 3.7, but for early-summer months (a,b) and late-summer months (c,d) in 1990–1999. A version of this plot without normalization is available in Figure A.6.

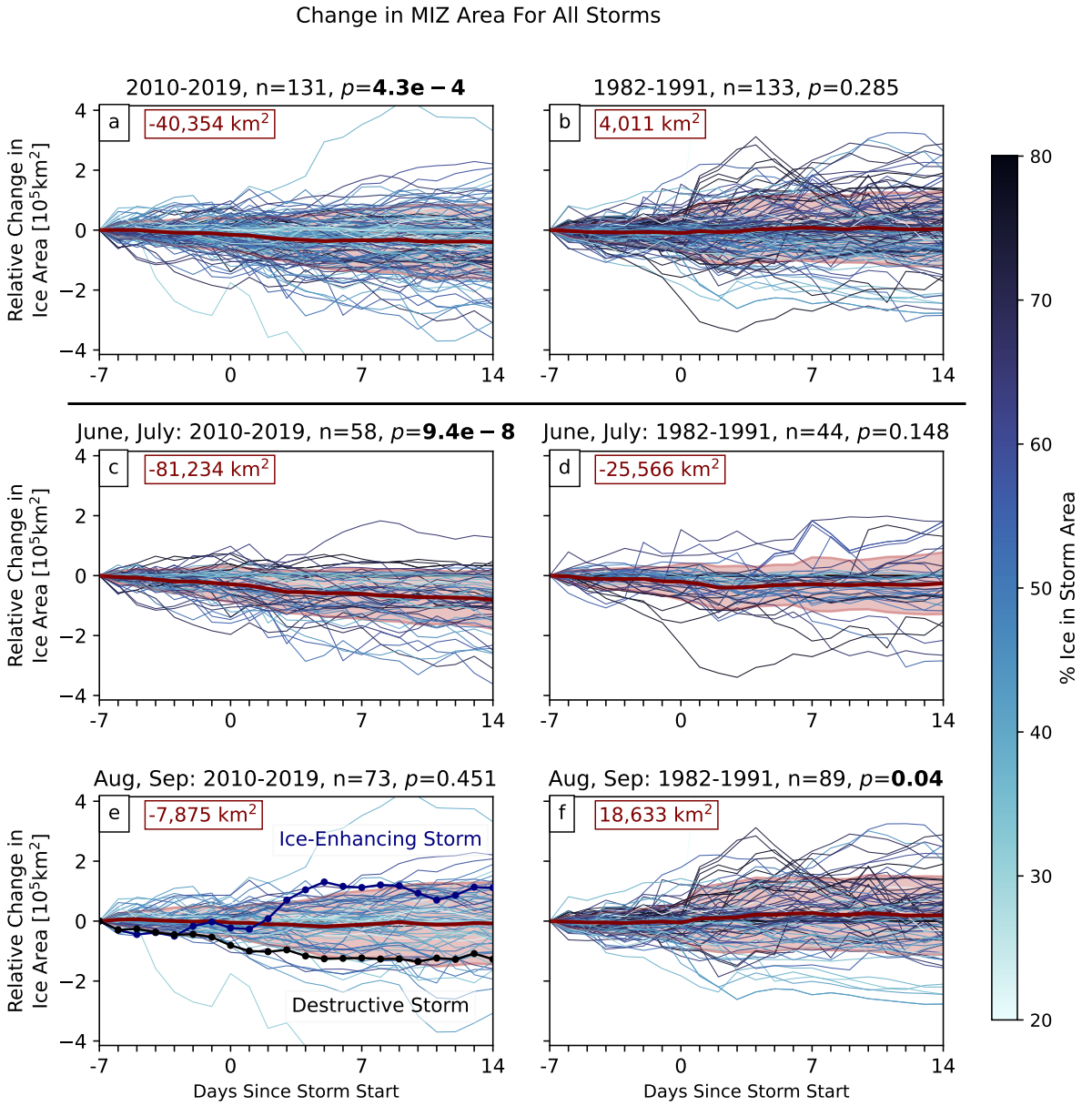

Figure 3.15: Net change in MIZ ice area for cyclones in the present-day Arctic (2010–2019, left column) and early in the satellite era (1982–1991, right column), for each decade (a,b), for early-summer months (c,d), and for late-summer months (e,f), relative to the climatological mean for each storm and the initial ice area one week before the start of the storm. Line coloring indicates the percentage of ice that is present within the storm area on the first day of the cyclone. The mean and standard deviation of all curves are plotted in red. The mean trends in (a), (c), and (f) are significantly different from zero based on a Student's t-test at the 95% level. Values in red (upper left) denote the mean net change in area after two weeks.

Chapter 4

Have Impacts of Intense Arctic Cyclones on Summer Sea Ice Reached a Maximum?

4.1 Introduction

As sea ice continues to decline in a warming Arctic, the role of summer cyclones in altering the ice edge may similarly evolve. Despite knowing that a changing ice state is important to the evolution of storm impacts, cyclone-sea ice interactions in global

This chapter is adapted from the peer-reviewed publication:
Mundi, C. L., L'Ecuyer, T. S., & DuVivier, A. K. (2025). Have Impacts of Intense Arctic Cyclones on Summer Sea Ice Reached a Maximum?. *Geophysical Research Letters*, 52(19), e2025GL117848.

climate models remain understudied. Previous modeling studies investigating cyclone-sea ice interactions have tended to focus on individual case studies such as “The Great Arctic Cyclone of August 2012" (Lukovich et al., 2021, Simmonds and Rudeva, 2012, Zhang et al., 2013), or the record cyclone in January 2022 (Blanchard-Wrigglesworth et al., 2024), which were unprecedentedly large and intense cyclones. Other studies have examined the effects of many cyclones in models by investigating the winter cyclone impacts in phase 5 of the Coupled Model Intercomparison Project (CMIP5; Cai et al., 2020) or by using reanalysis to force ice-ocean models (Clancy et al., 2022, Kriegsmann and Brümmer, 2014). Alternatively, regional and global climate models have been used to project increases in the total number of Arctic cyclones, though these trends are regionally variable (Akperov et al., 2015, Crawford and Serreze, 2017, Day et al., 2018, Nishii et al., 2015). Weaker and equatorward biases in northern hemisphere storm tracks may cause these increases to be underestimated (Harvey et al., 2020, Zappa et al., 2013), possibly due to the growing land-sea temperature contrast in the Arctic impacting modeled storm tracks differently than in observations (Day and Hodges, 2018) or biases in net poleward energy transport (Cox et al., 2024).

These differences in modeled cyclone patterns may imply an under-representation of the corresponding sea ice impacts. However, the integrated large-scale impacts of intense cyclones within the MIZ have yet to be investigated in models. In this chapter, we use the Community Earth System Model Version 2 Large Ensemble (CESM2-LE) to isolate the role of intense summer cyclones on MIZ ice evolution. We ask:

1. Do biases in intense cyclone characteristics influence modeled impacts on MIZ sea ice?

2. How are these impacts on the MIZ predicted to change in a warmer climate?

Historical storm impacts are compared with results found using satellite observations and reanalysis (Mundi and L'Ecuyer, 2025) to reveal differences in cyclone characteristics and their effects on the MIZ, which are then used to inform predictions about future cyclone-induced changes to the MIZ.

4.2 Adapting Cyclone Detection Methods to CESM2-LE

To account for the coarser resolution in CESM2, the pressure threshold used for detecting cyclones is increased to 986 hPa. This value was determined by scaling ERA5 data to the horizontal and temporal resolution of CESM2 and adjusting the pressure threshold to produce the same number of storms as the original ERA5 census, with comparable timings and durations. The storm area definition was adjusted similarly (increasing the daily contours to 1002 hPa to reproduce the areal extents of the original ERA5 storms). Also, when considering MIZ-interacting storms in CESM2, differences in sea ice concentration from satellite observations necessitated finding similar area fractions of MIZ and pack ice in CESM2 by determining the concentrations with the lowest root mean square difference

from 15% and 80% to establish which portions of the storm domain were covered by MIZ or pack ice. An example of these methods is shown in Figure B.1.

4.3 Results

4.3.1 Differences in Cyclone Detection

Adjusting the pressure threshold to account for resolution differences, we expect similar storm counts for both CESM2 and ERA5 in the historical period. Figures 4.1a,b show the mean number of low-pressure systems detected (before applying the additional criteria listed in Section 2.2) across the 40 CESM2 ensemble members and the total number of ERA5 storms for two decades from June through September. CESM2 has more storms overall, with over 100 intense storms each decade on average, whereas ERA5 has around 90. However, once these low-pressure systems are sorted to meet this study's conditions (colored bars), fewer CESM2 storms remain. The first filter (shown in blue) determines if the cyclone reaches the ice edge (within 1250 km) during its evolution. For ERA5, roughly 30% of storms are removed, while more than two-thirds of CESM2 storms fail this criterion, indicating an equatorward bias of intense storms in the model, consistent with Konstali et al. (2024) and Priestley and Catto (2021). The next filters are similar between the two datasets. About 70% of the remaining storms are removed due to storm characteristics (green; defined as not having a duration of 2 days) and approximately half of the remaining are removed for not sufficiently interacting the MIZ (purple; storm area containing 20-80% high-concentration ice). Subsequently, the equatorward bias in storm

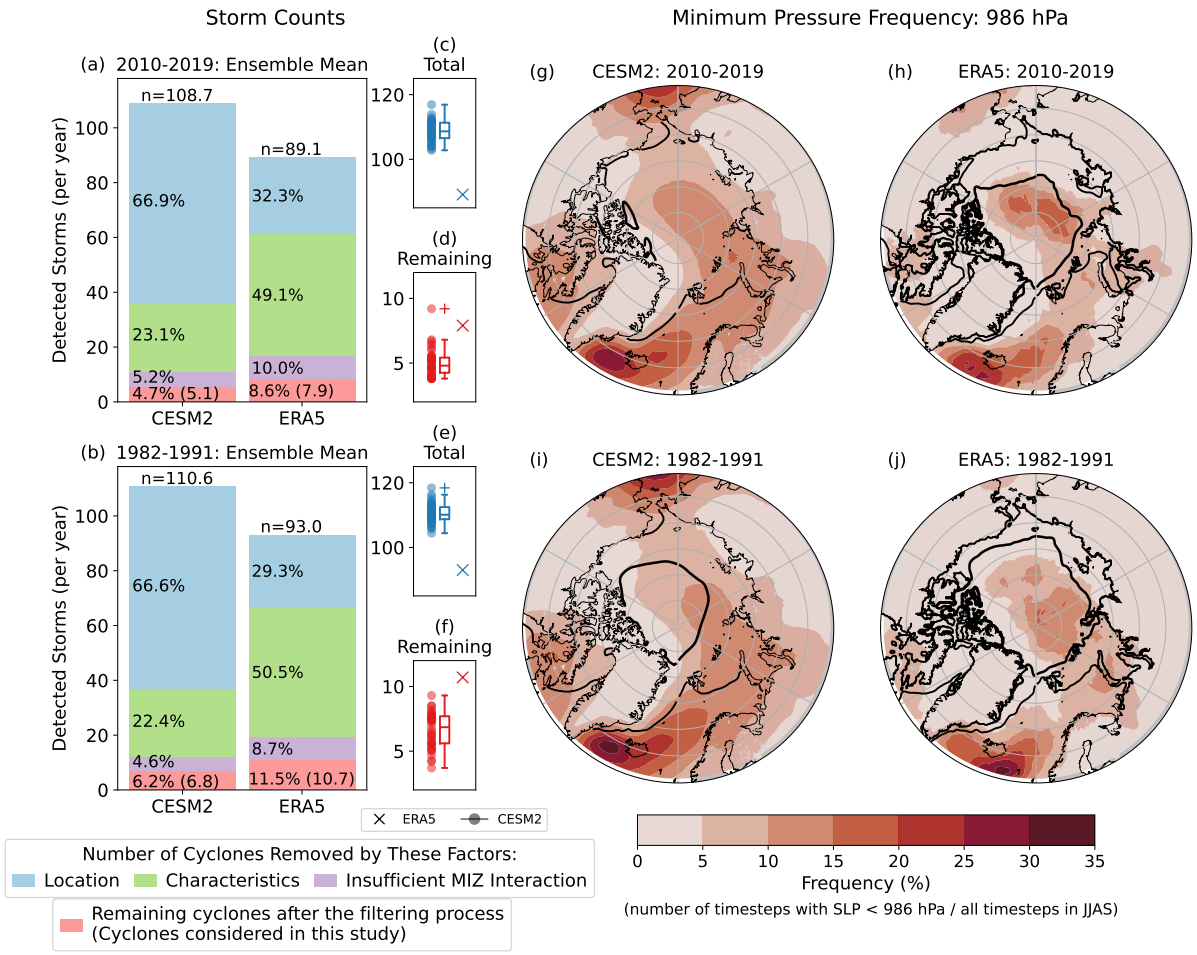

Figure 4.1: June through September storm counts for 2010-2019 (a) and 1982-1991 (b) in CESM (left) and ERA5 (right). The mean total annual count per ensemble member (n) is indicated at the top of each bar. Colors describe the filters applied to the census of cyclones and are discussed in text. “Remaining Cyclones" (red) are storms considered in this study, with the mean annual count shown in parentheses. (c-f) Distribution of ensemble annual-mean storm counts (dots and boxplot) compared with ERA5 (cross) for total storm counts (blue) and remaining cyclones (red). (g-j) Frequency of June-September mean sea level pressure values falling below 986 hPa. ERA5 data is scaled to match the resolution of CESM2.

development locations causes more storms to be removed in the first step, with CESM2 simulating considerably fewer MIZ-interacting cyclones than ERA5.

Figures 4.1g-j reinforce this result by showing the frequency of sea level pressure below the pressure threshold for both datasets. Although ERA5 may have biases in sea level pressure over the central Arctic and may not be fully representative as "ground truth," the dataset has been widely used in identifying Arctic cyclones (e.g., Chen et al., 2025, Crawford et al., 2021, Valkonen et al., 2025). ERA5 has two distinct maxima in low pressure frequency, with storms tending to reach minimum pressure values along the eastern coast of Greenland and over the sea ice in the Central Arctic Ocean. While the modeled distribution has the same Icelandic low maximum, the frequency of central Arctic low-pressure occurrences is reduced. The secondary low-pressure maximum appears much farther from the ice edge, in the Bering Sea, which does not appear as strongly in ERA5. These biases in storm frequency over the central Arctic are consistent with other global climate models, such as CMIP5 models (Zappa et al., 2013) and the previous version of CESM (Crawford and Serreze, 2017).

4.3.2 Impacts of Intense Cyclones on MIZ Ice Area

In addition to storm location differences, CESM2 and ERA5 indicate different MIZ responses to intense cyclones. Figures 4.2a-d show the net change in MIZ ice area relative to one week before the storm for early and late summer months in each decade. In all periods, the CESM2-LE composite-mean change in MIZ ice area is larger than the mean observed outcomes. Like ERA5, early summer storms in CESM2 tend to have greater

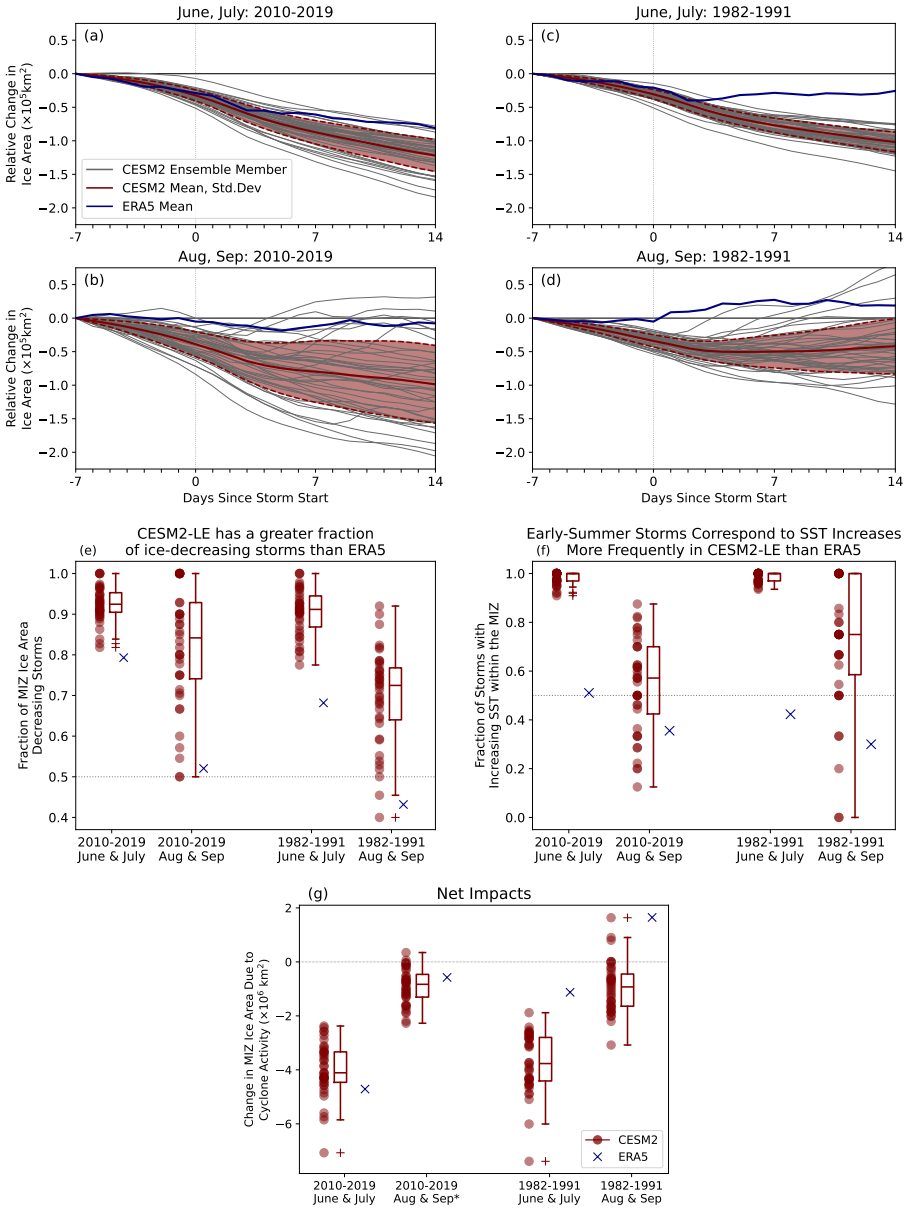

Figure 4.2: (a-d) Net change in MIZ ice area, relative to one week before the storm. Mean storm impact for each ensemble member is shown in gray, with the mean and standard deviation across members shown in red. The mean observational response is shown in blue. (e) Fraction of cyclones in each ensemble member that causes a net decrease in MIZ ice area two weeks after the storm's passage or (f) have a corresponding increase in SST during the storm lifetime. (g) Total net sea ice change for each month/decade grouping. Red dots and box plots show the distribution of ensemble member values. Blue crosses show the corresponding mean value for cyclones detected in ERA5. Asterisk depicts no statistically significant difference at the 99.9% level (e-f all show significant differences).

negative impacts on the MIZ than late summer storms (where modeled September storms generally increase the local ice area like in observations; Fig. B.2). All 40 ensemble members considered show net negative MIZ ice area changes in early summer months. The spread of ensemble members captures the observed mean MIZ impacts in the more recent decade, but model responses diverge substantially from the observed time series in the earlier decade. CESM2-LE has a much larger spread in outcomes two weeks after the storm in late summer, where a decline in MIZ ice is simulated initially, followed by significant spread after the storm (particularly in the earlier decade), with some ensemble members indicating continued decline and others increasing ice area. In all month-decade groupings, modeled storms tend to have longer-lasting effects on MIZ ice area. Possible explanations for these differences could be larger areas of lower sea ice concentration or melt pond coverage accelerating the ice-albedo feedback with the CESM2 MIZ, or differences in the non-cyclone-induced changes to the sea ice, since CESM2 is known to underestimate sea ice thickness (and subsequently extent) in summer months due to thinner spring clouds (DeRepentigny et al., 2020, DuVivier et al., 2020). The tendency towards lower-latitude storms could also explain the too-strong impacts in the model, as fewer storms travel over a thicker ice regime in the central Arctic, which are known to have differing impacts, as suggested by Lukovich et al. (2021).

Nearly all modeled cyclones decrease MIZ ice area in early summer months, a much larger fraction than observed storms (Fig. 4.2e), possibly because over 90% of storms also correspond to local SST increases (Fig. 4.2f). In late summer, most modeled cyclone cases also decreased MIZ ice area, as opposed to only about half of ERA5 storms. Late summer

storms in CESM2 also have coincident SST increases more often than observed. The combination of enhanced and prolonged sea ice loss with more ubiquitous SST warming highlights the importance of upper-ocean characteristics in representing sea ice changes (Blanchard-Wrigglesworth et al., 2024, Finocchio et al., 2022).

4.3.3 Net Impact

The preceding analysis suggests CESM2-LE under-represents the number of MIZ-interacting storms but predicts stronger-than-observed impacts. Figure 4.2g quantifies the implications of these competing biases on the accumulated MIZ impact of intense cyclones in CESM2 (defined as the 3-week change in MIZ ice area, minus climatology, summed over all storms). The observed storm impact falls within the range of CESM2 ensemble members in the more recent decade, however, in the earlier decade, all CESM2 ensemble members produce a too-negative ice response compared with observations. CESM2 may be demonstrating similar MIZ ice area net changes compared to observations due to compensating effects of reduced storm frequency and increased storm impacts.

4.4 Evolution of Intense Cyclone Impacts in Future Decades

Although CESM2-LE has biases capturing observed intense cyclone frequency and sea ice response, examining how these impacts may evolve in the future is still instructive. As emphasized above, both storm count and timing modify net MIZ ice area responses.

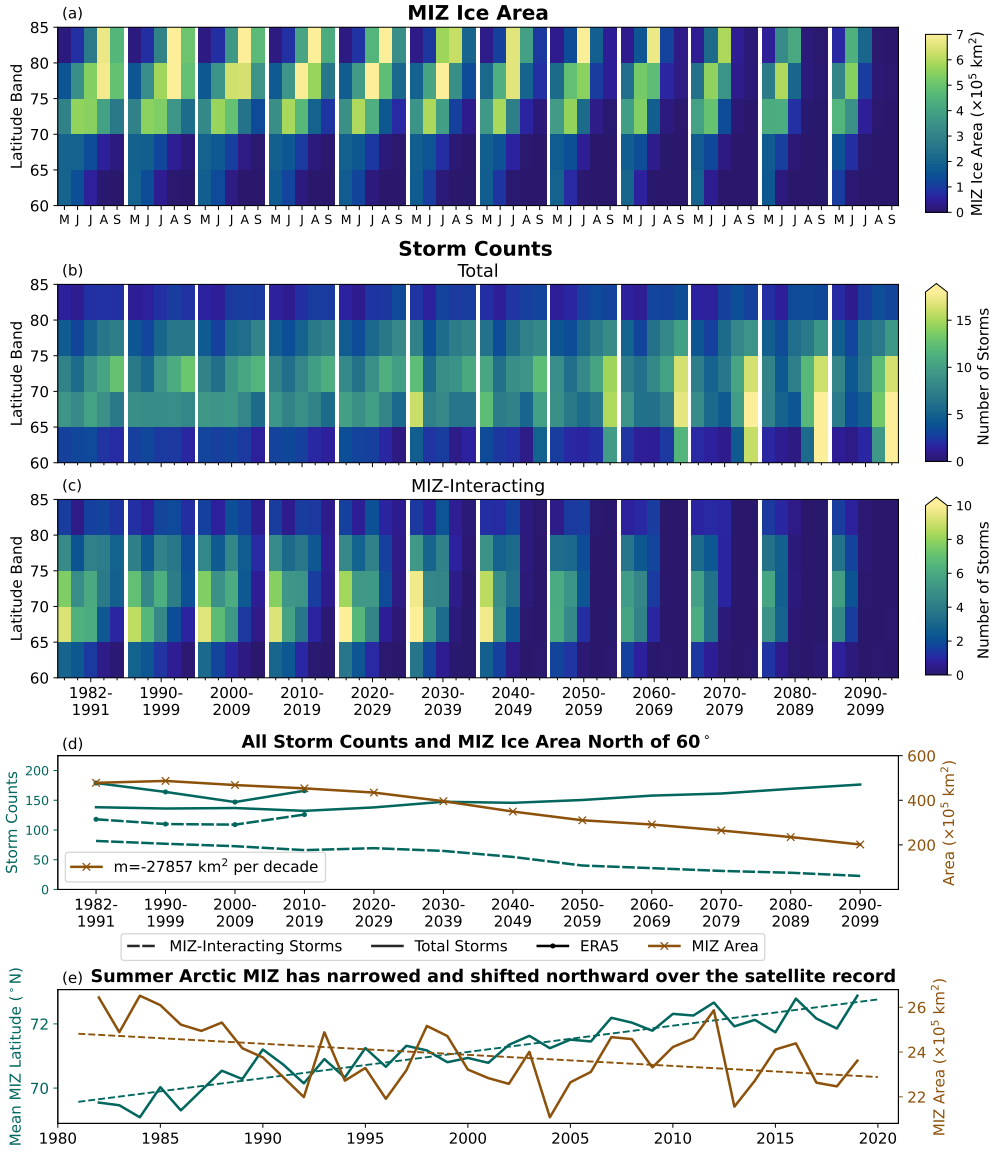

Figure 4.3: Monthly mean (a) MIZ ice area, (b) storm count, (c) number of storms that interact with the MIZ, per latitude band. (d) Annual storm counts (green) and MIZ area (brown crosses) for both CESM2-LE (no marker) and observed storms (circles). Dashed lines indicate storms that interact with the MIZ and solid lines show total storm count. (e) Observed annual mean MIZ latitude (green) and MIZ area (brown) over the satellite record.

CESM2-LE predicts increases in Arctic storm frequency overall, especially in late summer and in lower latitude bands (Fig. 4.3b). However, CESM2 composite mean trends suggest MIZ ice area will decrease by almost 30,000 km^2 per decade and shift poleward (Fig. 4.3a). A progression towards an earlier ice-free Arctic is also evident in future decades causing fewer storms to interact with the ice edge. In near-future decades, MIZ-interacting storms shift poleward. Then, after the 2040s, as September months become ice-free, storm interaction with the MIZ declines (Fig. 4.3c). This transition causes a predominance of early summer storms reaching the MIZ, which tend to decrease ice area more effectively than late summer storms. In later decades, as earlier months become ice-free, the number of early summer MIZ-interacting storms also decreases (relative to the lower number of storms compared with observations in recent years; Fig. 4.3d).

Figure 4.4 summarizes this transition, showing CESM2-LE composite-mean net cyclone impacts on the MIZ for each month. In the early satellite era (1980s) and present day (2020s), the largest MIZ ice area decreases occur in June and July, with weaker changes in August and slight increasing effects in September, consistent with observations (Mundi and L'Ecuyer, 2025). Generally, storm impacts increase from the 1980s to present as the MIZ becomes more vulnerable to external changes. Intense cyclone impacts in July (and also all months combined) reach their maximum in the 2000s and steadily decline after the 2020s. The decreased ice loss in the 2010s likely results from fewer July storms (Figure B.3). August and September storms have their largest influence on MIZ ice in the 1990s and 1980s, respectively, before transitioning to near-zero impacts around the 2040s. In the near and far future (2060s, 2090s), late summer intense cyclone impacts

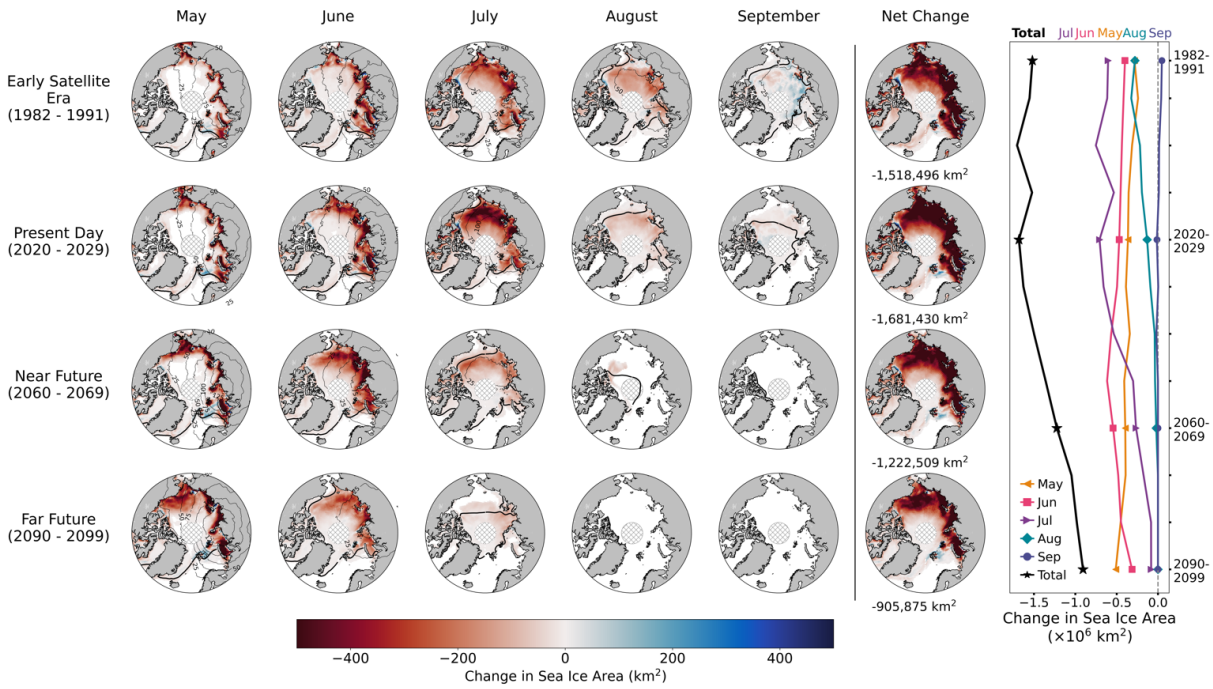

Figure 4.4: Changes in MIZ ice area due to cyclones for May, June, July, August, September, and total change for all five months (columns) and four selected decades (rows). Thick black lines depict the ensemble and decadal mean sea ice extent on the first day of the month. Thin contours indicate the mean number of days of each decade with storms occurring in that location. Monthly and total time series on the right show the change in MIZ area for all decades from the early satellite era through 2100. Markers correspond to the four selected decades shown in the maps.

are minimized as ice-free months become more common. In the far future, August and September become completely ice-free, and the greatest changes to the MIZ occur in May, shifting the largest intense cyclone impacts earlier as less MIZ ice is available later in the season. These predicted changes are plausible given the poleward shift and decrease in MIZ area in recent decades (Fig. 4.4e). As fewer intense storms reach the ice edge with this transition, the model's storm count bias is likely minimized. Since the modeled storm impacts are overestimated, the actual shift in storm impacts may be muted in comparison with this prediction.

4.5 Conclusions

As Arctic sea ice becomes less expansive and more vulnerable to external changes in recent years, intense cyclones are playing a more significant role in modulating sea ice cover. Storms can largely reduce MIZ ice area and potentially prompt the first ice-free day (Heuzé and Jahn, 2024). This ice cover loss significantly modifies the energy balance and contributes to the Arctic's amplified warming rate (Stroeve and Notz, 2018), highlighting the importance of predicting future changes in intense cyclone effects.

Our second research question asks how intense cyclone impacts are predicted to change in a warmer climate, and we find a temporary increase in MIZ ice area loss from the 1980s to present, as more susceptible sea ice becomes exposed to passing summer cyclones. Then, despite a predicted increase in future intense Arctic storms, shrinking ice cover and longer ice-free periods from continued climate forcings lead to fewer cyclones reaching the MIZ, reducing the impact of intense storms particularly in late summer (even when scaled by the MIZ ice area, not shown). As a result, the largest cyclone-induced ice area decreases occur earlier in the summer, transitioning from July to June around 2050, then to May toward the simulation's end, total ice-decreasing effects begin to decline after the 2020s, suggesting intense cyclone impacts on summertime sea ice may have reached a maximum.

Regarding our first research question on modeled biases of intense cyclone characteristics, CESM2-LE had fewer cyclones pass over the MIZ, but on average decreased ice area more than observed in past decades. Compared with observations, individual modeled storms

were more likely to decrease MIZ ice area, with early summer storms corresponding to SST increases more frequently, highlighting the ocean environment's importance in cyclone-sea ice interactions. The modeled sea ice state and cyclone distribution may also impact the net effect of storms. However, these biases in storm count and impact magnitude reproduced similar net impacts in the model compared with observed storms.

While these two discrepancies partially compensate, these biases limit the ability to assess future changes in CESM2 fully, particularly under changing ice conditions. Better representing Arctic cyclones and their impacts can reduce the uncertainties described in this analysis. Further investigating the key relationship between changing sea ice conditions and intense cyclone development near the ice could increase confidence in the number of storms reaching the ice edge (Valkonen et al., 2025). Additionally, we highlight the importance of upper ocean conditions (including upwelling or wave dynamics, as discussed in Blanchard-Wrigglesworth et al. (2024)) in improving modeled cyclone impacts on the MIZ. By addressing these concerns, predictions of future cyclone impacts can be more accurate. Regardless of model biases, this study emphasizes the significance of the evolving summer sea ice cover when considering intense cyclone impacts.

Chapter 5

Intense Storms Increase Global Ice Area

5.1 Preface

The previous chapters have underscored the importance of intense cyclone impacts on the summertime sea ice extent in the Arctic. However, sea ice cover in both hemispheres influences Earth's energy balance, and cyclones impact sea ice throughout the year. We use a combination of satellite observations and reanalyses to identify and analyze 2087 storms in both hemispheres and two decades (1982-1991 and 2010-2019) to quantify the net effects of intense cyclones on global sea ice area. This study specifically focuses on the

This chapter is a modified version of:
Mundi, C., & L'Ecuyer, T. (2026). Intense Storms Increase Global Ice Area. Under Review. *Nature Communications.*

subset of intense cyclones with minimum sea level pressures below 984 hPa in the Arctic and 957 hPa in the Antarctic that have the largest impacts. To understand the factors governing the impact of these storms on the MIZ, their impacts on mean meridional wind and ice speeds and changes in sea surface temperature (SST) in the MIZ are examined. The results are used to estimate the accumulated impact of all cyclones on the global MIZ area.

5.2 Adapting Methods to the Southern Hemisphere

Like previous chapters, we focus this study on more intense storms, using a minimum pressure threshold of 984 hPa in the Arctic and 957 hPa in the Antarctic. The Antarctic storm threshold is also similar to previously used values Hepworth et al. (2022). These thresholds may lead to higher storm counts in winter months when the mean sea level pressure tends to be lower, however, the findings are not sensitive to this bias (see Section 5.2.1). An effective “storm influence area" is defined using the maximum and minimum longitude and latitude of the daily 1000 hPa and 980 hPa mean sea level contours for the Arctic and Antarctic, respectively. To remove storms that minimally interact with the MIZ, we require between 20-80% of this storm area to contain pack ice. Due to this ice-interaction criteria, austral summer storms (January through March) seldom interact with the minimal MIZ around Antarctica and are excluded from the analysis.

5.2.1 Sensitivity to Chosen Thresholds

To establish error bars on the results, we perturbed all aspects of the methodology as follows:

1. the minimum pressure threshold for detection was increased by 10 hPa (to 994 hPa in the Arctic and 967 hPa in the Antarctic), and
2. the storm influence area was localized to to 990 and 970 hPa in the northern and southern hemispheres, respectively.

By including more storms, a larger accumulated change in MIZ ice area is noted, indicating the greater end of the spread in Fig. 5.4. Selecting a storm area more central to each storm's minimum pressure reduced the total ice area, providing a smaller estimate of net area changes.

5.3 Storms Can Expand or Reduce Ice Area

Recent publications analyzing cyclone case studies have tended to focus on large, destructive cyclones (e.g., Blanchard-Wrigglesworth et al., 2022, Graham et al., 2019b, Jena et al., 2022). However, there is considerable variability in storm impacts on sea ice, so these case studies may not be representative of all storms (Aue and Rinke, 2023, Mundi and L'Ecuyer, 2025, Schreiber and Serreze, 2020). In fact, despite the emphasis on destructive storms, many storms increase sea ice area. An example of such a storm occurred in mid

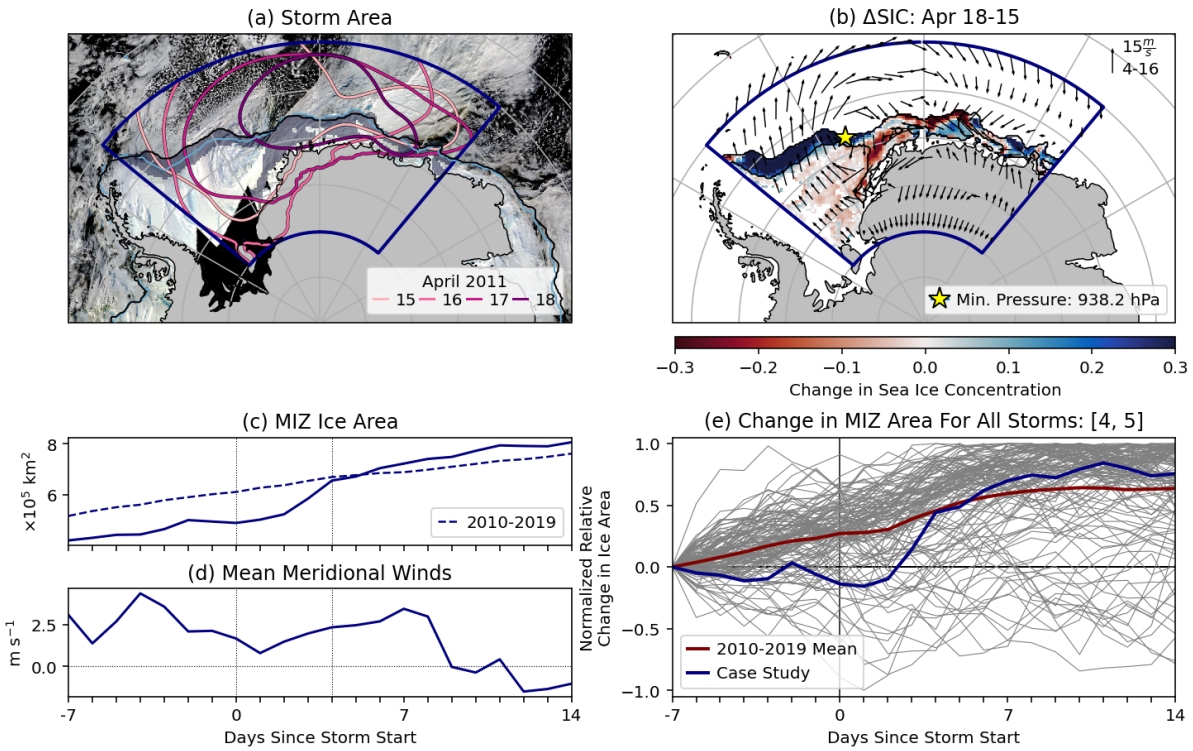

Figure 5.1: **Example Case Study: April 15, 2011. a**, Storm area (navy) defined by daily mean 980 hPa contours (pink). Shaded area indicates the MIZ. Light blue and black contours indicate the sea ice extent on the the first day (April 15) and the last day (April 18) of the storm. **b**, Change in sea ice concentration over the duration of the storm. Daily mean wind vectors are shown for the second day of the storm. The location of the storm's minimum pressure is noted with a yellow star. **c-d**, Daily time series from one week before the storm to two weeks after for (**c**) sea ice area (solid; dashed line depicts the climatological mean ice change for this storm area), (**d**) meridional winds, computed within the MIZ and storm area for this case. **e**, Normalized mean change in MIZ ice area for all southern hemisphere April and May storms in 2010-2019 (gray). The red line depicts the mean MIZ ice area evolution for these storms, and the blue line is the normalized time series for this case study.

April 2011, in the Eastern Weddell and Lazarev Seas (Fig. 5.1). This storm increased local MIZ area by 1.1 $\times 10^5$ km^2 (relative to the 10-year climatological mean) over its four day duration.

Following Mundi et al. (2025), for each cyclone event analyzed here, including this case study, the storm area is defined using daily sea level pressure contours, and a fixed area

of all MIZ points from one day before to one day after the storm is defined (see Methods; Fig. 5.1a). We then track the amount of ice area in this region from one week before the start of the storm to two weeks after and subtract the 10-year climatological mean change in MIZ area to isolate storm impacts (Fig. 5.1c).

The cyclone in Fig. 5.1 began to form on April 15, reaching a minimum sea level pressure of 938 hPa on the following day, eventually beginning to dissipate on April 18. Strong southerly winds on the west side of the storm likely contribute to equatorward spreading of ice, leading to an increase in ice area within the MIZ (Fig. 5.1b, c). Prior to the storm, there was less ice within the MIZ than the 2010-2019 average. However, a large increase in ice area occurred during the storm, bringing the ice area to above average in the two weeks after it passes.

Computing this time series of MIZ ice area for all cyclones, removing the mean climatology and normalizing to better compare storms of different sizes, we find that this behavior is largely typical of intense cyclones in April and May in the southern hemisphere (Fig. 5.1e). Over 90% of the 128 detected storms in this time period (116) lead to an increase in MIZ ice area relative to climatology two weeks after the storm.

Expanding this analysis to all months in both hemispheres, a clear seasonal signal in intense cyclone impacts is evident, with spring and summer cyclones causing the largest declines in MIZ ice area and autumn storms leading to the largest increases (Fig. 5.2). In both decades in the Arctic (Fig. 5.2a,b), the largest enhancement in MIZ ice area occurs in October and November, with September and December close behind in the more recent

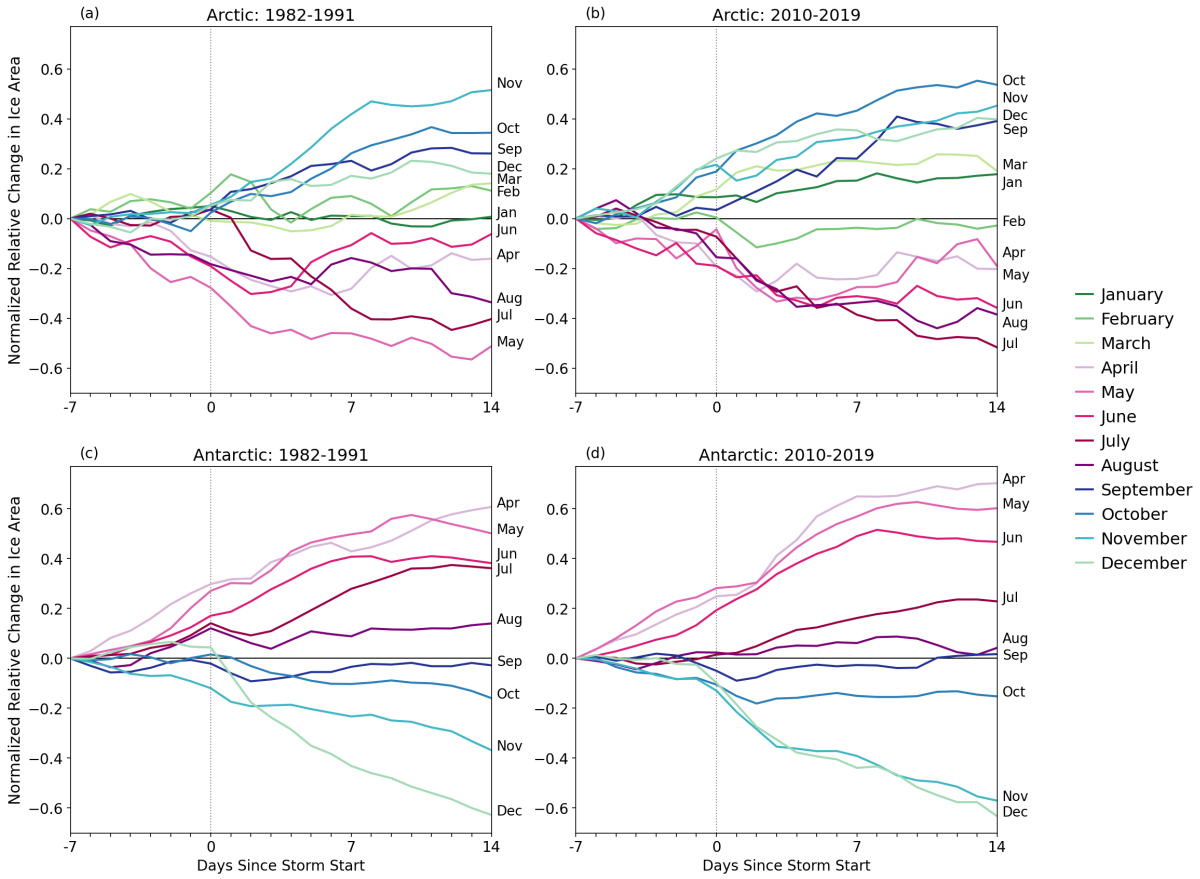

Figure 5.2: **Monthly Mean Change in MIZ Ice Area. a-d**, Normalized mean change in MIZ ice area for the northern (**a,b**) and southern (**c,d**) hemispheres across two decades (**a,c**) 1982-1991 and (**b,d**) 2010-2019. January-March months in the southern hemisphere are excluded due to small sample size.

period. During these months, sea ice is recovering from its smallest extent and has the greatest opportunity for cyclone-enhanced growth within the MIZ. Conversely, some of the greatest declines in Arctic ice area occur just before the minimum sea ice extent, in July and August. Early summer storms in April, May, and June also produce large decreases, especially in the days immediately following the storm. Cyclones in December, January, February, and March cause small increases in the MIZ ice area. In these months, sea ice is growing and reaching its maximum extent. The MIZ in these months is likely

less susceptible to external changes, and its extent is largely limited by land boundaries.

A similar seasonal trend is observed for Antarctic storms (Figs. 5.2c,d). During the ice growth season, from April through June, there is substantial enhanced growth during cyclone events that decreases in magnitude as the ice approaches its maximum extent. Then, in August, September, and October, smaller changes in MIZ ice area are observed as the ice is at its most resilient. Additionally, the ice extent may be limited by the Antarctic Circumpolar Current during these months (Goosse et al., 2025). The largest decreases in Antarctic MIZ ice area occur as the ice approaches its minimum extent, with the most rapid changes occurring right after storm passage, especially in December. Importantly, unlike the Arctic, three southern hemisphere months (January–March) exhibit negligible cyclone impacts on sea ice owing to the limited amount of MIZ ice around the Antarctic continent resulting in very few storms interacting with the ice.

Changes in MIZ ice area have generally increased relative to the 1980s, particularly for southern hemisphere storms, likely due to a generally more responsive present-day ice state and not a change in cyclone characteristics (Fig. C.1).

5.4 Storm-Induced Changes in the MIZ Environment

To better understand the observed seasonal cycle and apparent hemispheric symmetry in cyclone impacts on MIZ area, the modified Taylor diagrams in Fig. 5.3 show the relationship between the monthly mean cyclone impact on the MIZ ice area and several aspects of the cyclone environment. Here, the radial distances of each marker from the

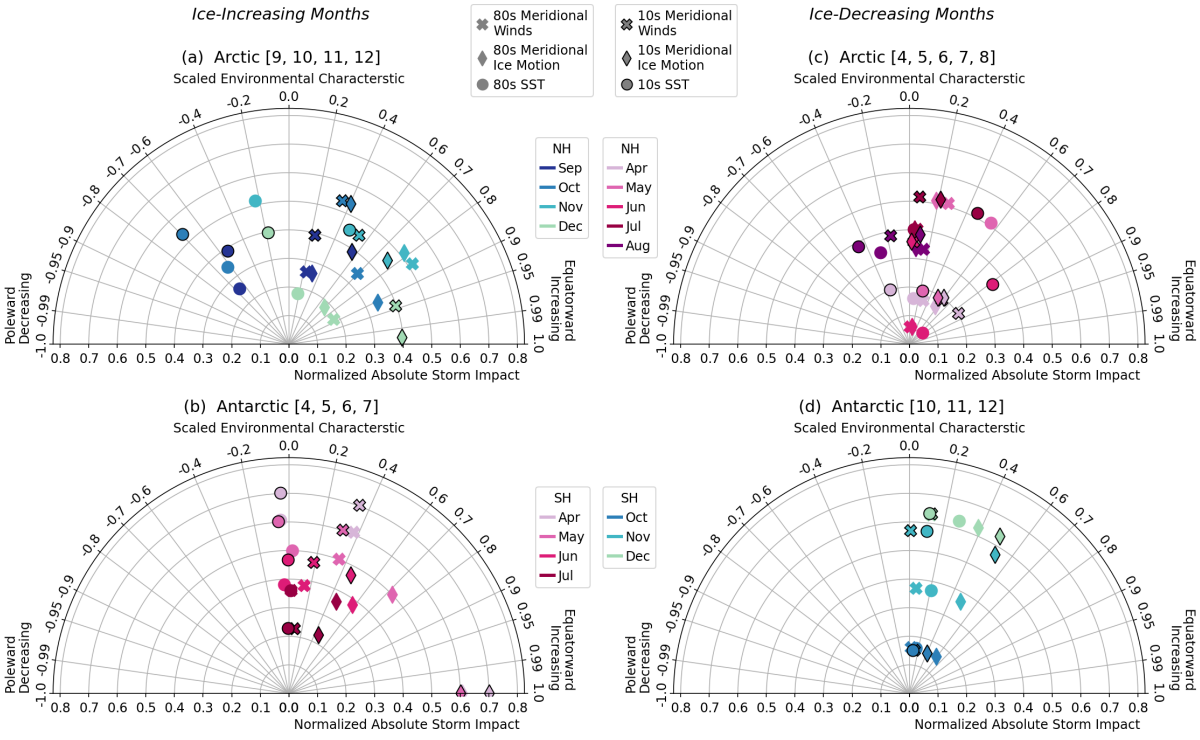

(e)	min	max
Meridional Winds	-3.5 m/s	3.5 m/s
Ice Motion	-3.5 cm/s	3.5 cm/s
Change in SST	-0.45 ˚C	0.45 ˚C

Figure 5.3: **Modified Taylor Diagram Showing Main Environmental Conditions.** **a-d**, Monthly mean meridional wind (X), ice motion (diamond), and change in SST (circle) for (**a**,**b**) ice-increasing months and (**c**,**d**) ice-decreasing months in the Arctic and Antarctic, with outlined markers indicating the more recent decade. **e**, Range of values for each environmental variable.

center show the mean normalized storm impact for each month two weeks after the start of the storm (as in Fig. 5.2) and the angle depicts the magnitude of each environmental characteristic scaled from -1 to 1 based on the range of observed changes listed in Fig. 5.3e. These variables describe the MIZ environment during the storm within the predefined storm area, and they are not necessarily independent of one another (Fig. C.2).

In ice-increasing months, mean cyclone-induced equatorward winds tend to dominate over the MIZ (northerly winds in the Arctic and southerly winds in the Antarctic), whereas

poleward winds play a larger role in ice-decreasing months. These meridional wind values align with the observed mean ice motion characteristics. During periods of sea ice growth, equatorward advection of ice tends to increase ice area due to the opening of leads that then refreeze (Wagner et al., 2021). In the warmer, ice-decreasing months, storm impacts are likely to have a larger compressive component, where thinner ice more easily compacts under poleward advection (Feltham, 2008). However, as the ice ridges, it becomes more resilient to further changes (Maslanik et al., 2007, Schreiber and Serreze, 2020).

Nearby ocean temperatures also affect how winds influence the underlying ice cover. Changes in SST within the MIZ during the two weeks following the storm show trends consistent with seasonal changes. Storms tend to advect ice into cooler water in ice-increasing months and warmer water in ice-decreasing months, compared with conditions at the start of the storm. These SST effects are generally larger in the northern hemisphere, where solar energy is more readily absorbed to heat the mixed layer. SST changes likely supplement the effects of the detected ice motion: the equatorward growth of ice is amplified by cooling oceans in ice-increasing months, while in ice-decreasing months, the slight equatorward drift is coupled with warming trends, promoting the loss of ice. This is particularly effective within the MIZ, where ice is more susceptible to these environmental changes (Clancy et al., 2022).

The changes in SST are generally smaller one week after the storm than two weeks after it, suggesting the ocean environment plays a role in determining cyclone impacts on longer timescales, whereas the impacts of mechanical forces like wind speeds are similar

across both timescales (Fig. C.3). Upper ocean temperatures, significant wave heights, air temperature, mean starting ice concentration, and ice concentration gradient exert second-order effects on the observed changes in ice area (Figs. C.4, C.5, C.6). Winter months near the maximum ice extent that do not experience significant changes in MIZ ice area are clustered near the origin (Fig. C.7).

5.5 The Net Cyclone Impact on Global Sea Ice

A variety of mechanisms lead to different MIZ ice responses to intense cyclones in either hemisphere, though the net effects exhibit some seasonal symmetry. As a result, there is a degree of compensation when the impacts on global ice cover within the MIZ are estimated by summing the total change in area due to all intense cyclones in both hemispheres. This seasonal symmetry is evident in Fig. 5.4a with opposing enhancements and declines occurring in each month in either hemisphere. The southern hemisphere has a larger ice response in most months compared with the northern hemisphere, particularly in austral autumn and early winter, due to the large number of intense Southern Ocean storms interacting with the MIZ (Fig. C.8). These results are robust even when the pressure threshold used to identify storms and the definition of storm area are varied (Section 5.2.1).

The larger impacts of southern hemisphere cyclones in most months coupled with the lack of a significant MIZ around Antarctica in southern hemisphere summer months (January–March) breaks the seasonal symmetry in global cyclone impacts leading to a

net positive cyclone impact on global ice area. Southern hemisphere storms contribute over two thirds of the global net MIZ ice area change two weeks after storm passage (Fig. 5.4b). The results further suggest that total annual changes have amplified in the more recent decade (Fig. C.9). On this timescale, intense cyclones increase the global MIZ ice area by over 26 million km^2 in the 2010s (about 13% of the mean annual ice area), compared to 21 million km^2 in the 1980s over the course of the year. Interestingly, storm impacts are slightly larger one week after storm passage (with a net change of almost 28 million km^2 in the 2010s) but considerably smaller just 3 days after storm passage. While the trajectory of sea ice area varies widely between storms, this provides some indication of the mean timescale of cyclone influence on MIZ area. Globally, August storms have shifted from enhancing ice to destroying it in the more recent decade suggesting more destructive storm-ice interactions recently.

5.6 Discussion

Despite the prevailing attention on the destructive nature of cyclones on sea ice, this study finds that the net effect of intense storms on marginal sea ice globally is to increase ice area over the course of the year. However, net cyclone impacts vary seasonally, with cyclones tending to amplify the seasonal ice cycle within the MIZ in both hemispheres, increasing ice area during the cold season and destroying it during the warm melt season.

We find that the storm's dominant meridional wind and resultant ice motion within the MIZ describes the net changes in ice area. Stronger equatorward winds and ice motion

lead to increases in MIZ ice area in the cold season, whereas the meridional advection directions are more balanced in warmer months. Given the nature of sea ice, particularly within the MIZ, it is easier for storms to pull the ice equatorward than compress it poleward (Wang et al., 2022). During the warm season, the more susceptible ice easily forms ridges under poleward advection whereas the stronger winter ice is more resistant (Maslanik et al., 2007). As storms advect ice poleward, ice can easily grow behind it, allowing for large increases in MIZ ice area during the cold season (Wagner et al., 2021). However, ridged ice in summer becomes more resilient to additional changes minimizing the storm's overall impact. The observed changes in SST further augment the seasonal storm impacts, limiting the expansion of ice in the summer with nearby increases in SST and aiding the growth of ice in the winter with cooling temperatures.

Southern hemisphere storms tend to dominate the annual cycle of global sea ice cover, likely due to the increased frequency of storms around Antarctica during the cold season. Ultimately, this tendency towards more impactful storm characteristics around Antarctica leads to a net increase of MIZ ice area over the year, due to the lack of MIZ area around the continent in late austral summer. Overall, we find that with the presence of intense storms in the polar regions, there is a greater area of MIZ ice than without. This effect has increased in magnitude in recent years relative to earlier in the satellite era, consistent with sea ice becoming increasingly vulnerable to storms (Mundi and L'Ecuyer, 2025, Mundi et al., 2025). As the climate continues to warm, we may continue to see amplified or otherwise changing storm impacts on the MIZ (Mundi et al., 2025) and, in turn, the ocean surface energy balance.

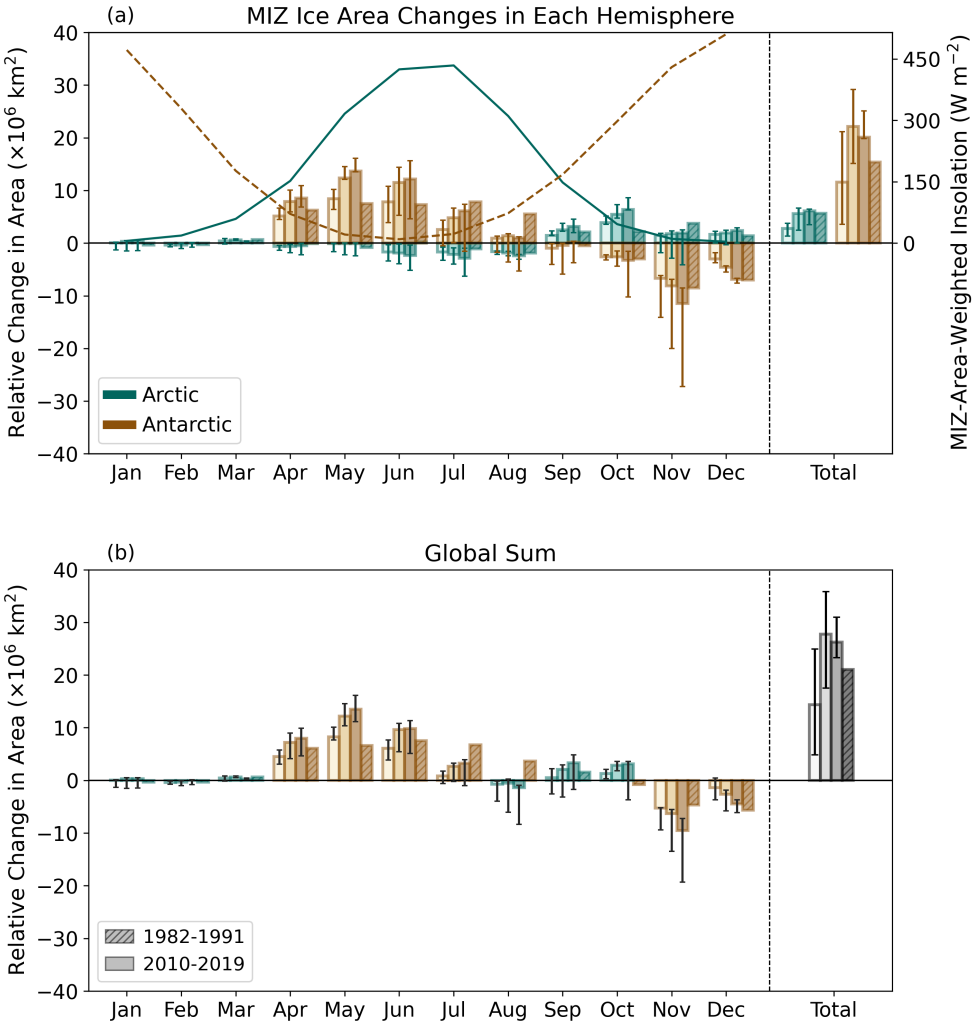

Figure 5.4: **Monthly Mean 3-, 7-, and 14-day Changes in MIZ Ice Area. a**, Monthly changes in MIZ ice area due to cyclone influence across three timescales (light = 3 days, medium = 7 days, and dark = 14 days) in the Arctic (blue) and Antarctic (brown) for 2010-2019 (solid) and the two-week change for 1982-1991 (dashed). Net annual changes are shown for each hemisphere (Total). The MIZ-area-weighted monthly mean insolation is shown for the northern (blue solid line) and southern (brown dashed line) hemispheres for reference. **b**, Summed changes for each month. Colors indicate which hemisphere has the larger impact in each month. The total global change across all months is shown in grayscale.

Chapter 6

Conclusions

6.1 Synthesis

Sea ice plays an important role in modulating energy at the surface, and understanding processes that impact the changing ice cover are increasingly important in a warming climate. The aim of the present research was to investigate the impact of cyclones on the marginal ice zone during the vulnerable Arctic summer both early in the satellite era and present-day, as well as in the future under changing sea ice conditions, and then consider how global MIZ ice impacts evolve throughout the year. In doing so, we asked three main research questions. The questions are restated here and the key points are summarized.

1. Is the modern Arctic MIZ more susceptible to summer cyclones?

In Chapter 3, we analyzed a census of over 250 cyclone cases, sorting by mean meridional wind direction and SST within the MIZ in the region of each storm, guided by the opposing mechanisms of two case studies. We find that more than half of these storms decrease ice area within the MIZ relative to climatology, and that present-day storms are more likely to have ice-decreasing storms than earlier in the satellite record. This result corresponds with a shift towards more early summer storms in the recent decade, which are also more likely to decrease ice area than late summer storms. The effects of cyclones on sea ice are also found to vary depending on the dominant wind direction and, to a lesser extent, nearby ocean temperatures. Cyclones that primarily enhance southerly winds result in decreases in MIZ ice area, and cyclones that enhance northerly winds result in increases in MIZ ice area. Yet considerable variations in individual cyclones' impacts remain even when controlling for these factors. These bulk diagnostics therefore only explain part of the complex ice-cyclone relationship.

2. Have impacts of intense Arctic cyclones on summer sea ice reached a maximum?

Chapter 4 builds upon the differences observed between 2010s storms and 1980s storms in the previous chapter, and assesses how intense cyclone impacts may evolve in the future. First, CESM2-LE was evaluated for how well it replicated observations of past cyclones. We found that CESM2-LE reproduces observed recent cyclone impacts on MIZ ice but exhibits compensating biases: too few storms exerting too strong impacts. And although these biases exist, CESM2-LE is still a useful model for predicting how cyclone impacts may evolve in the future. We find that total MIZ summer ice loss by storms is predicted

to decline after present day, suggesting intense cyclone impacts have reached a maximum. As late-summer sea ice recedes in the future, fewer storms reach the MIZ and the largest decreases in ice area occur earlier in the summer.

3. How do storm impacts vary seasonally and in the southern hemisphere?

Finally, we expanded the impacts of intense storms within the observational record to include all months of the year and southern hemisphere storms. We have shown that cyclone impacts vary seasonally, with cyclones tending to amplify the seasonal ice cycle within the MIZ in both hemispheres. We find that the storm's dominant meridional wind and subsequent ice motion within the MIZ describes the net changes in ice area. Stronger equatorward winds and ice motion lead to increases in MIZ ice area in the cold season, whereas the meridional advection directions are more balanced in warmer months. Southern hemisphere storms largely dominate the annual cycle, with especially large increases in MIZ ice area during autumn and early winter months likely due to the increased frequency of intense storms around Antarctica during these months. These increases are partially offset by ice losses in early austral summer, however a net increase in MIZ ice area over the year is still observed as the low overall ice extent limits further losses in area in late summer months. This asymmetric annual cycle results in a greater area of global MIZ ice when storms are present in the polar regions than without, an effect that has increased in recent years.

In answering these three research questions, we have highlighted the complex role of cyclone impacts on the ice edge and have explored how they may change in a warming

climate with changing ice conditions.

6.2 Future Work

Despite the conclusions outlined here, more work remains in understanding the role of cyclones in the polar climate system. Chapter 5 emphasized the opposite cyclone impacts that occur in spring and summer months compared with the months leading up to the maximum ice extent, and Chapter 4 highlighted how summertime storm impacts may evolve in a warming climate. A further study could investigate how fall and winter storm impacts will also change in future decades. With lesser ice extents going into the cold season, there could be more open ocean for the advective mechanism of cyclones to further enhance ice growth as summer ice minima tend to decline. Additionally, Chapter 4 identified key biases in understanding modeled storm impacts in the Arctic. The question still remains if these biases occur in the southern hemisphere as well. And through additionally examining the cyclones around Antarctica, we can quantify the net global ice area change within the CESM2-LE. By having a complete picture of seasonal and hemispheric cyclone impacts in global climate models, predictions of future cyclone impacts and sea ice changes can be more accurate.

Appendix A

Supplementary Information for Chapter 3

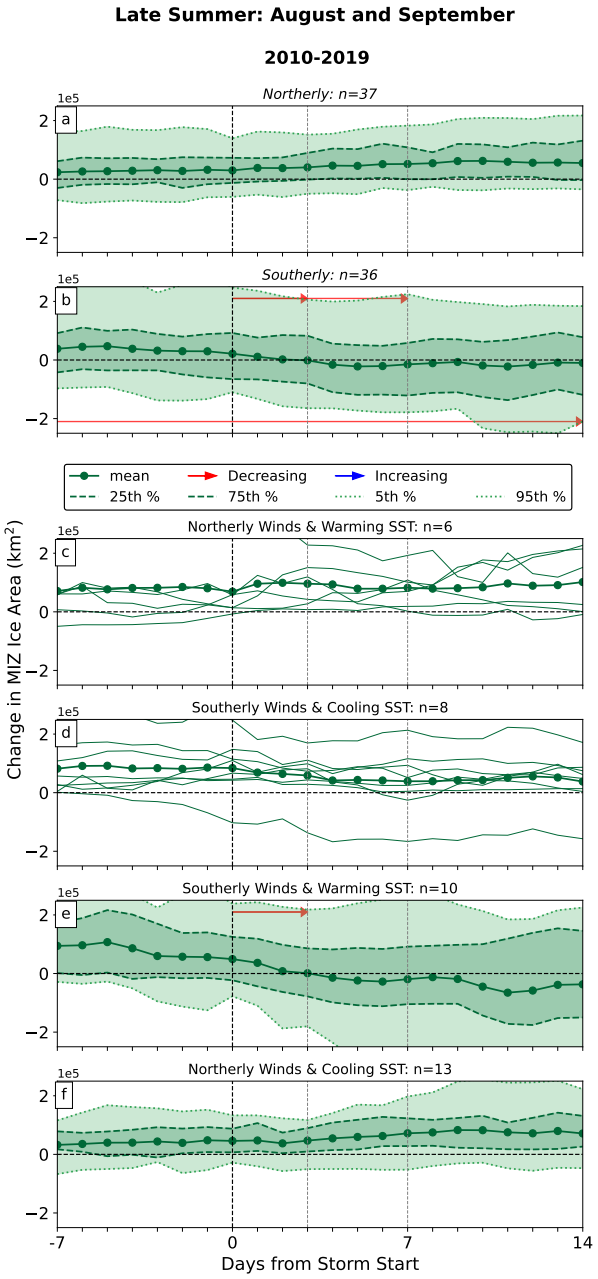

Figure A.1: Composite plots showing the change in MIZ ice area for the three weeks around cyclones occurring in late-summer 2010–2019 (as in Section 3c of the main text, but without the normalization procedure applied). (a-b) Categories based on the primary wind direction and within the storm area. (c-f) Categories are based on the primary wind direction and SST trend during the time of the cyclone. The mean values and the 5th, 25th, 75th, and 95th percentiles are plotted. The arrows represent the portion of the plot where the distribution of slopes of the mean normalized area time series has a statistically significant ($p < 0.05$) difference from zero. The slopes are computed over different sections of the time series: the week leading up to the storm (days -7 to 0; top of plots), after the storm (days 0 to 3, 0 to 7, 0 to 14; top of plots), or over the full three-week time series (days -7 to 14; bottom of plots).

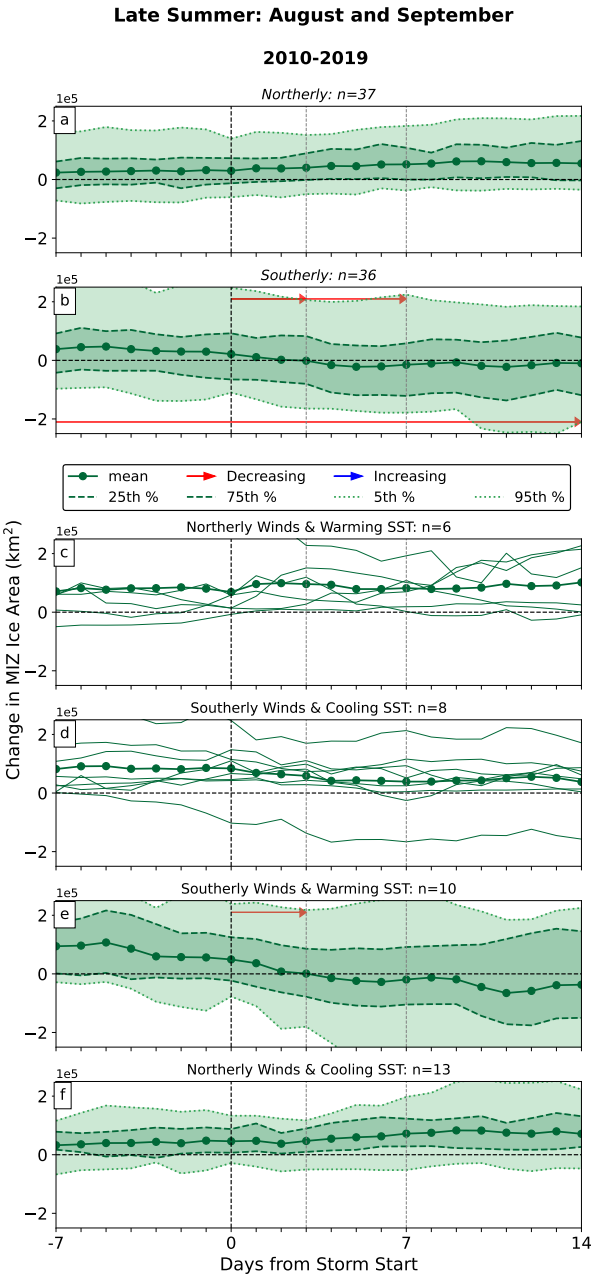

Figure A.2: As in Figure A.1, but for early-summer months in 2010–2019.

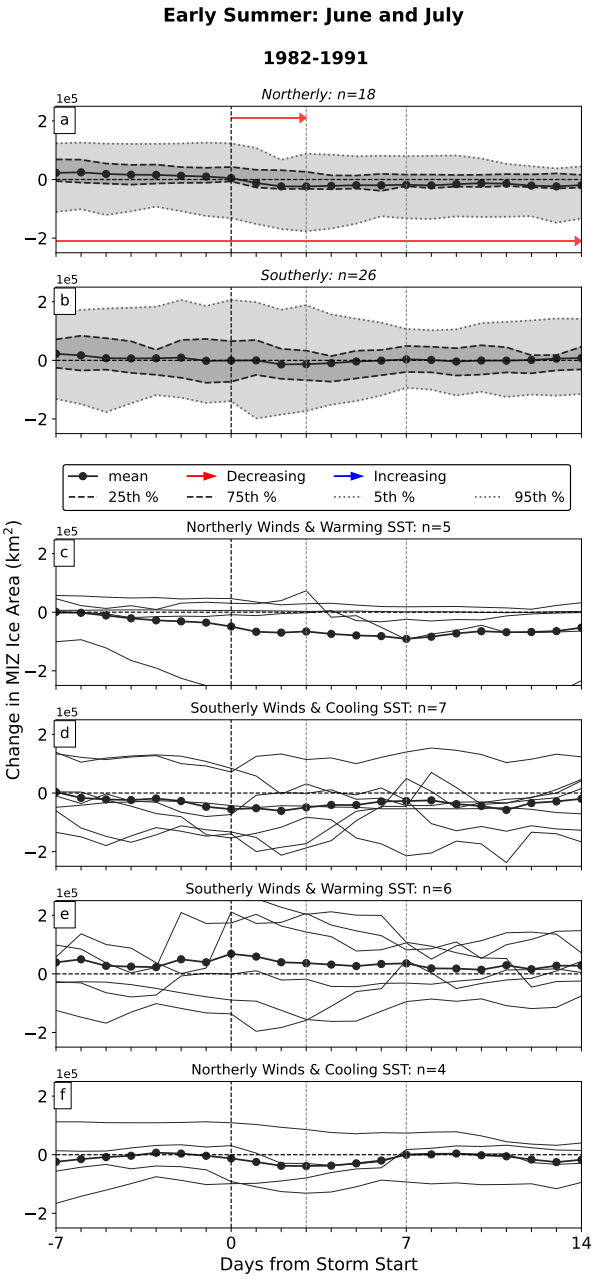

Figure A.3: As in Figure A.1, but for late-summer months in 1982–1991.

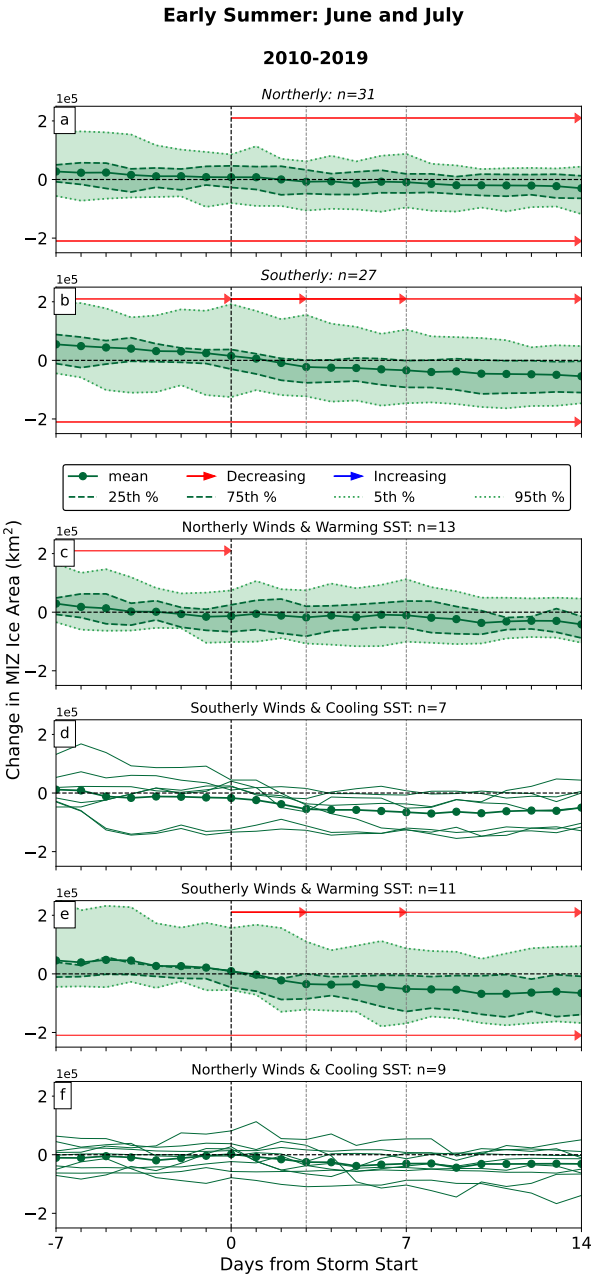

Figure A.4: As in Figure A.1, but for early-summer months in 1982–1991.

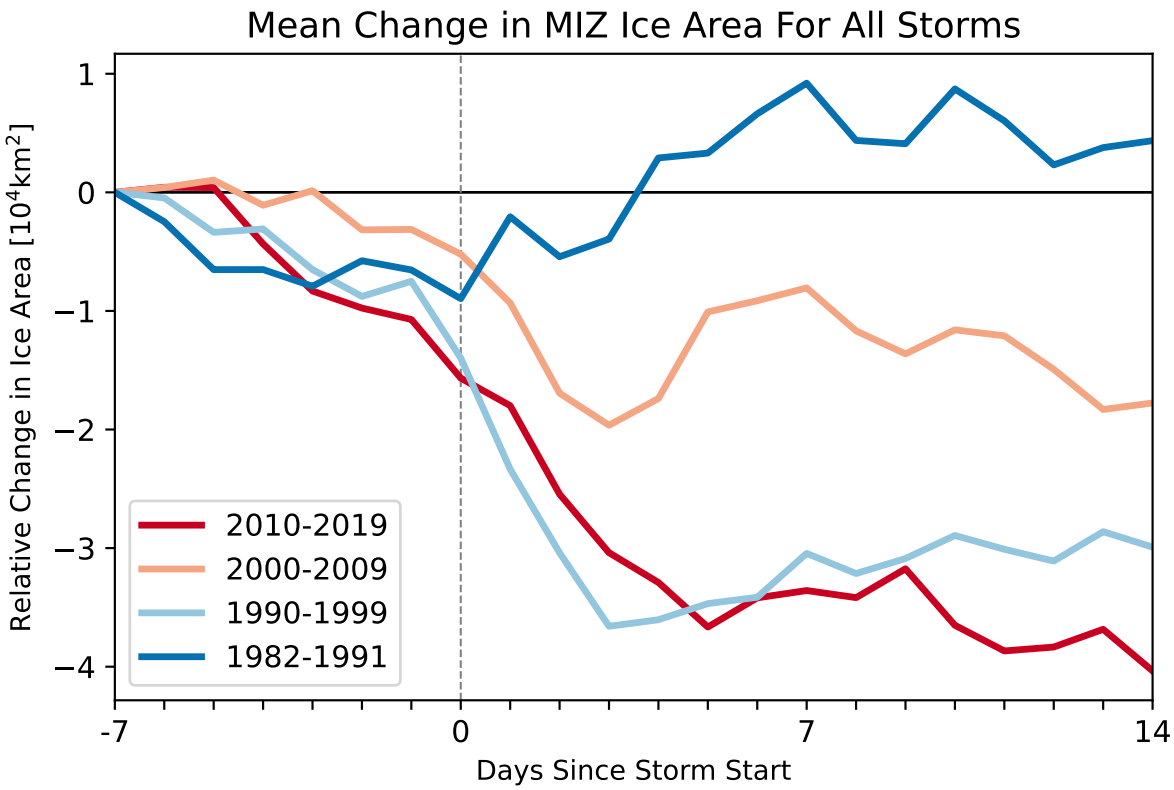

Figure A.5: Change in MIZ ice area relative to the start of the analysis time window for four decades of cyclone events (as in Figure 14a of Chapter 3, but without the normalization procedure applied).

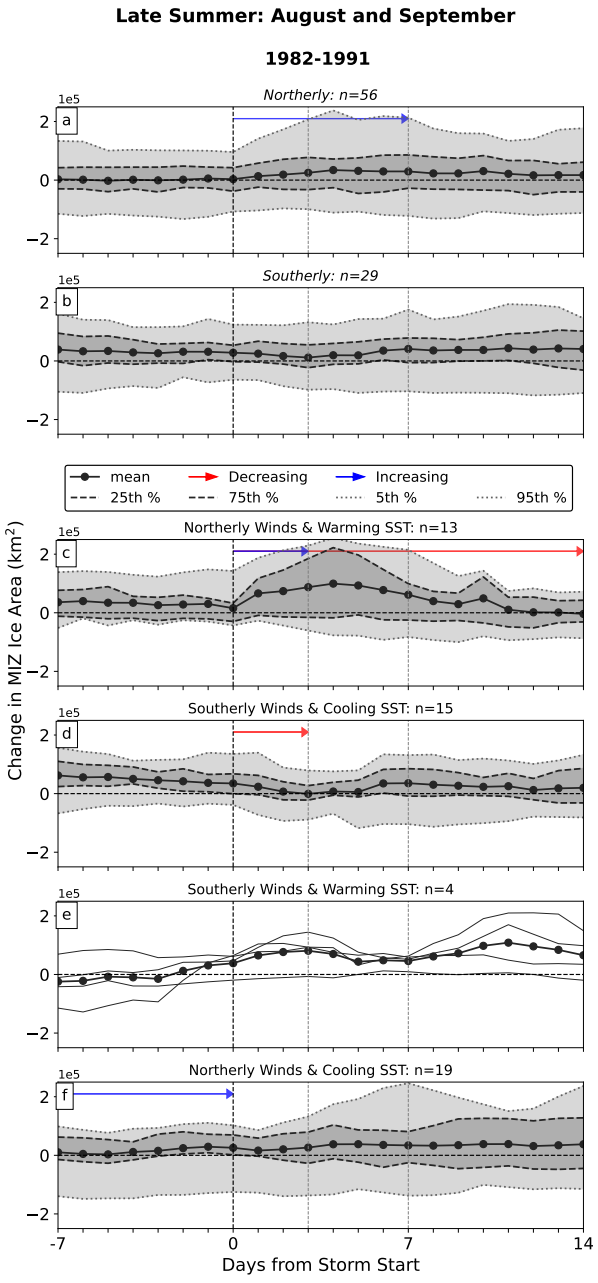

Figure A.6: As in Figure 15 of Chapter 3, but without the normalization procedure applied. Categories are based on the primary wind direction for early-summer months (a,b) and late-summer months (c,d) in 1990–1999.

Appendix B

Supplementary Information for Chapter 4

Figures B.1a-c show the beginning stages of a cyclone identified in ERA5 that develops and moves across the East Siberian and Chukchi seas from August 5-7, 2017, eventually reaching a minimum pressure of 981.5 hPa. The sea level pressure first reaches below the threshold on the first day of the storm at 16Z. To obtain a similar start date and trajectory at the resolution of CESM2, the selected pressure threshold must be increased by 2 hPa (as shown in Figures S1d-f). This ensures that a similar duration and spatial extent of the storm is reproduced at the modeled resolution throughout the evolution of this cyclone. As a result of these modifications, the minimum pressure used to identify intense cyclones was increased from 984 hPa to 986 hPa. A constant pressure threshold is suitable for summer months as the background pressure of the Arctic does not substantially change

over the selected four months. Therefore, this value represents the same deviation from the mean. To establish sufficient interaction with the ice edge, we found the sea ice concentrations with the lowest root mean square difference from 15% and 80%. This new definition of the marginal ice zone (MIZ) is shown in Figures B.1g-f.

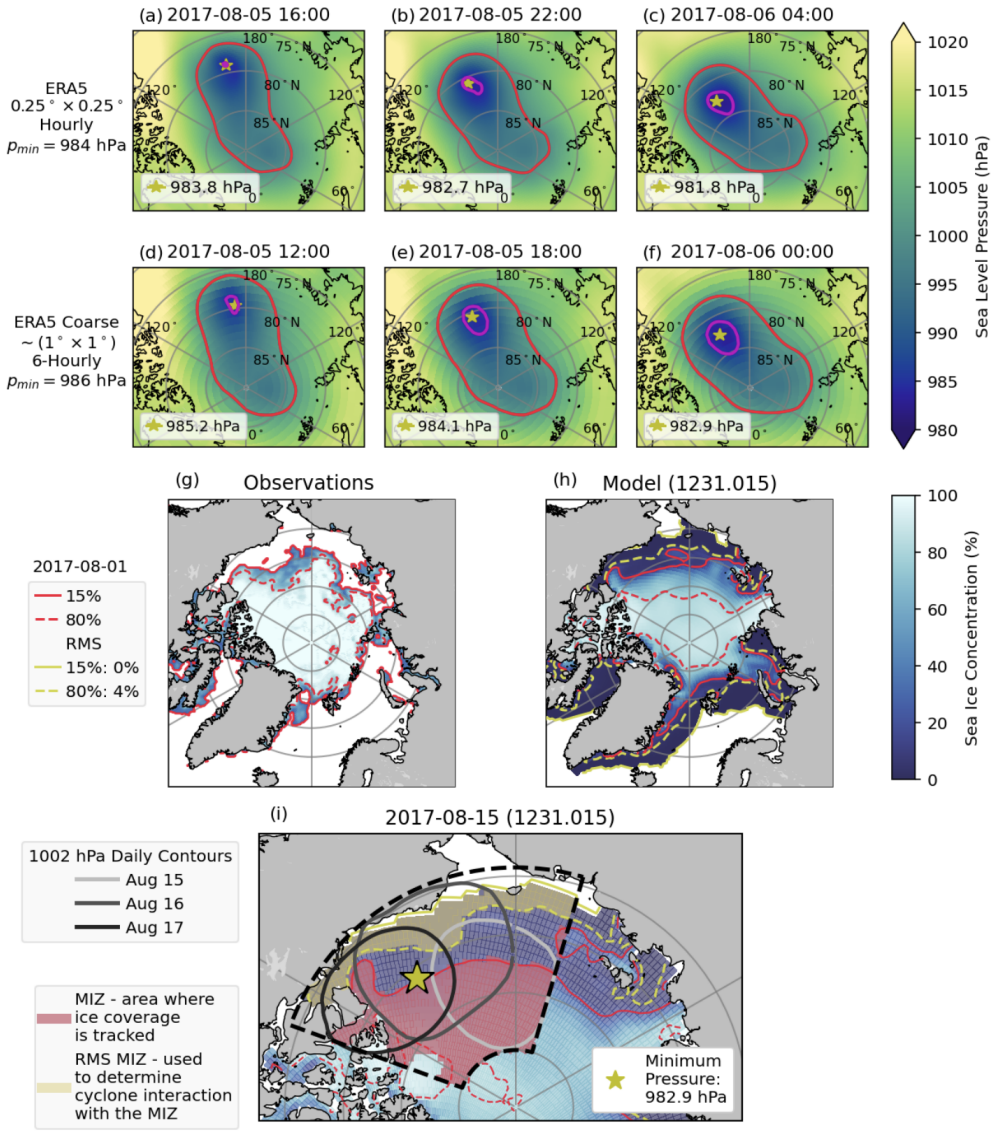

Figure B.1: ERA5 mean sea level pressure at the original resolution (a-c) and scaled to match the resolution of CESM2 (d-f). Magenta and red contours indicate the 984 and 1000 hPa isobars in (a-c) and the 986 and 1002 hPa isobars in (d-f). Yellow stars mark the location of the minimum pressure. The horizontal and temporal resolutions of the datasets are listed alongside the minimum pressure (p_{min}) used for cyclone detection. Sea ice concentration for August 1, 2017, from (g) satellite observations and (h) one ensemble member of the CESM2-LE. Sea ice concentration contours for 15% (solid) and 80% (dashed) are shown in red. The root mean square (RMS) equivalent contours are shown in yellow, indicating the same fractional area as the 15% and 80% contours in satellite observations. (i) Example cyclone event. Black dashed line indicates the storm area based on the daily 1002 mb contours (grayscale). Yellow shaded area is the equivalent MIZ area used to determine the cyclone's interaction with the MIZ. Red shaded area is region MIZ ice area is tracked, defined as all 15%-80% sea ice concentration points from one day before to one day after the storm.

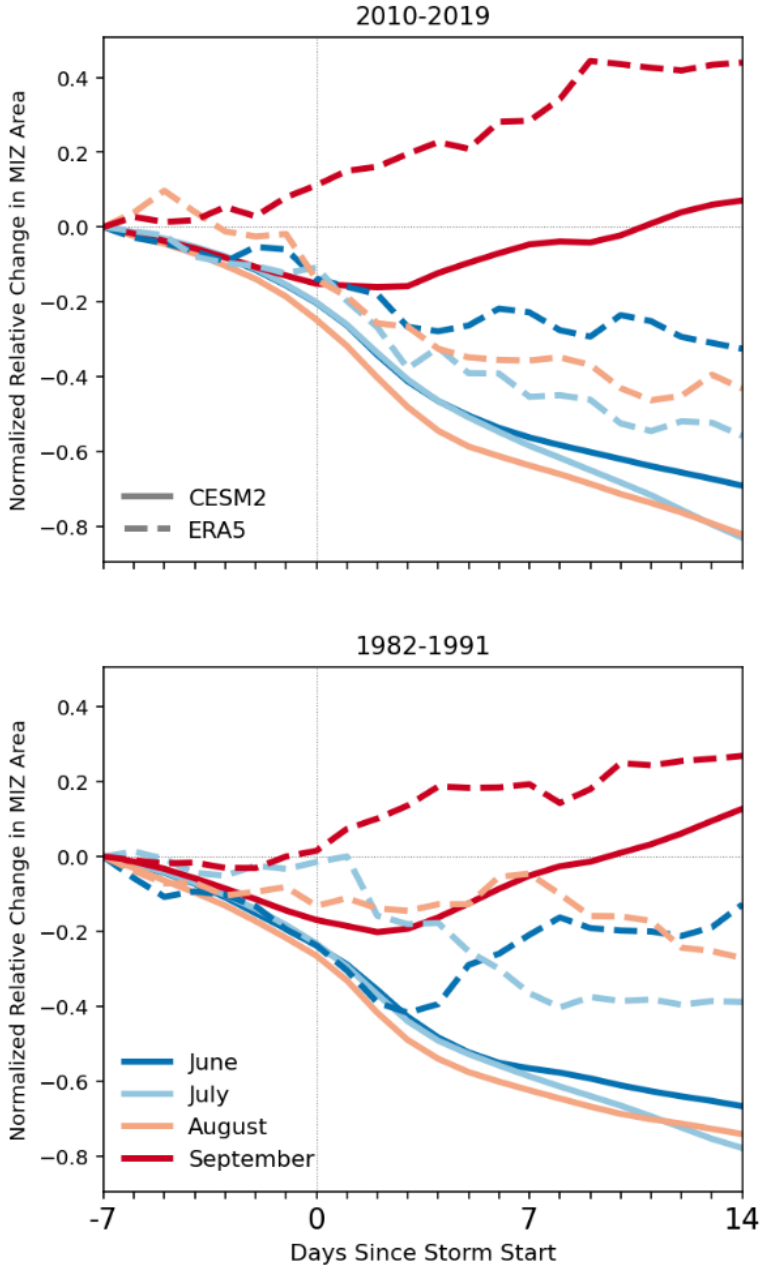

Figure B.2: Normalized changes in the MIZ ice area relative to the start of the analysis time window for each month in (top) 2010–19 and (bottom) 1982–91 for modeled (solid) and observed (dashed) storms. Storm time series were normalized by the range (minimum value subtracted from the maximum value) of the series to composite cyclone effects without preferentially weighting spatially larger storms, as in Mundi and L'Ecuyer (2025).

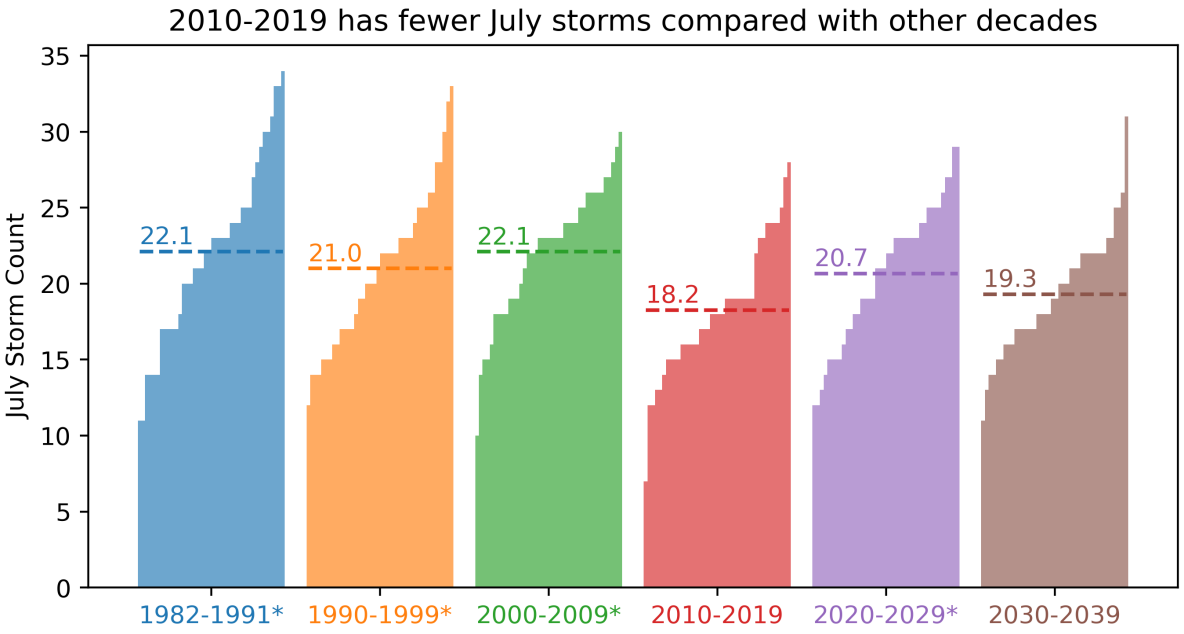

Figure B.3: Number of July storms across the 40 ensemble members considered for the six decades from the 1980s to the 2030s. Value and dashed line indicate the average storm count across the ensemble members for each decade. Asterisk depicts a statistically significant difference in count distributions at the 95% level. The 2010s has the fewest number of cyclones, contributing to the minimum in total cyclone impacts in Figure 4.4.

Appendix C

Supplementary Information for Chapter 5

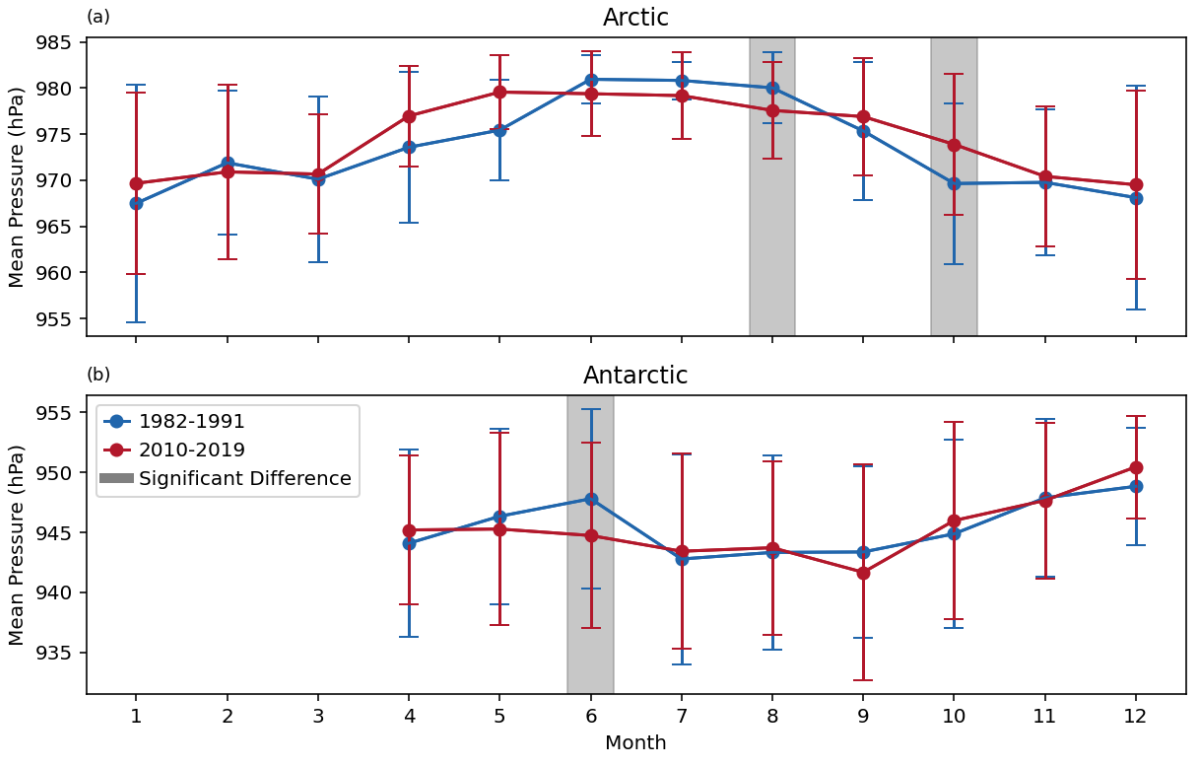

Figure C.1: **Monthly Minimum Storm Pressures. a-b**, Mean and standard deviation minimum storm pressures for each month for (**a**) Arctic and (**b**) Antarctic storms, with the 1980s shown in blue and 2010s in red. Shaded regions indicate statistically significant distributions in central pressures between the two decades.

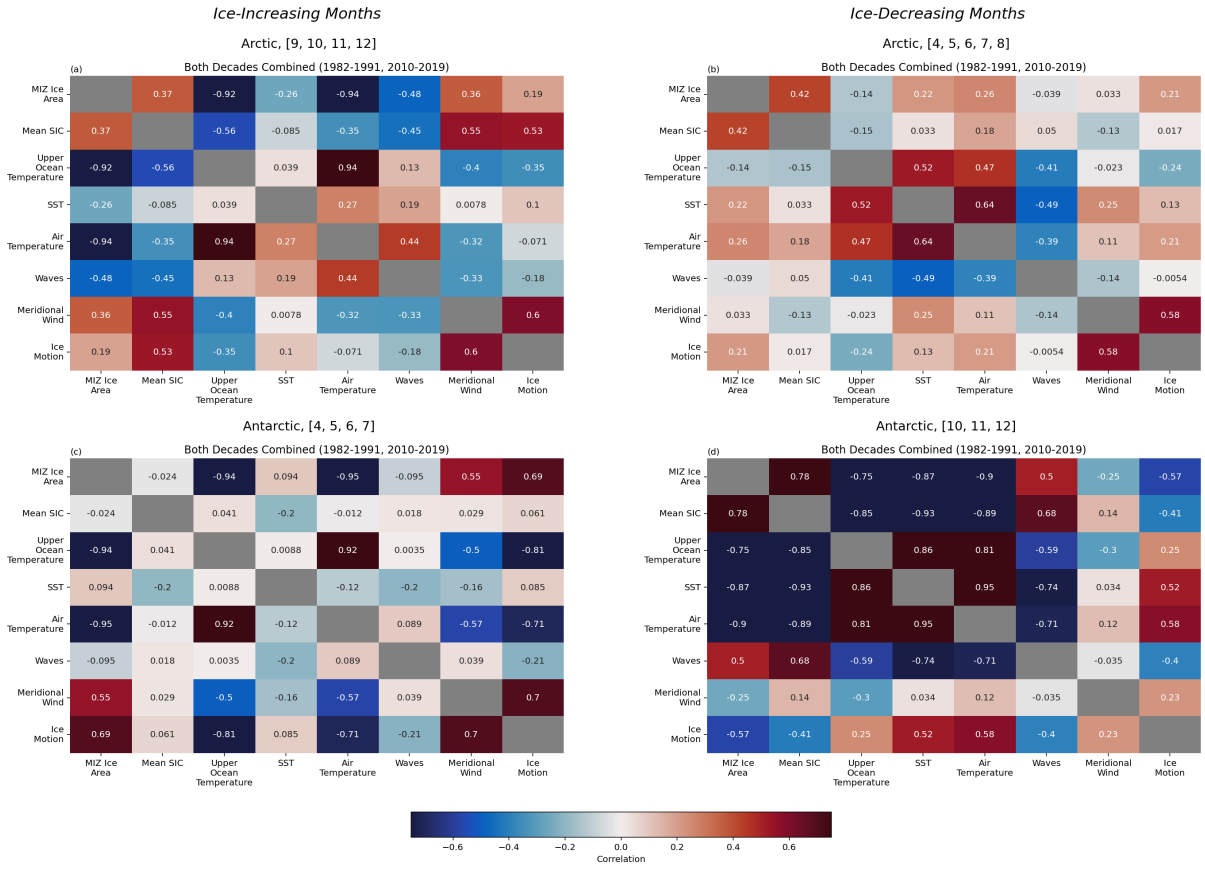

Figure C.2: **Correlation Matrix of Environmental Characteristics. a-d**, Correlation values for mean changes in each variables over two weeks following storm starts from both decades for (**a**,**c**) ice-increasing months and (**b**,**d**) ice-decreasing months in the Arctic and Antarctic.

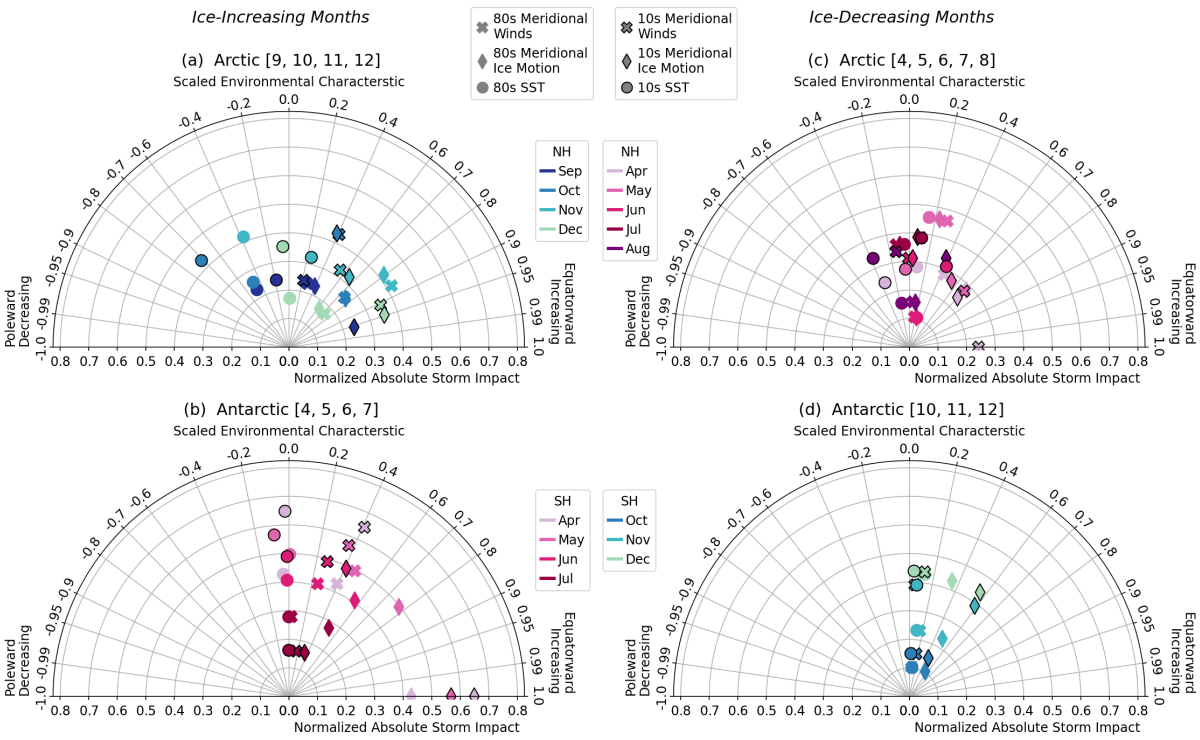

	min	max
Meridional Winds	-3.5 m/s	3.5 m/s
Ice Motion	-3.5 cm/s	3.5 cm/s
Change in SST	-0.45 °C	0.45 °C

Figure C.3: **Modified Taylor Diagram Showing Main Environmental Conditions One Week After Storm. a-d**, Monthly mean meridional wind (X), ice motion (diamond), and change in SST (circle) for (**a**,**b**) ice-increasing months and (**c**,**d**) ice-decreasing months in the Arctic (**a**,**c**) and Antarctic (**b**,**d**), with outlined markers indicating the more recent decade. The range of values for each environmental variable is shown in the table.

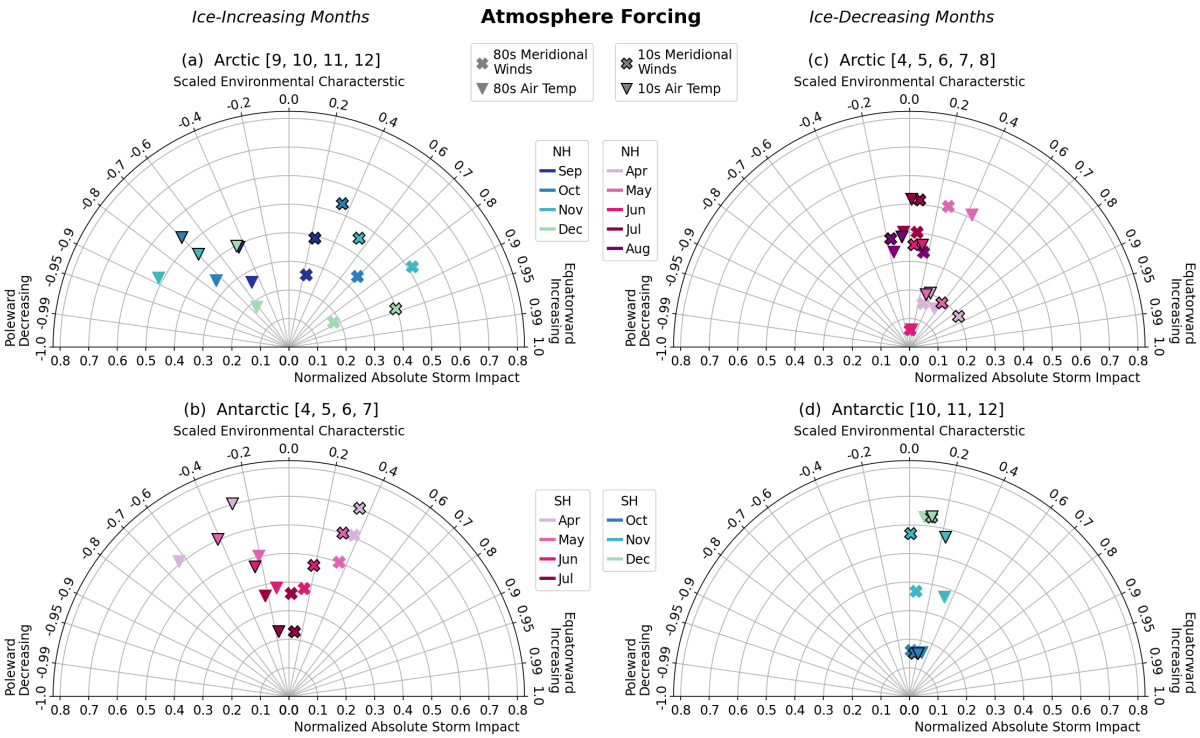

	min	max
Meridional Winds	-3.5 m/s	3.5 m/s
Air Temperature	-0.45 ˚C	0.45 ˚C

Figure C.4: **Modified Taylor Diagram Showing Atmosphere Conditions. a-d**, Monthly mean atmosphere conditions during intense cyclone events. Mean meridional wind (X) and 2 m air temperature (triangle) for (**a**,**b**) ice-increasing months and (**c**,**d**) ice-decreasing months in the Arctic and Antarctic, are shown with outlined markers indicating the more recent decade. The range of values for each environmental variable is shown in the table.

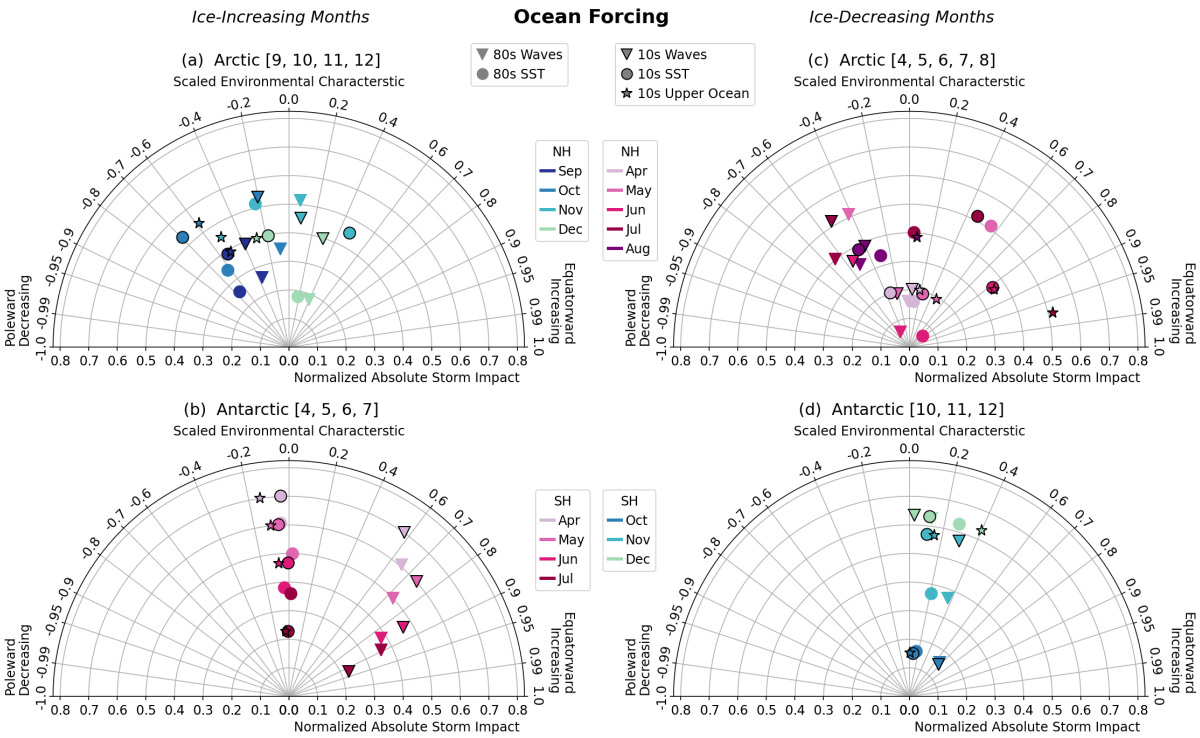

(e)	min	max
Wave Height	0 m	3.5 m
Change in SST	-0.45 ˚C	0.45 ˚C
Change in Upper Ocean Temperature	-1 ˚C	1 ˚C

Figure C.5: **Modified Taylor Diagram Showing Ocean Conditions. a-d**, Monthly mean ocean conditions during intense cyclone events. Mean significant wave height (triangle), change in SST (circle), and change in upper ocean temperature (star) for (**a**,**b**) ice-increasing months and (**c**,**d**) ice-decreasing months in the Arctic and Antarctic, are shown, with outlined markers indicating the more recent decade. The range of values for each environmental variable is shown in the table.

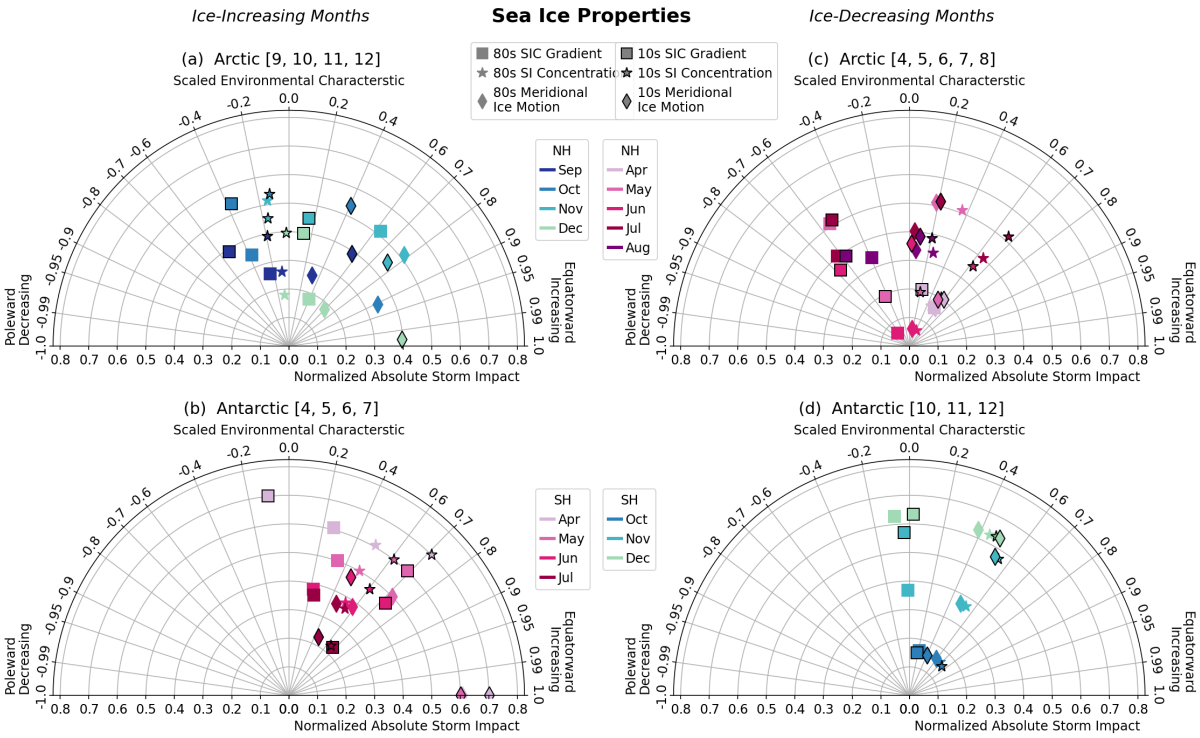

	min	max
SIC Gradient	0% km^{-1}	10% km^{-1}
Sea Ice Concentration	40%	60%
Ice Motion	-3.5 cm/s	3.5 cm/s

Figure C.6: **Modified Taylor Diagram Showing Sea Ice Conditions. a-d**, Monthly mean ocean conditions during intense cyclone events. Mean sea ice concentration (SIC) gradient (square), mean SIC at the start of each storm (star), and mean meridional ice motion (diamond) for (**a**,**b**) ice-increasing months and (**c**,**d**) ice-decreasing months in the Arctic and Antarctic, are shown, with outlined markers indicating the more recent decade. The range of values for each environmental variable is shown in the table.

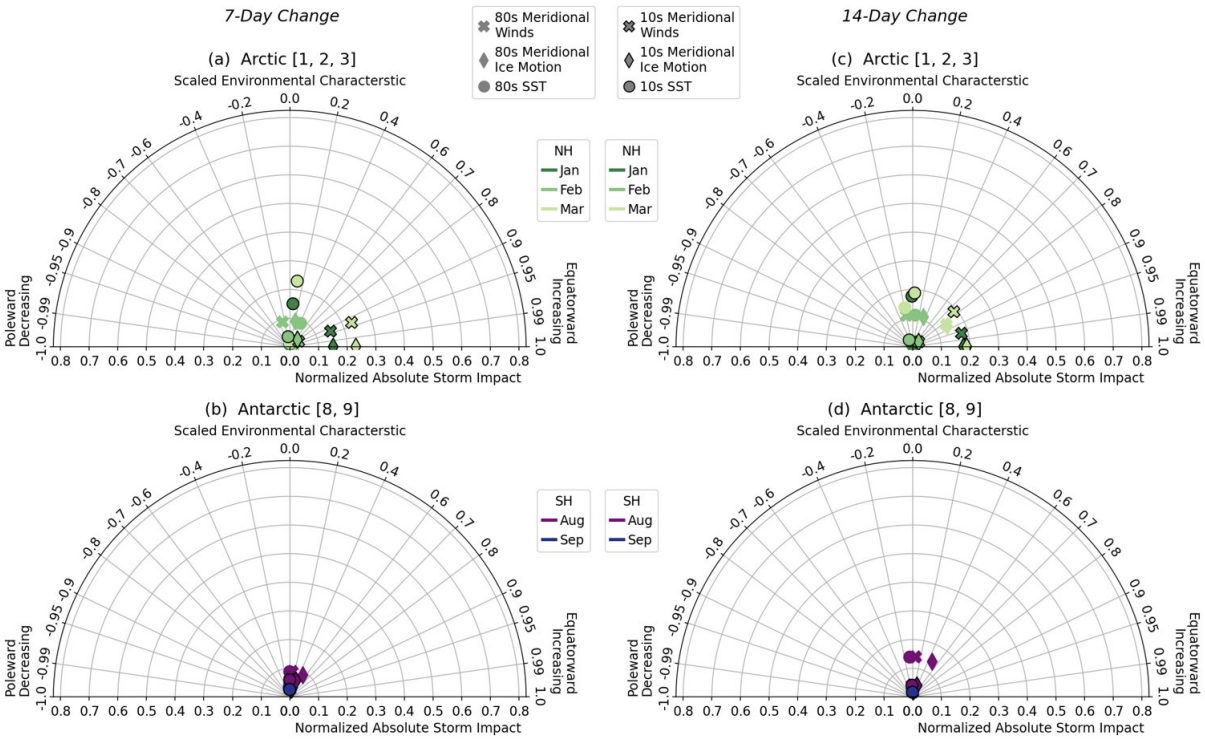

	min	max
Meridional Winds	-3.5 m/s	3.5 m/s
Ice Motion	-3.5 cm/s	3.5 cm/s
Change in SST	-0.45 ° C	0.45 ° C

Figure C.7: **Modified Taylor Diagram Showing Main Environmental Conditions during Ice Maximum Months. a-d**, Monthly mean meridional wind (X), ice motion (diamond), and change in SST (circle) for (**a**,**b**) one-week timescales and (**c**,**d**) two-week timescales in the Arctic (**a**,**c**) and Antarctic (**b**,**d**), with outlined markers indicating the more recent decade. The range of values for each environmental variable is shown in the table.

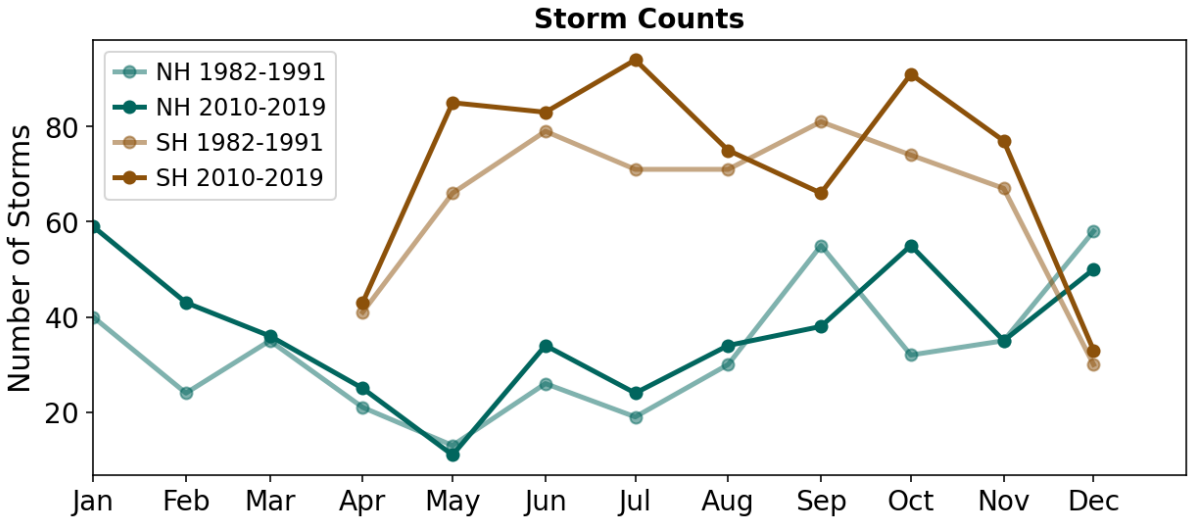

Figure C.8: **Monthly Storm Counts.** Monthly intense cyclone counts for Northern Hemisphere (blue) and Southern Hemisphere (brown) for each decade.

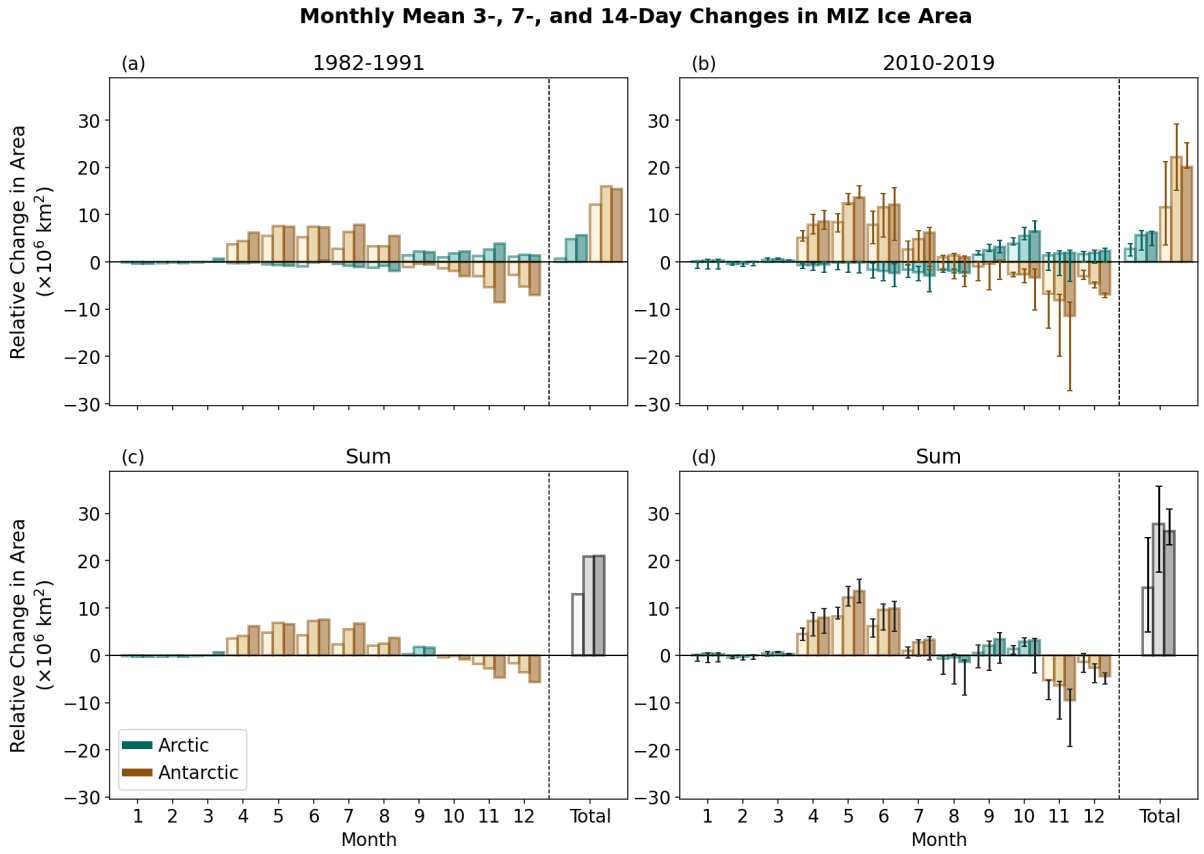

Figure C.9: **Monthly Mean 3-, 7-, and 14-day Changes in MIZ Ice Area. a-b**, Monthly changes in MIZ ice area due to cyclone influence across three timescales (light = 3 days, medium = 7 days, and dark = 14 days) in the Arctic (blue) and Antarctic (brown) for (**a**) 1982-1991 and (**b**) 2010-2019 Net annual changes are shown for each hemisphere (Total). **c-d** Summed changes for each month for (**c**) 1982-1991 and (**d**) 2010-2019. Colors indicate which hemisphere has the larger impact in each month. The total global change across all months is shown in grayscale.

Bibliography

Akperov, M., I. Mokhov, A. Rinke, K. Dethloff, and H. Matthes, 2015: Cyclones and their possible changes in the Arctic by the end of the twenty first century from regional climate model simulations. *Theoretical and Applied Climatology*, **122**, 85–96.

Aue, L. and A. Rinke, 2023: Cyclone impacts on sea ice concentration in the Atlantic Arctic Ocean: Annual cycle and recent changes. *Geophysical Research Letters*, **50**, e2023GL104657.

Aue, L., T. Vihma, P. Uotila, and A. Rinke, 2022: New insights into cyclone impacts on sea ice in the Atlantic sector of the Arctic Ocean in winter. *Geophysical Research Letters*, e2022GL100051.

Bailey, D. A., M. M. Holland, A. K. DuVivier, E. C. Hunke, and A. K. Turner, 2020: Impact of a new sea ice thermodynamic formulation in the CESM2 sea ice component. *Journal of Advances in Modeling Earth Systems*, **12**, e2020MS002154.

Blanchard-Wrigglesworth, E., S. Brenner, M. Webster, C. Horvat, Ø. Foss, and C. M. Bitz, 2024: Model biases in simulating extreme sea ice loss associated with the record January

2022 Arctic cyclone. *Journal of Geophysical Research: Oceans*, **129**, e2024JC021127.

Blanchard-Wrigglesworth, E., M. Webster, L. Boisvert, C. Parker, and C. Horvat, 2022: Record Arctic cyclone of January 2022: Characteristics, impacts, and predictability. *Journal of Geophysical Research: Atmospheres*, **127**, e2022JD037161.

Box, J. E., W. T. Colgan, T. R. Christensen, N. M. Schmidt, M. Lund, F.-J. W. Parmentier, R. Brown, U. S. Bhatt, E. S. Euskirchen, V. E. Romanovsky, et al., 2019: Key indicators of Arctic climate change: 1971–2017. *Environmental Research Letters*, **14**, 045010.

Brümmer, B., D. Schröder, G. Müller, G. Spreen, A. Jahnke-Bornemann, and J. Launiainen, 2008: Impact of a Fram Strait cyclone on ice edge, drift, divergence, and concentration: Possibilities and limits of an observational analysis. *Journal of Geophysical Research: Oceans*, **113**.

C3S, 2023: ERA5 hourly data on single levels from 1940 to present. *Copernicus Climate Change Service (C3S) Climate Data Store (CDS)*, doi:10.24381/cds.adbb2d47.

Cai, L., V. A. Alexeev, and J. E. Walsh, 2020: Arctic sea ice growth in response to synoptic-and large-scale atmospheric forcing from CMIP5 models. *Journal of Climate*, **33**, 6083–6099.

Carmack, E., I. Polyakov, L. Padman, I. Fer, E. Hunke, J. Hutchings, J. Jackson, D. Kelley, R. Kwok, C. Layton, et al., 2015: Toward quantifying the increasing role of oceanic

heat in sea ice loss in the new Arctic. *Bulletin of the American Meteorological Society*, **96**, 2079–2105.

Chen, Y., Y. Liang, X. Chen, and H. Bi, 2025: Arctic cyclone activity changes under a warming climate. *npj Climate and Atmospheric Science*.

Clancy, R., C. M. Bitz, E. Blanchard-Wrigglesworth, M. C. McGraw, and S. M. Cavallo, 2022: A cyclone-centered perspective on the drivers of asymmetric patterns in the atmosphere and sea ice during Arctic cyclones. *Journal of Climate*, **35**, 73–89.

Comiso, J. C., 2012: Large decadal decline of the Arctic multiyear ice cover. *Journal of Climate*, **25**, 1176–1193.

Cox, T., A. Donohoe, K. C. Armour, D. M. Frierson, and G. H. Roe, 2024: Trends in atmospheric heat transport since 1980. *Journal of Climate*, **37**, 1539–1550.

Crawford, A. D., E. A. Schreiber, N. Sommer, M. C. Serreze, J. C. Stroeve, and D. G. Barber, 2021: Sensitivity of northern hemisphere cyclone detection and tracking results to fine spatial and temporal resolution using ERA5. *Monthly Weather Review*, **149**, 2581–2598.

Crawford, A. D. and M. C. Serreze, 2016: Does the summer Arctic frontal zone influence Arctic Ocean cyclone activity? *Journal of Climate*, **29**, 4977–4993.

— 2017: Projected changes in the Arctic frontal zone and summer Arctic cyclone activity in the CESM large ensemble. *Journal of Climate*, **30**, 9847–9869.

Danabasoglu, G., J.-F. Lamarque, J. Bacmeister, D. Bailey, A. DuVivier, J. Edwards, L. Emmons, J. Fasullo, R. Garcia, A. Gettelman, et al., 2020: The community earth system model version 2 (CESM2). *Journal of Advances in Modeling Earth Systems*, **12**, e2019MS001916.

Day, J. J. and K. I. Hodges, 2018: Growing land-sea temperature contrast and the intensification of Arctic cyclones. *Geophysical Research Letters*, **45**, 3673–3681.

Day, J. J., M. M. Holland, and K. I. Hodges, 2018: Seasonal differences in the response of Arctic cyclones to climate change in CESM1. *Climate Dynamics*, **50**, 3885–3903.

DeRepentigny, P., A. Jahn, M. M. Holland, J. E. Kay, J. Fasullo, J.-F. Lamarque, S. Tilmes, C. Hannay, M. J. Mills, D. A. Bailey, et al., 2022: Enhanced simulated early 21st century arctic sea ice loss due to cmip6 biomass burning emissions. *Science Advances*, **8**, eabo2405.

DeRepentigny, P., A. Jahn, M. M. Holland, and A. Smith, 2020: Arctic sea ice in two configurations of the cesm2 during the 20th and 21st centuries. *Journal of Geophysical Research: Oceans*, **125**, e2020JC016133.

DuVivier, A. K., M. M. Holland, J. E. Kay, S. Tilmes, A. Gettelman, and D. A. Bailey, 2020: Arctic and Antarctic sea ice mean state in the Community Earth System Model version 2 and the influence of atmospheric chemistry. *Journal of Geophysical Research: Oceans*, **125**, e2019JC015934.

Eayrs, C., X. Li, M. N. Raphael, and D. M. Holland, 2021: Rapid decline in Antarctic sea ice in recent years hints at future change. *Nature Geoscience*, **14**, 460–464.

Feltham, D. L., 2008: Sea ice rheology. *Annu. Rev. Fluid Mech.*, **40**, 91–112.

Finocchio, P. M. and J. D. Doyle, 2021: Summer cyclones and their association with short-term sea ice variability in the Pacific sector of the Arctic. *Frontiers in Earth Science*, **9**, 738497.

Finocchio, P. M., J. D. Doyle, and D. P. Stern, 2022: Accelerated sea ice loss from late summer cyclones in the New Arctic. *Journal of Climate*, **35**, 4151–4169.

Finocchio, P. M., J. D. Doyle, D. P. Stern, and M. G. Fearon, 2020: Short-term impacts of Arctic summer cyclones on sea ice extent in the marginal ice zone. *Geophysical Research Letters*, **47**, e2020GL088338.

Goosse, H., S. Libera, A. C. Naveira Garabato, B. Richaud, A. Silvano, and M. Vancoppenolle, 2025: Winter sea ice edge shaped by Antarctic Circumpolar Current pathways. *The Cryosphere*, **19**, 5763–5779.

Graham, R. M., S. R. Hudson, and M. Maturilli, 2019a: Improved performance of ERA5 in Arctic gateway relative to four global atmospheric reanalyses. *Geophysical Research Letters*, **46**, 6138–6147.

Graham, R. M., P. Itkin, A. Meyer, A. Sundfjord, G. Spreen, L. H. Smedsrud, G. E. Liston, B. Cheng, L. Cohen, D. Divine, et al., 2019b: Winter storms accelerate the demise of sea ice in the Atlantic sector of the Arctic Ocean. *Scientific Reports*, **9**, 9222.

Haine, T. W. and T. Martin, 2017: The Arctic-Subarctic sea ice system is entering a seasonal regime: Implications for future Arctic amplification. *Scientific Reports*, **7**, 4618.

Hansen, J., M. Sato, P. Kharecha, and K. Von Schuckmann, 2011: Earth's energy imbalance and implications. *Atmospheric Chemistry and Physics*, **11**, 13421–13449.

Harvey, B., P. Cook, L. Shaffrey, and R. Schiemann, 2020: The response of the northern hemisphere storm tracks and jet streams to climate change in the CMIP3, CMIP5, and CMIP6 climate models. *Journal of Geophysical Research: Atmospheres*, **125**, e2020JD032701.

Hepworth, E., G. Messori, and M. Vichi, 2022: Association between extreme atmospheric anomalies over Antarctic sea ice, Southern Ocean polar cyclones and atmospheric rivers. *Journal of Geophysical Research: Atmospheres*, **127**, e2021JD036121.

Hersbach, H., B. Bell, P. Berrisford, S. Hirahara, A. Horányi, J. Muñoz-Sabater, J. Nicolas, C. Peubey, R. Radu, D. Schepers, et al., 2020: The ERA5 global reanalysis. *Quarterly Journal of the Royal Meteorological Society*, **146**, 1999–2049.

Heuzé, C. and A. Jahn, 2024: The first ice-free day in the arctic ocean could occur before 2030. *Nature Communications*, **15**, 1–10.

Holt, B. and S. Martin, 2001: The effect of a storm on the 1992 summer sea ice cover of the Beaufort, Chukchi, and East Siberian Seas. *Journal of Geophysical Research: Oceans*, **106**, 1017–1032.

Hoskins, B. J. and K. I. Hodges, 2002: New perspectives on the northern hemisphere winter storm tracks. *Journal of the Atmospheric Sciences*, **59**, 1041–1061.

Huang, B., C. Liu, V. Banzon, E. Freeman, G. Graham, B. Hankins, T. Smith, and H.-M. Zhang, 2021: Improvements of the daily optimum interpolation sea surface temperature (DOISST) version 2.1. *Journal of Climate*, **34**, 2923–2939.

Hunke, E., W. Lipscomb, P. Jones, A. Turner, N. Jeffery, and S. Elliott, 2017: CICE, the Los Alamos sea ice model. Technical report, Los Alamos National Laboratory (LANL), Los Alamos, NM (United States).

Itkin, P., G. Spreen, B. Cheng, M. Doble, F. Girard-Ardhuin, J. Haapala, N. Hughes, L. Kaleschke, M. Nicolaus, and J. Wilkinson, 2017: Thin ice and storms: Sea ice deformation from buoy arrays deployed during N-ICE 2015. *Journal of Geophysical Research: Oceans*, **122**, 4661–4674.

Jena, B., C. Bajish, J. Turner, M. Ravichandran, N. Anilkumar, and S. Kshitija, 2022: Record low sea ice extent in the Weddell Sea, Antarctica in April/May 2019 driven by intense and explosive polar cyclones. *Npj Climate and Atmospheric Science*, **5**, 19.

Kapsch, M.-L., R. G. Graversen, M. Tjernström, and R. Bintanja, 2016: The effect of downwelling longwave and shortwave radiation on Arctic summer sea ice. *Journal of Climate*, **29**, 1143–1159.

Konstali, K., T. Spengler, C. Spensberger, and A. Sorteberg, 2024: Linking future precipitation changes to weather features in cesm2-le. *Journal of Geophysical Research: Atmospheres*, **129**, e2024JD041190.

Koyama, T., J. Stroeve, J. Cassano, and A. Crawford, 2017: Sea ice loss and Arctic cyclone activity from 1979 to 2014. *Journal of Climate*, **30**, 4735–4754.

Kriegsmann, A. and B. Brümmer, 2014: Cyclone impact on sea ice in the central Arctic Ocean: a statistical study. *The Cryosphere*, **8**, 303–317.

Kwok, R., G. Spreen, and S. Pang, 2013: Arctic sea ice circulation and drift speed: Decadal trends and ocean currents. *Journal of Geophysical Research: Oceans*, **118**, 2408–2425.

Landrum, L. and M. M. Holland, 2020: Extremes become routine in an emerging new Arctic. *Nature Climate Change*, **10**, 1108–1115.

Lellouche, J.-M., E. Greiner, R. Bourdallé-Badie, G. Garric, A. Melet, M. Drévillon, C. Bricaud, M. Hamon, O. Le Galloudec, C. , Regnier, et al., 2021: The Copernicus global 1/12 oceanic and sea ice GLORYS12 reanalysis. *Frontiers in Earth Science*, **9**, 698876.

Lindsay, R. and A. Schweiger, 2015: Arctic sea ice thickness loss determined using subsurface, aircraft, and satellite observations. *The Cryosphere*, **9**, 269–283.

Lukovich, J. V., J. C. Stroeve, A. Crawford, L. Hamilton, M. Tsamados, H. Heorton, and F. Massonnet, 2021: Summer extreme cyclone impacts on Arctic sea ice. *Journal of Climate*, **34**, 4817–4834.

Madec, G., R. Bourdallé-Badie, P.-A. Bouttier, C. Bricaud, D. Bruciaferri, D. Calvert, J. Chanut, E. Clementi, A. Coward, D. Delrosso, et al., 2017: NEMO ocean engine.

Maslanik, J., C. Fowler, J. Stroeve, S. Drobot, J. Zwally, D. Yi, and W. Emery, 2007: A younger, thinner Arctic ice cover: Increased potential for rapid, extensive sea-ice loss. *Geophysical Research Letters*, **34**.

Meier, W. N., F. Fetterer, M. Savoie, S. Mallory, R. Duerr, and J. Stroeve, 2017: NOAA/NSIDC Climate Data Record of Passive Microwave Sea Ice Concentration, Version 3. Boulder, Colorado USA. NSIDC: National Snow and Ice Data Center. doi:https://doi.org/10.7265/N59P2ZTG.

Mundi, C. and T. L'Ecuyer, 2025: Is the modern Arctic marginal ice zone more susceptible to summer cyclones? *Journal of Climate*, **38**, 403–422.

Mundi, C., T. L'Ecuyer, and A. DuVivier, 2025: Have impacts of intense Arctic cyclones on summer sea ice reached a maximum? *Geophysical Research Letters*, **52**, e2025GL117848.

Neu, U., M. G. Akperov, N. Bellenbaum, R. Benestad, R. Blender, R. Caballero, A. Cocozza, H. F. Dacre, Y. Feng, K. Fraedrich, et al., 2013: IMILAST: A community effort

to intercompare extratropical cyclone detection and tracking algorithms. *Bulletin of the American Meteorological Society*, **94**, 529–547.

Nishii, K., H. Nakamura, and Y. J. Orsolini, 2015: Arctic summer storm track in CMIP3/5 climate models. *Climate Dynamics*, **44**, 1311–1327.

Ogi, M., I. G. Rigor, M. G. McPhee, and J. M. Wallace, 2008: Summer retreat of Arctic sea ice: Role of summer winds. *Geophysical Research Letters*, **35**.

Peng, G., W. N. Meier, D. J. Scott, and M. H. Savoie, 2013: A long-term and reproducible passive microwave sea ice concentration data record for climate studies and monitoring. *Earth System Science Data*, **5**, 311–318, doi:10.5194/essd-5-311-2013.
URL `https://essd.copernicus.org/articles/5/311/2013/`

Peng, L., X. Zhang, J.-H. Kim, K.-H. Cho, B.-M. Kim, Z. Wang, and H. Tang, 2021: Role of intense Arctic storm in accelerating summer sea ice melt: An in situ observational study. *Geophysical Research Letters*, **48**, e2021GL092714.

Perovich, D. K., J. A. Richter-Menge, K. F. Jones, and B. Light, 2008: Sunlight, water, and ice: Extreme Arctic sea ice melt during the summer of 2007. *Geophysical Research Letters*, **35**.

Priestley, M. D. and J. L. Catto, 2021: Future changes in the extratropical storm tracks and cyclone intensity, wind speed, and structure. *Weather and Climate Dynamics Discussions*, **2021**, 1–40.

Prince, H. D. and T. S. L'Ecuyer, 2024: Observed energetic adjustment of the Arctic and Antarctic in a warming world. *Journal of Climate*, **37**, 2611–2627.

Rinke, A., M. Maturilli, R. M. Graham, H. Matthes, D. Handorf, L. Cohen, S. R. Hudson, and J. C. Moore, 2017: Extreme cyclone events in the Arctic: Wintertime variability and trends. *Environmental Research Letters*, **12**, 094006.

Rodgers, K. B., S.-S. Lee, N. Rosenbloom, A. Timmermann, G. Danabasoglu, C. Deser, J. Edwards, J.-E. Kim, I. R. Simpson, K. Stein, et al., 2021: Ubiquity of human-induced changes in climate variability. *Earth System Dynamics*, **12**, 1393–1411.

Rolph, R. J., D. L. Feltham, and D. Schröder, 2020: Changes of the Arctic marginal ice zone during the satellite era. *The Cryosphere*, **14**, 1971–1984.

Schreiber, E. A. and M. C. Serreze, 2020: Impacts of synoptic-scale cyclones on Arctic sea-ice concentration: a systematic analysis. *Annals of Glaciology*, **61**, 139–153.

Screen, J. A. and I. Simmonds, 2012: Declining summer snowfall in the Arctic: Causes, impacts and feedbacks. *Climate dynamics*, **38**, 2243–2256.

Serreze, M. C., 1995: Climatological aspects of cyclone development and decay in the arctic. *Atmosphere-Ocean*, **33**, 1–23.

Serreze, M. C. and R. G. Barry, 2011: Processes and impacts of Arctic amplification: A research synthesis. *Global and planetary change*, **77**, 85–96.

Serreze, M. C., F. Carse, R. G. Barry, and J. C. Rogers, 1997: Icelandic low cyclone activity: Climatological features, linkages with the NAO, and relationships with recent changes in the northern hemisphere circulation. *Journal of Climate*, **10**, 453–464.

Sickmöller, M., R. Blender, and K. Fraedrich, 2000: Observed winter cyclone tracks in the northern hemisphere in re-analysed ECMWF data. *Quarterly Journal of the Royal Meteorological Society*, **126**, 591–620.

Simmonds, I. and I. Rudeva, 2012: The great Arctic cyclone of August 2012. *Geophysical Research Letters*, **39**.

Simpson, I. R., J. Bacmeister, R. B. Neale, C. Hannay, A. Gettelman, R. R. Garcia, P. H. Lauritzen, D. R. Marsh, M. J. Mills, B. Medeiros, et al., 2020: An evaluation of the large-scale atmospheric circulation and its variability in CESM2 and other CMIP models. *Journal of Geophysical Research: Atmospheres*, **125**, e2020JD032835.

Sledd, A., T. L'Ecuyer, J. Kay, and M. Steele, 2023: Clouds increasingly influence Arctic sea surface temperatures as CO2 rises. *Geophysical Research Letters*, **50**, e2023GL102850.

Song, J.-N., G. Fu, Y. Xu, Z.-Y. Han, Q.-Z. Sun, and H. Wang, 2021: Assessment of the capability of CMIP6 global climate models to simulate Arctic cyclones. *Advances in Climate Change Research*, **12**, 660–676.

Spensberger, C., G. Boutin, H. Regan, and T. Spengler, 2026: Limited overall impact of cyclones on arctic sea ice tendencies throughout all seasons. *Journal of Climate*, **39**, 439–458.

Spreen, G., R. Kwok, and D. Menemenlis, 2011: Trends in Arctic sea ice drift and role of wind forcing: 1992–2009. *Geophysical Research Letters*, **38**.

Steele, M., J. Zhang, and W. Ermold, 2010: Mechanisms of summertime upper arctic ocean warming and the effect on sea ice melt. *Journal of Geophysical Research: Oceans*, **115**.

Stroeve, J. and D. Notz, 2018: Changing state of Arctic sea ice across all seasons. *Environmental Research Letters*, **13**, 103001.

Stroeve, J. C., T. Markus, L. Boisvert, J. Miller, and A. Barrett, 2014: Changes in Arctic melt season and implications for sea ice loss. *Geophysical Research Letters*, **41**, 1216–1225.

Stroeve, J. C., M. C. Serreze, M. M. Holland, J. E. Kay, J. Malanik, and A. P. Barrett, 2012: The Arctic's rapidly shrinking sea ice cover: a research synthesis. *Climatic change*, **110**, 1005–1027.

Strong, C. and I. G. Rigor, 2013: Arctic marginal ice zone trending wider in summer and narrower in winter. *Geophysical Research Letters*, **40**, 4864–4868.

Thorndike, A. and R. Colony, 1982: Sea ice motion in response to geostrophic winds. *Journal of Geophysical Research: Oceans*, **87**, 5845–5852.

Trenberth, K. E., J. T. Fasullo, and M. A. Balmaseda, 2014: Earth's energy imbalance. *Journal of Climate*, **27**, 3129–3144.

Tsamados, M., D. Feltham, A. Petty, D. Schroeder, and D. Flocco, 2015: Processes controlling surface, bottom and lateral melt of Arctic sea ice in a state of the art sea ice model. *Philosophical Transactions of the Royal Society A: Mathematical, Physical and Engineering Sciences*, **373**, 20140167.

Tschudi, M., W. Meier, J. Stewart, C. Fowler, and J. Maslanik, 2019: Polar pathfinder daily 25 km ease-grid sea ice motion vectors, version 4.
URL `http://nsidc.org/data/NSIDC-0116/versions/4`

Tschudi, M. A., W. N. Meier, and J. S. Stewart, 2020: An enhancement to sea ice motion and age products at the National Snow and Ice Data Center (NSIDC). *The Cryosphere*, **14**, 1519–1536.

Valkonen, E., J. Cassano, and E. Cassano, 2021: Arctic cyclones and their interactions with the declining sea ice: A recent climatology. *Journal of Geophysical Research: Atmospheres*, **126**, e2020JD034366.

Valkonen, E., J. Cassano, E. Cassano, M. Seefeldt, and C. Parker, 2025: Cmip6 representation of declining sea ice and arctic cyclones in the current climate. *Journal of Geophysical Research: Atmospheres*, **130**, e2024JD042388.

Vichi, M., C. Eayrs, A. Alberello, A. Bekker, L. Bennetts, D. Holland, E. de Jong, W. Joubert, K. MacHutchon, G. Messori, et al., 2019: Effects of an explosive polar

cyclone crossing the Antarctic marginal ice zone. *Geophysical Research Letters*, **46**, 5948–5958.

von Schuckmann, K., M. Palmer, K. E. Trenberth, A. Cazenave, D. Chambers, N. Champollion, J. Hansen, S. Josey, N. Loeb, P.-P. Mathieu, et al., 2016: An imperative to monitor Earth's energy imbalance. *Nature Climate Change*, **6**, 138–144.

Wagner, T., I. Eisenman, and H. Mason, 2021: How sea ice drift influences sea ice area and volume. *Geophysical Research Letters*, **48**, e2021GL093069.

Wang, Q., Z. Li, P. Lu, Y. Xu, and Z. Li, 2022: Flexural and compressive strength of the landfast sea ice in the Prydz Bay, East Antarctic. *The Cryosphere*, **16**, 1941–1961.

Wang, Y., H. Bi, H. Huang, Y. Liu, Y. Liu, X. Liang, M. Fu, and Z. Zhang, 2019: Satellite-observed trends in the Arctic sea ice concentration for the period 1979–2016. *Journal of Oceanology and Limnology*, **37**, 18–37.

Ward, J. L., A. E. Payne, and C. Pettersen, 2023: Present-day regional Antarctic sea ice response to extratropical cyclones. *Journal of Geophysical Research: Atmospheres*, **128**, e2023JD038914.

Wei, J., X. Zhang, and Z. Wang, 2019: Reexamination of Fram Strait sea ice export and its role in recently accelerated Arctic sea ice retreat. *Climate Dynamics*, **53**, 1823–1841.

Wernli, H. and C. Schwierz, 2006: Surface cyclones in the ERA-40 dataset (1958–2001). Part I: Novel identification method and global climatology. *Journal of the Atmospheric Sciences*, **63**, 2486–2507.

Zappa, G., L. C. Shaffrey, and K. I. Hodges, 2013: The ability of CMIP5 models to simulate north atlantic extratropical cyclones. *Journal of Climate*, **26**, 5379–5396.

Zhang, J., R. Lindsay, A. Schweiger, and M. Steele, 2013: The impact of an intense summer cyclone on 2012 Arctic sea ice retreat. *Geophysical Research Letters*, **40**, 720–726.

Zhang, X., H. Tang, J. Zhang, J. E. Walsh, E. L. Roesler, B. Hillman, T. J. Ballinger, and W. Weijer, 2023: Arctic cyclones have become more intense and longer-lived over the past seven decades. *Communications Earth & Environment*, **4**, 348.

Zhang, X., J. E. Walsh, J. Zhang, U. S. Bhatt, and M. Ikeda, 2004: Climatology and interannual variability of Arctic cyclone activity: 1948–2002. *Journal of Climate*, **17**, 2300–2317.

Zhou, C., Q. Wang, I. Tan, L. Zhang, M. D. Zelinka, M. Wang, and J. Bloch-Johnson, 2025: Sea ice pattern effect on Earth's energy budget is characterized by hemispheric asymmetry. *Science Advances*, **11**, eadr4248.